A Thesis for the Degree of Ph.D. in Engineering

Development of Haptic End-effector for Medicine and Manufacturing

August 2017

Graduate School of Science and Technology
Keio University

MATSUNAGA, Takuya

Acknowledgements

I have completed this dissertation as a summary of my research from April 2013 through August 2017 as a member of Ohnishi laboratory, Graduate School of Science and Technology, Keio University. I would like to express my acknowledgments to those who have helped me to complete my research.

First of all, I would like to express my heartfelt grateful to Professor Dr. Kouhei Ohnishi. His enormous support and insightful comments were invaluable for my research. In addition, he gave me opportunities to take part in state of the art projects and develop various haptic robots. Activities in Ohnishi laboratory were precious experiences for me.

I greatly appreciate to the members of SUM committee in Keio University, Professor Dr. Toshiyuki Murakami, Professor Dr. Hiroaki Nishi, Associate Professor Dr. Takahiro Yakoh, Associate Professor Dr. Seiichiro Katsura, and Assistant Professor Dr. Takahiro Nozaki for giving me a lot of valuable advices and comments.

My deepest appreciation goes to Professor Dr. Yuko Kitagawa and Senior Assistant Professor Dr. Norihito Wada. They gave me appropriate feedback about medical haptic applications.

I would like to offer my special thanks to Associate Professor Dr. Tomoyuki Shimono, Yokohama National University, and Mr. Wataru Iida, Haptics Research Center. Their constructive comments and warm encouragement have been a great help in my research activity.

Dr. Takahiro Mizoguchi, Kanagawa Institute of Industrial Science and Technology, Mr. Kazuki Tanida, Sumitomo Heavy Industries, Ltd., Mr. Yuki Saito, Yokogawa Electric Corporation, Mr. Kasun Prasanga, Dr. Koyo Yu, KEYENCE CORPORATION, and Mr. Kenji Ogawa gave me a lot of valuable and practical advices as the seniors of the laboratory. Without their guidance and persistent help, my Ph. D dissertation would not have been possible.

As Ph. D. candidates, I have had encouragement of Mr. Hiroshi Asai, Yokohama National University. Also, I have had encouragement of Mr. Shuhei Shimizu, Mr. Yoshiyuki Kambara, and Mr. Mehdi Hazaz, who are my contemporaries in Ohnishi laboratory. Mr. Daisuke Tomizuka made enormous contribution to projects and experiments. I received tremendous support for activities in Ohnishi laboratory from Mr. Toshiaki Okano.

I am deeply grateful to my parents and sister for giving me tremendous support. Without their supports, I could not dedicate myself to this research.

There are a lot of people who helped me although I could not mentioned here. I would like to express my sincere gratitude again to all people who have supported me.

August, 2017

Takuya Matsunaga

Contents

List of Figures

List of Tables

Chapter 1

Introduction

1.1 Background

1.1.1 Robotic technologies for modern society

The modern society has many serious problems. An aging society with fewer children causes a shortage of labor force. Production capacity will be deteriorated in accordance with the reduction of labor force in human working area such as factories and farms. Human skills which are necessary to achieve tasks will be lost by the lack of successors. Besides, tasks conducted in places that human workers should not approach have been increasing. Disaster areas, radioactive pollution areas, and the outer space are dangerous for human workers. In a clean room, since dust deteriorates the quality of products, human workers must take care not to bring dust from the outside. In addition, there are tasks requiring motions beyond human abilities. Manipulation of micro objects such as cells and electronic parts is difficult for human workers. Dexterous motions in a narrow space such as surgical procedures are also requires skill of surgeons. Therefore, technologies to support or substitute for human workers are necessary for these problems. Robotic technologies are useful to solve difficulties in the modern society. Robots can be driven in various environments and conduct difficult tasks for human workers from the perspective of the ability and the safety of human workers. Besides, robotic labor force can be increased as needed by manufacturing robots. Therefore, various robots have been studied and developed by many researchers.

Since the 1960s, robotic technologies have been applied to industrial robots in factories [1]. Industrial robots can achieve target tasks automatically and repetitively in a closed working area. Tasks such as welding and coating are conducted by robotic motions with the high precision positioning instead of human workers. Although industrial robots contribute to improve the efficiency of production works, the substitution of the human recognition ability and the technical skill is difficult. Human workers are still necessary to execute tasks which require the human recognition ability and the skill, even if the task is danger for human workers.

As robots that human components remain in the control loop, teleoperation robots have been studied and developed. A method of teleoperation is the master-slave system composed of a master robot (master) at an operator side and a slave robot (slave) at a working area [2]. The slave conducts tasks by following motion of the master manipulated by the human operator. Especially, the realization of motion of upper limbs is important to conduct complex tasks by the teleoperation robots. A practical application of the master-slave system to realize motion of upper limbs is robotic systems for surgery [3]. Surgeons conduct complex surgical procedures by using multi degree of freedom (DoF) forceps robots which are components of a robotic system for surgery. Besides, the human abilities can be extended by using robotic functions such as the motion scaling and the hand shake suppression. Commercialized systems are used for minimally invasive surgery and experiments [4][5]. In addition, robotic systems for neurosurgery [6], retinal surgery [7], Natural Orifice Translumenal Endoscopic Surgery (NOTES) [8][9], and so on have been studied and developed.

An issue of these robots is utilization of haptic information composed of position information and force information. Although conventional teleoperation robots can achieve high precision positioning, the capability to transmit the force information is insufficient. Since the operator cannot control the force applied to objects which contacts with the slave, the lack of force sensation causes failure of tasks by the excessive and the shortage of the output force [10][11]. To achieve tasks requiring the human recognition ability and the technical skill by robotic motion, the utilization of the haptic information for robots which have the motion of upper limbs is necessary.

1.1.2 Haptic technologies

There are technologies to utilize the haptic information for robots and machines. The bilateral control is a method to transmit the haptic information between the master and the slave in teleoperation. Many researchers have worked on the bilateral control to transmit clear force sensation to the operator [12]. Hannaford expressed relation of the position information and the force information communicated between the master and the slave by the hybrid parameter [13]. Lawrence expressed the performance of the bilateral control by the transparency [14]. Iida et al. realized transmission of the clear force sensation

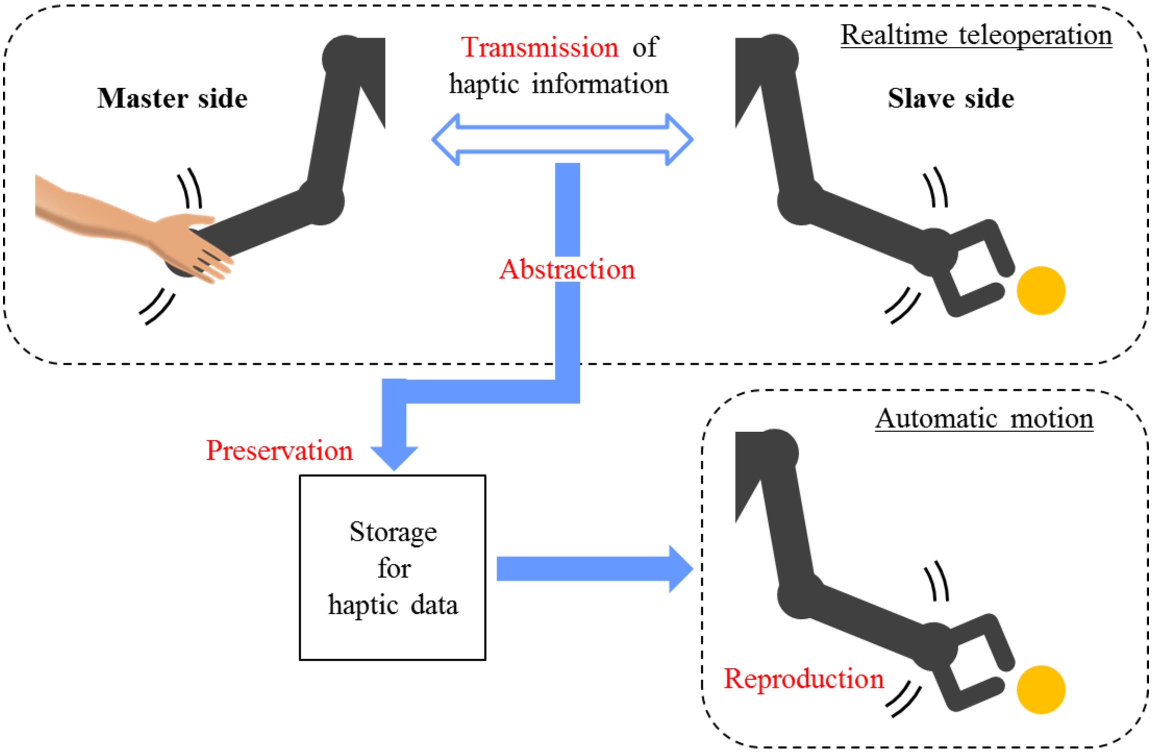

Fig. 1-1: Utilization of haptic information.

by the acceleration based four-channel bilateral control and expressed the transparency as operationality and reproducibility [15].

Haptic information is necessary for analysis of human motion to realize robotic motion with human technical skill. As a method to analyze human motion, the motion capture system have been used [16]. Human motion is captured by cameras and saved as position and posture information. However, force information cannot be obtained by the visual information. Yokokura et al. proposed the motion-copying system to save haptic information transmitted by master-slave systems and reproduce motion of the slave by the saved haptic information [17]. Nozaki et al. proposed a method of elemental separation of human motion extracted by the master-slave system with the bilateral control and presented mathematical expression of human motion which can be used for the motion reproduction system [18]. Therefore, the acceleration based four-channel bilateral control can be used not only for transmission, but also for abstraction and preservation of human motion as haptic information. The motion reproduction system realizes automatic motion based on human motion as shown in Fig. 1-1.

The master and the slave have the number of DoF and the structure according to target tasks. Although the bilateral control can transmit precise haptic information between the master and the slave, the actual performance of haptic robots depends on mechanical components to obtain haptic information. The performance to obtain haptic information is deteriorated by backdrivability of movable parts, stiffness of mechanical parts to transmit driving force, and backlash between movable parts and fixed parts. The backdrivability can be considered as the impedance [19]. The mass of movable parts and the friction decrease the backdrivability. The influence of these mechanical components is not ignorable when the number of DoF is increased. Although methods to improve the backdrivability of the robot have been proposed [20], additional sensors causes problems such as the complexity of the structure and the increase of the size. To realize the utilization of the precise haptic information, the mechanical design of haptic devices must be considered.

1.1.3 Mechanism of multi DoF robots

To realize the motion of an upper limb by robots, large number of DoF is required. Suzuki et al. and Nozaki et al. developed master-slave systems which have the similar structure and the number of DoF with a human hand [21][22]. However, only motion of a human hand was focused on. Since the large number of DoF increases the cost and the complexity, simplified structure is applied to many teleoperation robots. A simplified function of a human hand is grasping motion. Due to the versatile usage, various mechanisms including the grasping mechanism as an end-effector have been proposed.

Wire drive mechanism which realizes transmission of driving force in narrow spaces is applied to commercialized robotic systems for surgery [4][5], multi DoF forceps robots [23][24], and flexible endoscopic robots for NOTES [8][9][25][26]. However, the wire drive mechanism has problems such as the elasticity and the durability of wires. Besides, flexible parts of robots deteriorate the performance of the wire drive mechanism in the case of flexible endoscopic robots, since wires going through the inside of flexible parts cause the friction and the backlash. Instead of the wire drive mechanism, multi DoF forceps robots driven by fluid actuators have been proposed [27][28]. The mechanism driven by fluid can reduce the weight of movable parts and improve the backdrivability. However, fluid actuators have some difficulties such as the compressibility of air, the complexity of the calibration, and the leak of fluid.

As a method to transmit driving force by rigid components, multi DoF forceps robots with the parallel link mechanism have been developed. The parallel link mechanism is applied to the bending mechanism at the tip of forceps robots. Ibrahim et al. developed the bending mechanism with four rigid links [29]. Although two DoF bending motion is realized by the parallel link mechanism, required actuators are more than the number of DoF. Kishi et al. proposed the bending mechanism composed of gears and rigid rods [30]. Arata et al. developed a link driven four DoF forceps robot [31]. To realize two DoF bending motion, these robots have two joints at the tip of the forceps. The bending mechanism with more than two joints is unlike the structure of a human wrist. Ishii et al. applied the double-screw-drive mechanism for the bending mechanism [32]. Arata et al. developed the parallel link mechanism composed of the spring-link mechanism [33]. However, these mechanisms deteriorate the backdrivability of bending parts. The accuracy of force information can be improved by force sensors at the tip of tool [34]. King et al. implemented force sensor to contact surfaces of the gripper of a forceps to obtain grasping force information [35]. Kim et al. developed a gripper utilizing dielectric substrate to obtain force information of three translational direction and grasping motion [36]. However, force information cannot be measured correctly when objects do not contact with the sensing part of the force sensors. Besides, the implementation of force sensors constrains the size and the shape of the gripper.

As a haptic application, Katsura et al. applied the acceleration based four-channel bilateral control to a master-slave forceps robot [15]. Tanaka et al. developed a multi DoF forceps robot with the bilateral control [37]. However, large manipulating force is generated by the mechanism of the robot to realize multi DoF motion. Besides, the bending mechanism with two joints is unlike the structure of a human wrist. Ishii et al. developed a four DoF haptic forceps robot with the parallel link mechanism driven by linear motors [38]. Although translational motion, pitch motion, and yaw motion are realized in modal space, the robot does not have roll motion. The linear motors directly connected with rigid rods of the parallel link mechanism make the roll motion difficult. Therefore, not only the bending mechanism but also a method to transmit driving force to the tip must be considered when the parallel link mechanism with rigid links is utilized.

1.2 Orientation of this research

The purpose of this research is to develop the five DoF Haptic End-effector for Medicine and Manufacturing (HEM^2) which can transmit haptic information and reproduce human motion by preserved haptic information. Motion of upper limb is essential to both medical treatments and manufacturing tasks, although detailed specifications depend on tasks. HEM^2 is a master-slave system to realize motion

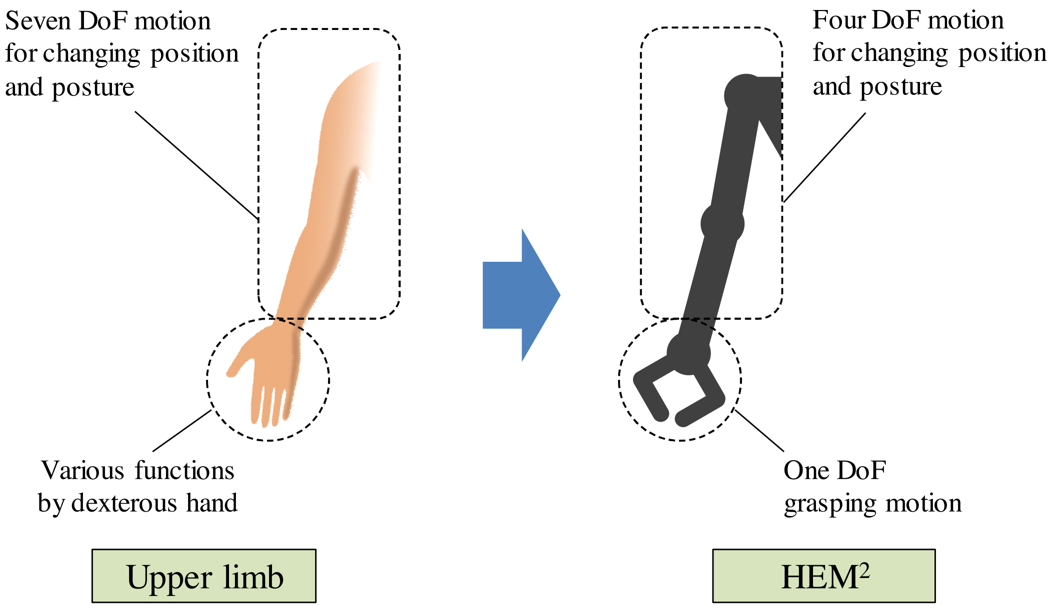

Fig. 1-2: Motion of upper limb and HEM^2.

of an upper limb. The correspondence between an upper limb and HEM^2 is shown in Fig. 1-2. The human arm and wrist have seven DoF motion used to change the position and the posture of the dexterous hand. In this research, one DoF grasping motion, three DoF wrist motion, and one DoF translational motion are chosen as the simplified motion of an upper limb. By using the five DoF motion of HEM^2, complex tasks are realized by bilateral teleoperation and automatic motion based on human motion. For the purpose, three types of the master-slave system with haptic technologies are developed.

First, a two DoF serial link robot constructed by high backdrivability actuators, high stiffness mechanical parts, and less backlash mechanism is developed. Two DoF motion is composed of grasping motion and translational motion which are correspond to the simplified motion of the human hand and arm. The end-effector for the grasping motion is composed of slider crank mechanisms. Besides, the bilateral control with the kinematics of slider crank mechanisms is regarded as the scaling bilateral control by approximation.

Second, a one DoF miniature haptic forceps robot with a flexible tube is developed as a slave of a flexible haptic forceps robot. The miniature haptic forceps robot composed of a small motor with a high reduction ratio gear head realizes the grasping motion not depending on the posture of flexible parts. Mechanical components such as high reduction ratio mechanisms cause the deterioration of the efficiency to transmit driving force and the accuracy of force information. Therefore, the efficiency of the torque transmission mechanism of the miniature haptic forceps robot is calculated by a preliminary experiment. The force information is corrected by the efficiency.

Third, two prototypes of the five DoF HEM^2 are developed. Five DoF motion is the minimum number of DoF to realize the human wrist motion and the simplified hand and arm motion. Since the serial link mechanism with large number of DoF deteriorates the performance, two DoF serial link mechanism, parallel link mechanism, and gear mechanism are combined and driven by parallel drive mechanism. Besides, the efficiency of driving force transmission mechanisms is used to obtain force information. The performance of the second prototype is validated by experiments

Finally, a ten DoF double arm teleoperation robot composed of two sets of the five DoF HEM^2 is constructed. A ligation task which is a surgical procedure is conducted by both the teleoperation and automatic motion. The force information is important when tightening a knot [39]. Although Motooka et al. developed a 16 DoF double arm haptic forceps robot, the bilateral control was implemented to only two DoF motion for each arm [40]. Two DoF motion is not enough to achieve complex tasks. The ligation task is conducted by bilateral teleoperation using the teleoperation robot. Besides, the motion of the operator is preserved and reproduced.

1.3 Chapter organization

The rest of this thesis is organized as follows; the chapter organization is shown in Fig. 1-3.

Chapter 2 describes the motion control based on robust acceleration control. As a method to realize the robust acceleration control, Disturbance OBserver (DOB) is explained [41]. Besides, Reaction Force OBserver (RFOB) is referred to estimate force information [42]. Then, position control and force control based on the acceleration control are described.

Chapter 3 describes control systems for haptic applications. The acceleration based four-channel bilateral control is explained as a method to transmit clear force sensation. As control systems based on the bilateral control, the oblique coordinate control [43] and the motion reproduction system is described [17]. The bilateral control using the oblique coordinate control eliminates the influence of the interference. The motion reproduction system preserves human motion as haptic information and reproduces motion by saved haptic information.

Chapter 4 describes the two DoF haptic robot composed of high backdrivability mechanisms, high

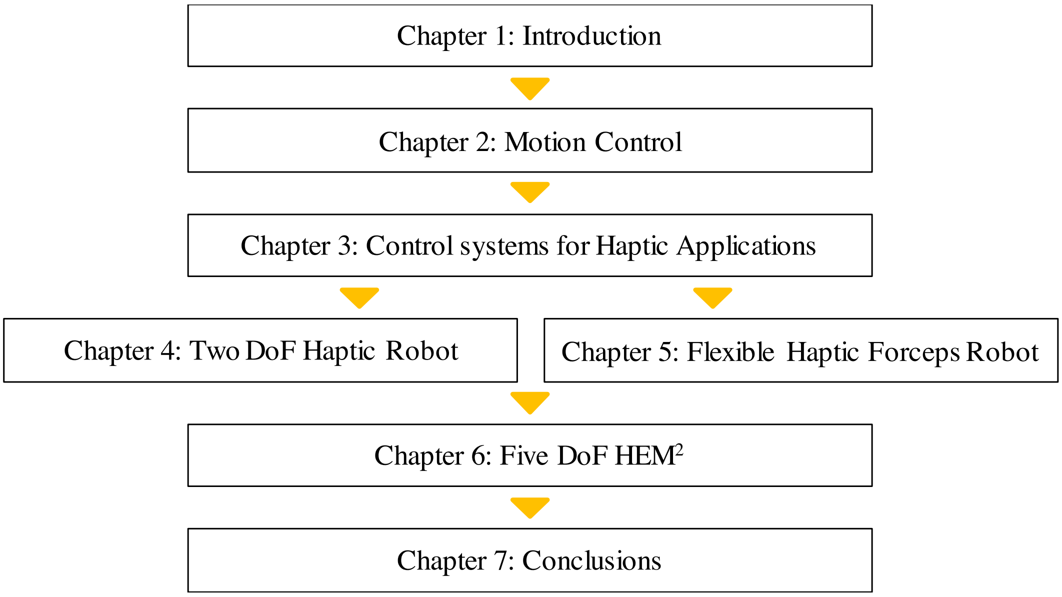

Fig. 1-3: Chapter organization.

stiffness parts to transmit driving force, and less backlash mechanisms. The serial link mechanism with an end-effector composed of slider crank mechanisms is applied to both the master and the slave. The validity of these mechanisms for the bilateral control and the motion reproduction system is confirmed by experiments.

Chapter 5 describes the one DoF flexible haptic forceps robot. A small motor with a high reduction ratio gear head is implemented to the slave of the DoF flexible haptic forceps robot. The efficiency of the mechanical component to transmit the driving force is used to correct the estimated value of RFOB in the bilateral teleoperation.

Chapter 6 describes two prototypes of the five DoF HEM^2. Five DoF motion with force sensation is realized by the first prototype. The parallel drive mechanism to combine the serial link mechanism with slider crank mechanisms, the parallel link mechanism, and the no-backlash gear is constructed for the second prototype. The efficiency of the mechanical components to transmit driving force is considered to correct force information. For more complex tasks, the double arm teleoperation robot composed two prototypes of the HEM^2 is constructed. The ligation task is conducted by both bilateral teleoperation and reproduced motion.

Chapter 7 concludes this research. The symbols and subscripts are shown as Table 1.1 and Table 1.2.

Table 1.1: Symbols and descriptions

Symbols	Descripsions	Units
x	Position	m
f	Force	N
M	Mass	kg
q, ϕ, θ, ψ	Angle	rad
τ	Torque	Nm
J	Inertia	kg m^2
I_a	Current	A
K_t	Thrust coefficient or torque coefficient	N/A or Nm/A
C_p	Position controller	-
C_f	Force controller	-
K_p	Position gain	s^{-2}
K_v	Velocity gain	s^{-1}
K_f	Force gain	-
s	Laplace operator	-
g	Cutoff frequency	rad/s

Table 1.2: Superscripts, subscripts, and descriptions

Superscripts and subscripts	Descripsions
n	Nominal value
dis	Disturbance
int	Internal
ext	External
fric	Friction
g	Gravity
cmp	Compensation
ref	Reference
res	Response
cmd	Command
dob	Disturbance observer
rfob	Reaction force observer
M	Master
S	Slave
m	Motor space
j	Joint space
w	Work space
G	Grasping motion
L	Translational motion
R	Roll motion
P	Pitch motion
Y	Yaw motion

Chapter 2

Motion Control

2.1 Introduction

Robust motion control of actuators is essential to realize desired motion of robots and achieve target tasks. To utilize haptic information composed of position information and force information for master-slave systems, position and force of actuators must be controlled. Position control and force control can be achieved by robust acceleration control.

In this chapter, motion control of electric motors based on robust acceleration control is explained. First, a model of a linear motor is explained in Section 2.2. Second, DOB [41] for robust acceleration control and RFOB [42] for estimation of force information are described in Section 2.3. Third, robust position control and robust force control in motor space is explained in Section 2.4. Finally, robust position control and robust force control in joint space is explained in Section 2.5.

2.2 Model of motor

A motion equation of a linear motor is given as,

$$Ms^2X = F_{\mathrm{a}} - F_{\mathrm{load}}. \tag{2.1}$$

F_{a} and F_{load} are driving force of the linear motor and load force. Assuming that a current reference $I_{\mathrm{a}}^{\mathrm{ref}}$ accords with a armature current of the linear motor, the driving force of the linear motor F_{a} is given as,

$$F_{\mathrm{a}} = K_{\mathrm{t}} I_{\mathrm{a}}^{\mathrm{ref}}. \tag{2.2}$$

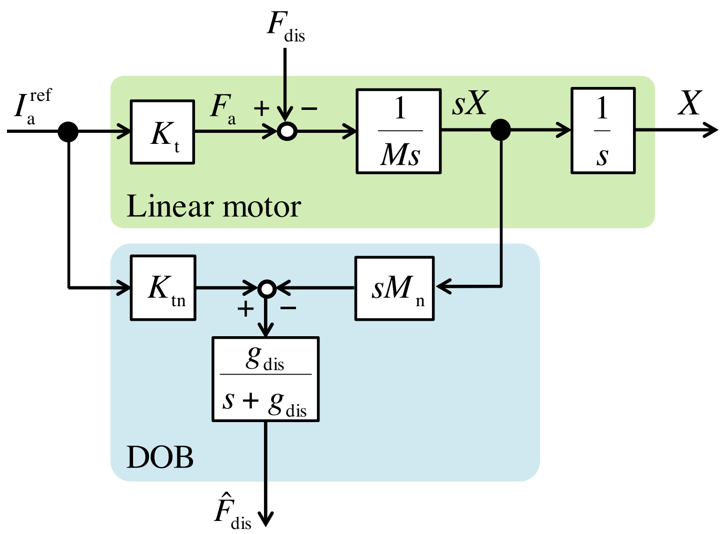

Fig. 2-1: Disturbance observer.

The composition of the load force F_{load} is given as,

$$F_{\mathrm{load}} = F^{\mathrm{ext}} + F^{\mathrm{int}} + F^{\mathrm{fric}} + F^{\mathrm{g}}. \tag{2.3}$$

F^{ext}, F^{int}, F^{fric}, and F^{g} denote external force, internal force, friction force, and gravity force, respectively. From eq. (2.1), eq. (2.2), and eq. (2.3), the motion equation of the linear motor is given as,

$$Ms^2X = K_{\mathrm{t}}I_{\mathrm{a}}^{\mathrm{ref}} - \left(F^{\mathrm{ext}} + F^{\mathrm{int}} + F^{\mathrm{fric}} + F^{\mathrm{g}}\right). \tag{2.4}$$

The model can be applied not only to linear motors but also to rotary motors.

2.3 Disturbance observer and reaction force observer

In actual control systems, nominal mass M_{n} and nominal thrust coefficient K_{tn} are used instead of actual mass M and actual thrust coefficient K_{t}. Errors between the real values and the nominal values are given as,

$$M = M_{\mathrm{n}} + \Delta M, \tag{2.5}$$

$$K_{\mathrm{t}} = K_{\mathrm{tn}} + \Delta K_{\mathrm{t}}. \tag{2.6}$$

Hence, disturbance F_{dis} including the load force F_{load} and the parameter errors is given as,

$$F_{\mathrm{dis}} = F_{\mathrm{load}} - \Delta K_{\mathrm{t}}I_{\mathrm{a}}^{\mathrm{ref}} + \Delta Ms^2X. \tag{2.7}$$

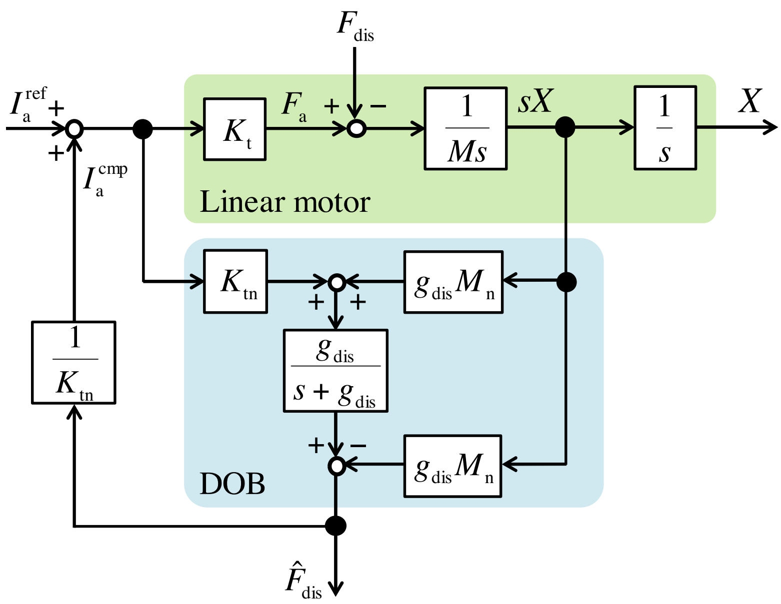

Fig. 2-2: Feedback of compensation current.

From eq. (2.5), eq. (2.6), and eq. (2.7), the disturbance F_{dis} is rewritten as,

$$F_{\mathrm{dis}} = K_{\mathrm{tn}} I_{\mathrm{a}}^{\mathrm{ref}} - M_{\mathrm{n}} s^2 X. \tag{2.8}$$

DOB estimates the disturbance F_{dis} by the current reference $I_{\mathrm{a}}^{\mathrm{ref}}$ and the acceleration response s^2X. Since high frequency noise is amplified by differential operations, DOB includes a Low Pass Filter (LPF). Therefore, estimated disturbance $\hat{F}_{\mathrm{dis}}$ is given as,

$$\hat{F}_{\mathrm{dis}} = \frac{g_{\mathrm{dis}}}{s + g_{\mathrm{dis}}} F_{\mathrm{dis}}. \tag{2.9}$$

g_{dis} is a cutoff frequency of DOB. The block diagram of DOB is shown in Fig. 2-1.

Robust acceleration control with DOB is achieved by feedback of compensation current $I_{\mathrm{a}}^{\mathrm{cmp}}$ given as,

$$I_{\mathrm{a}}^{\mathrm{cmp}} = \frac{1}{K_{\mathrm{tn}}} \hat{F}_{\mathrm{dis}}. \tag{2.10}$$

The block diagram of DOB expressed by an integrator and the compensation current $I_{\mathrm{a}}^{\mathrm{cmp}}$ is shown in Fig. 2-2. The disturbance F_{dis} in a low frequency band can be suppressed by setting the high cutoff frequency of LPF. However, the system becomes unstable when the cutoff frequency is excessively high.

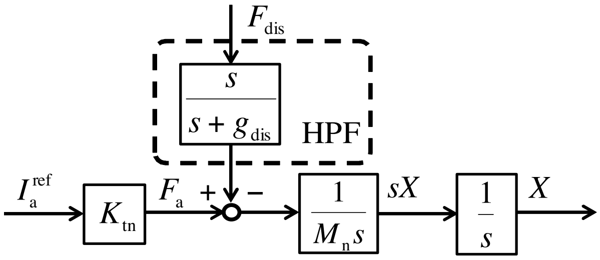

Fig. 2-3: Equivalent transformation of disturbance observer with compensation current.

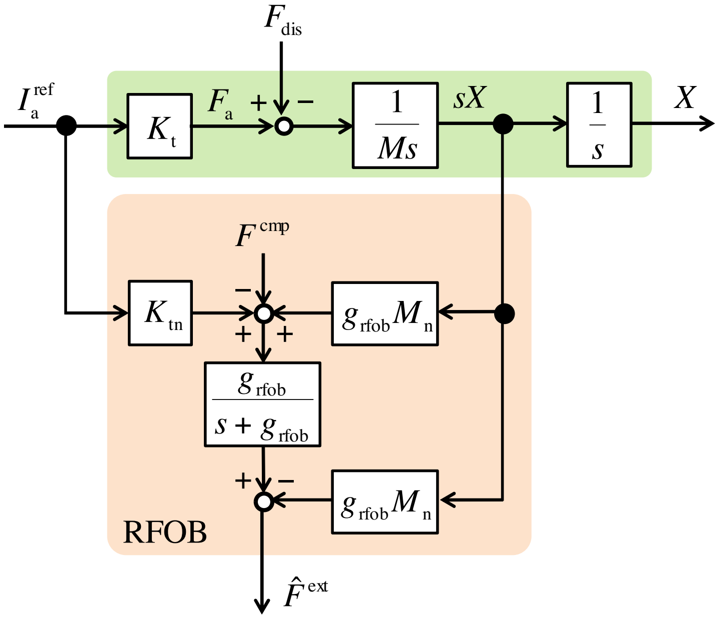

Fig. 2-4: Reaction force observer.

A transformed structure of DOB is shown in Fig. 2-3. The disturbance in the low frequency band is suppressed by a High Pass Filter (HPF).

From eq. (2.3) and eq. (2.7), the disturbance F_{dis} includes the external force F^{ext} given as,

$$F^{\text{ext}} = K_{\text{tn}} I_{\text{a}}^{\text{ref}} - M_{\text{n}} s^2 X + \Delta K_{\text{tn}} I_{\text{a}}^{\text{ref}} - \Delta M s^2 X - \left(F^{\text{int}} + F^{\text{fric}} + F^{\text{g}}\right). \tag{2.11}$$

RFOB estimates the external force F^{ext} by eliminating the components of the disturbance except the external force. The block diagram of RFOB is shown in Fig. 2-4. g_{rfob} is a cutoff frequency of RFOB. Although DOB suppresses the influence of ΔM and ΔK_{t} as disturbance, the parameter errors deteriorate the estimation accuracy of RFOB.

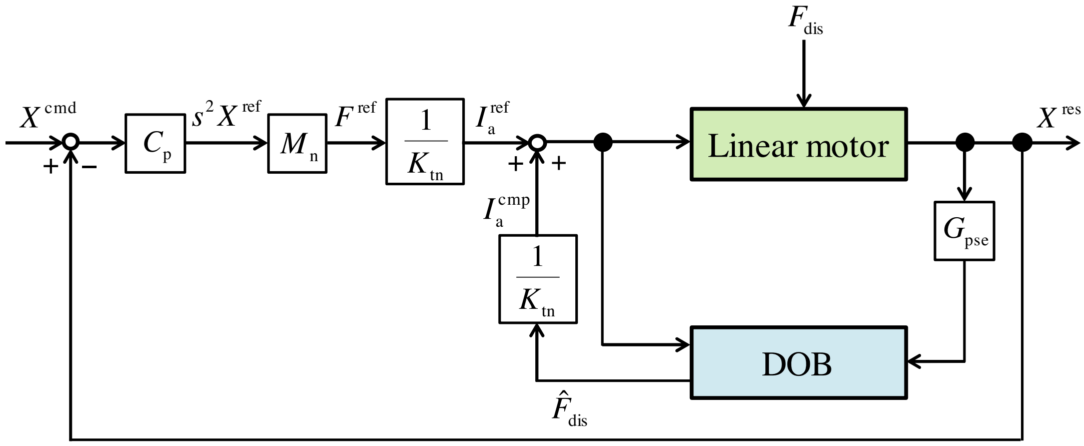

Fig. 2-5: Position control based on the acceleration control with DOB.

2.4 Robust acceleration control in motor space

Robust position control and robust force control can be achieved by the acceleration control with DOB. A controller of the robust control is constructed in motor space to control motion of the motor.

2.4.1 Position control

In ideal position control, a position response X^{res} accords with a desired position X^{cmd}. Assuming that the controlled system is the second order system, a transfer function is given as,

$$\begin{aligned}\frac{X^{\mathrm{res}}}{X^{\mathrm{cmd}}} &= \frac{s^2 + K_{\mathrm{v}}s + K_{\mathrm{p}}}{s^2 + K_{\mathrm{v}}s + K_{\mathrm{p}}} \\ &= 1. \end{aligned} \tag{2.12}$$

K_{p} and K_{v} are position gain and velocity gain, respectively. Hence, an ideal acceleration response s^2X^{res} is given as,

$$s^2X^{\mathrm{res}} = s^2X^{\mathrm{cmd}} + K_{\mathrm{v}}s\left(X^{\mathrm{cmd}} - X^{\mathrm{res}}\right) + K_{\mathrm{p}}\left(X^{\mathrm{cmd}} - X^{\mathrm{res}}\right). \tag{2.13}$$

A position controller C_{p} is defined as,

$$C_{\mathrm{p}} = K_{\mathrm{v}}s + K_{\mathrm{p}}. \tag{2.14}$$

Therefore, the ideal acceleration response s^2X^{res} is given as,

$$s^2X^{\mathrm{res}} = s^2X^{\mathrm{cmd}} + C_{\mathrm{p}}\left(X^{\mathrm{cmd}} - X^{\mathrm{res}}\right). \tag{2.15}$$

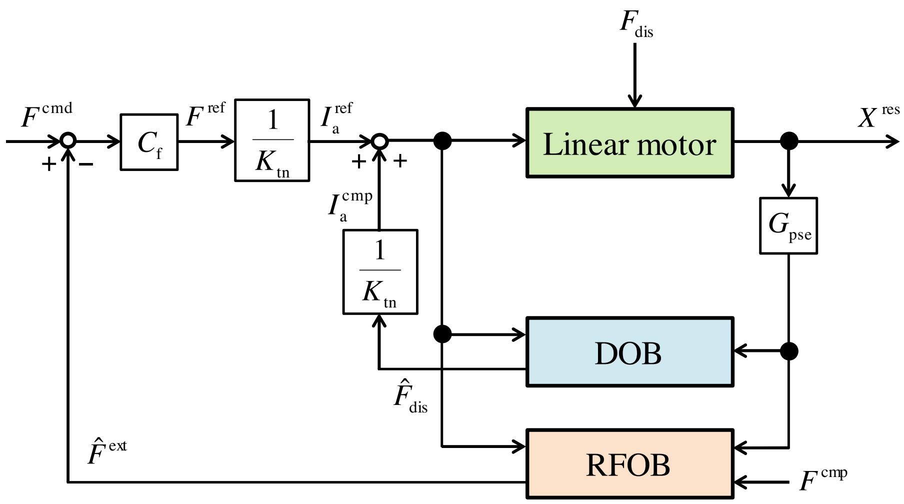

Fig. 2-6: Force control based on the acceleration control with DOB and RFOB.

A critical damped response is achieved by a condition given as,

$$K_{\mathrm{v}} = 2\sqrt{K_{\mathrm{p}}}. \tag{2.16}$$

The block diagram of the position control based on the robust acceleration control with DOB is shown in Fig. 2-5. Instead of a differential operation, a pseudo differential operation is implemented to calculate the velocity information. The pseudo differential operation G_{pse} is given as,

$$G_{\mathrm{pse}} = \frac{s g_{\mathrm{pse}}}{s + g_{\mathrm{pse}}}. \tag{2.17}$$

g_{pse} is a cutoff frequency of the pseudo differential operation.

2.4.2 Force control

In ideal force control, the external force applied by contacted objects F^{ext} accords with a desired force F^{cmd}. The block diagram of the force control based on the robust acceleration control with DOB is shown in Fig. 2-6. By implementing RFOB, the force information can be obtained without force sensors. A force reference for the motor F^{ref} is given as,

$$F^{\mathrm{ref}} = \frac{C_{\mathrm{f}}}{M_{\mathrm{n}}} \left(F^{\mathrm{cmd}} - \hat{F}^{\mathrm{ext}} \right). \tag{2.18}$$

C_{f} is a force controller.

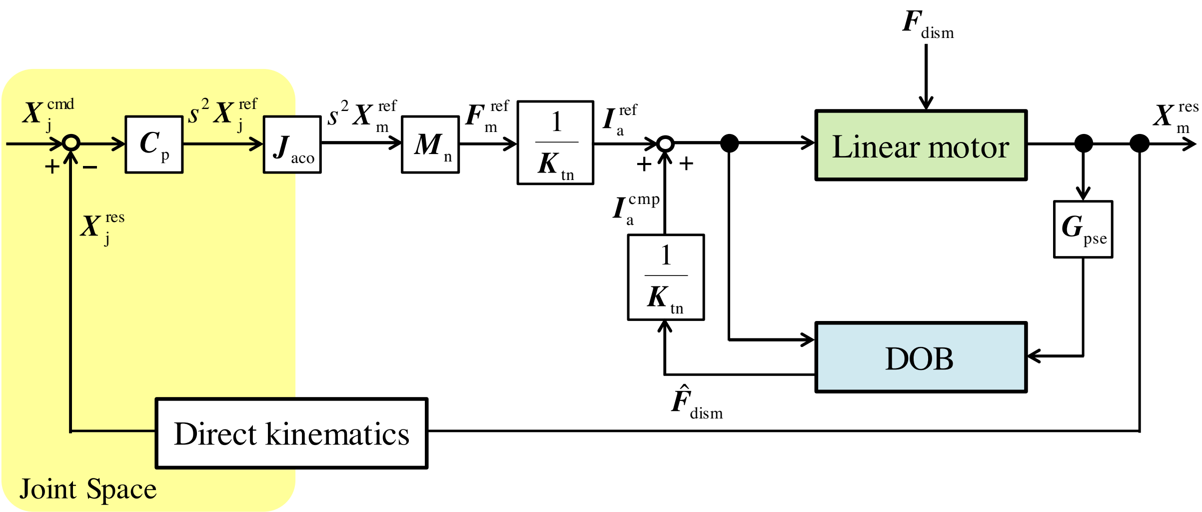

Fig. 2-7: Position control in joint space based on the acceleration control with DOB.

2.5 Robust acceleration control in joint space

Motion of active joints in joint space is different from motion of motors, when mechanical components such as gears and link mechanisms are used to transmit driving force. To construct a controller of the robust control for active joints of robots, motion in the motor space must be converted into motion in the joint space.

2.5.1 Position control in joint space

Assuming that a two DoF serial link robot composed of two linear motors is controlled, a position vector $\boldsymbol{x}_{\mathrm{m}}$ and a force vector $\boldsymbol{f}_{\mathrm{m}}$ in the motor space are given as,

$$\boldsymbol{x}_{\mathrm{m}} = \begin{bmatrix} x_{\mathrm{m1}} & x_{\mathrm{m2}} \end{bmatrix}^{\mathrm{T}}, \tag{2.19}$$

$$\boldsymbol{f}_{\mathrm{m}} = \begin{bmatrix} f_{\mathrm{m1}} & f_{\mathrm{m2}} \end{bmatrix}^{\mathrm{T}}. \tag{2.20}$$

The subscripts 1 and 2 denote link number. A position vector $\boldsymbol{x}_{\mathrm{j}}$ and A force vector $\boldsymbol{f}_{\mathrm{j}}$ in the joint space are given as,

$$\boldsymbol{x}_{\mathrm{j}} = \begin{bmatrix} x_{\mathrm{j1}} & x_{\mathrm{j2}} \end{bmatrix}^{\mathrm{T}}, \tag{2.21}$$

$$\boldsymbol{f}_{\mathrm{j}} = \begin{bmatrix} f_{\mathrm{j1}} & f_{\mathrm{j2}} \end{bmatrix}^{\mathrm{T}}. \tag{2.22}$$

The position vector in the motor space $\boldsymbol{x}_{\mathrm{m}}$ is converted into the position vector in the joint space $\boldsymbol{x}_{\mathrm{j}}$ by kinematics of the robot. Relation between the velocity vector in the motor space and the joint space is expressed by a Jacobian matrix $\boldsymbol{J}_{\mathrm{aco}}$ given as,

$$\dot{\boldsymbol{x}}_{\mathrm{j}} = \boldsymbol{J}_{\mathrm{aco}} \dot{\boldsymbol{x}}_{\mathrm{m}}, \tag{2.23}$$

$$\boldsymbol{J}_{\mathrm{aco}} = \begin{bmatrix} \dfrac{\partial x_{\mathrm{j1}}}{\partial x_{\mathrm{m1}}} & \dfrac{\partial x_{\mathrm{j1}}}{\partial x_{\mathrm{m2}}} \\ \dfrac{\partial x_{\mathrm{j2}}}{\partial x_{\mathrm{m1}}} & \dfrac{\partial x_{\mathrm{j2}}}{\partial x_{\mathrm{m2}}} \end{bmatrix}. \tag{2.24}$$

Besides, an acceleration vector in the joint space is given as,

$$\ddot{\boldsymbol{x}}_{\mathrm{j}} = \boldsymbol{J}_{\mathrm{aco}} \ddot{\boldsymbol{x}}_{\mathrm{m}} + \dot{\boldsymbol{J}}_{\mathrm{aco}} \dot{\boldsymbol{x}}_{\mathrm{m}}. \tag{2.25}$$

The second term of the right side in eq. (2.25) is ignorable. Relation between the force vector in the motor space and the joint space derived by the principle of virtual work is given as,

$$\boldsymbol{f}_{\mathrm{m}} = \boldsymbol{J}_{\mathrm{aco}}{}^{\mathrm{T}} \boldsymbol{f}_{\mathrm{j}}. \tag{2.26}$$

The block diagram of the position control in the joint space is shown in Fig. 2-7. Matrices $\boldsymbol{C}_{\mathrm{p}}$, $\boldsymbol{M}_{\mathrm{n}}$, $\boldsymbol{K}_{\mathrm{tn}}$, $\boldsymbol{I}_{\mathrm{a}}$, and $\boldsymbol{G}_{\mathrm{pse}}$ are given as,

$$\boldsymbol{C}_{\mathrm{p}} = \begin{bmatrix} C_{\mathrm{p1}} & 0 \\ 0 & C_{\mathrm{p2}} \end{bmatrix}, \tag{2.27}$$

$$\boldsymbol{M}_{\mathrm{n}} = \begin{bmatrix} M_{\mathrm{n1}} & 0 \\ 0 & M_{\mathrm{n2}} \end{bmatrix}, \tag{2.28}$$

$$\boldsymbol{K}_{\mathrm{tn}} = \begin{bmatrix} K_{\mathrm{tn1}} & 0 \\ 0 & K_{\mathrm{tn2}} \end{bmatrix}, \tag{2.29}$$

$$\boldsymbol{I}_{\mathrm{a}} = \begin{bmatrix} I_{\mathrm{a1}} & 0 \\ 0 & I_{\mathrm{a2}} \end{bmatrix}, \tag{2.30}$$

$$\boldsymbol{G}_{\mathrm{pse}} = \begin{bmatrix} G_{\mathrm{pse1}} & 0 \\ 0 & G_{\mathrm{pse2}} \end{bmatrix}. \tag{2.31}$$

A position response vector in the motor space $\boldsymbol{X}_{\mathrm{m}}^{\mathrm{res}}$ is converted into a position response vector in the joint space $\boldsymbol{X}_{\mathrm{j}}^{\mathrm{res}}$ by the kinematics. A force reference vector $\boldsymbol{F}_{\mathrm{j}}^{\mathrm{ref}}$ is calculated by the controller constructed in the joint space and converted into references in the motor space. DOB is constructed in the motor space and realize the robust acceleration control.

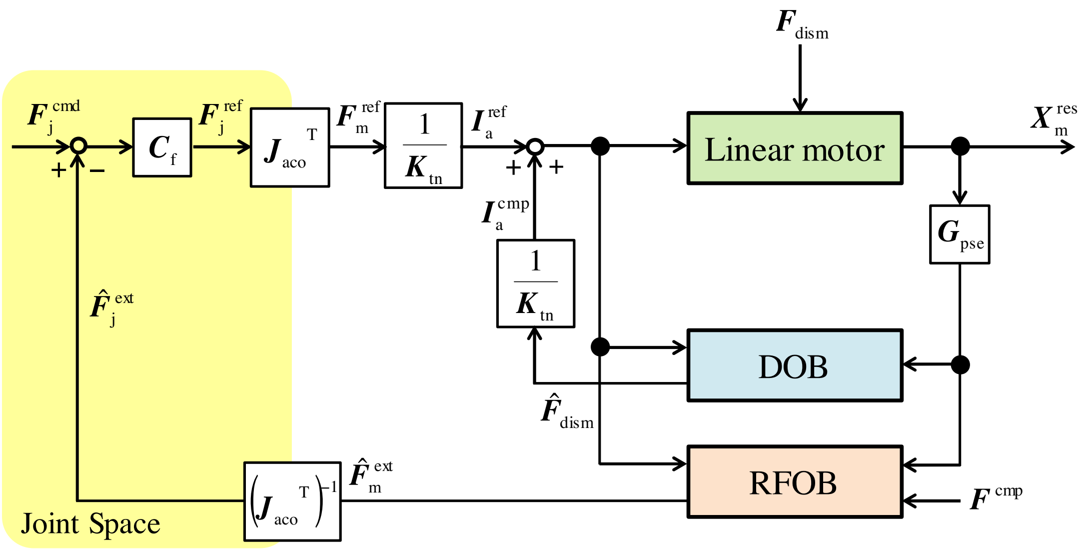

Fig. 2-8: Force control in joint space based on the acceleration control with DOB.

2.5.2 Force control in joint space

The block diagram of the force control in the joint space is shown in Fig. 2-8. A force controller matrix $\boldsymbol{C}_{\rm f}$ is given as,

$$\boldsymbol{C}_{\rm f} = \begin{bmatrix} C_{\rm f1} & 0 \\ 0 & C_{\rm f2} \end{bmatrix} \tag{2.32}$$

Both DOB and RFOB are constructed in the motor space. The conversion of estimated external force vector $\hat{\boldsymbol{F}}^{\rm ext}$ between the motor space and the joint space is conducted according to eq. (2.26). DOB and RFOB are constructed in the motor space.

2.6 Summary

In this chapter, the motion control of electric motors based on the robust acceleration control was explained. A linear motor was modeled as an electric motor. Then, DOB for the robust acceleration control and RFOB for estimating the external force were described. The position control and the force control based on the robust acceleration control with DOB were constructed in the motor space and the joint space. The contents of this chapter are the fundamental knowledge of this research.

Chapter 3

Control Systems for Haptic Applications

3.1 Introduction

The master-slave system is widely used as a method to manipulate robots intuitively. Haptic information composed of position information and force information is important for safer teleoperation. The lack of the force sensation causes failures in teleoperation such as damage for objects and drop of objects. There are some control systems to utilize haptic information.

In this chapter, control systems for haptic applications are explained. First, the acceleration based four-channel bilateral control to transmit clear force sensation in bilateral teleoperation is described in Section 3.2. Second, the acceleration based bilateral control using oblique coordinate control is explained in Section 3.3. Finally, the motion reproduction system to preserve and reproduce human motions is explained in Section 3.4.

3.2 Acceleration based bilateral control

The acceleration based four-channel bilateral control is a method to transmit clear force sensation between the master and the slave. The concept of the acceleration based bilateral teleoperation is shown in Fig. 3-1. When a human hand contacts with an object and applies action force, reaction force is generated by the object. From Newton's third law, the magnitude of the action force is the same with one of the reaction force. In bilateral teleoperation, Newton's third law is realized via master-slave systems. The master and the slave reproduce the reaction force and the action force, while achieving the coincident

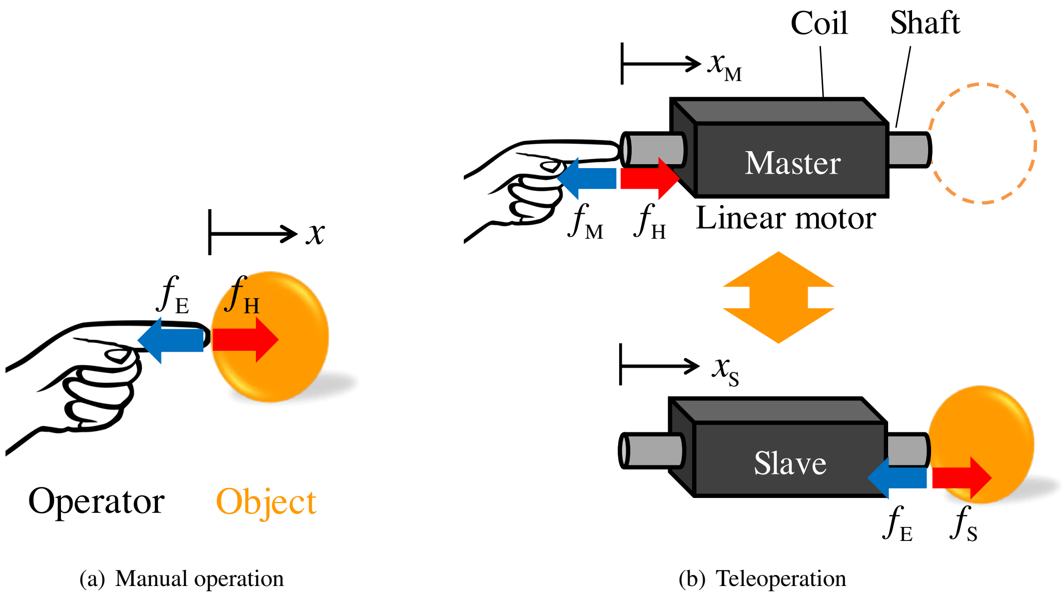

Fig. 3-1: Concept of bilateral teleoperation.

of the position. Therefore, control targets of the acceleration based bilateral control are given as,

$$X_{\rm M} - X_{\rm S} = 0, \tag{3.1}$$

$$F_{\rm M} + F_{\rm S} = 0. \tag{3.2}$$

Position tracking between the master and the slave is realized by eq. (3.1). Newton's third law is realized by eq. (3.2).

The control targets of the acceleration based four-channel bilateral control system are achieved in modal space. A modal transformed position and a modal transformed force are given as,

$$\begin{bmatrix} X_{\rm dif} \\ X_{\rm com} \end{bmatrix} = \boldsymbol{T} \begin{bmatrix} X_{\rm M} \\ X_{\rm S} \end{bmatrix}, \tag{3.3}$$

$$\begin{bmatrix} F_{\rm dif} \\ F_{\rm com} \end{bmatrix} = \boldsymbol{T} \begin{bmatrix} F_{\rm M} \\ F_{\rm S} \end{bmatrix}, \tag{3.4}$$

$$\boldsymbol{T} = \begin{bmatrix} 1 & -1 \\ 1 & 1 \end{bmatrix}. \tag{3.5}$$

$\boldsymbol{T}$ is a transformation matrix from the motor space to the modal space. A differential mode of the position $X_{\rm dif}$ and A common mode of the force $F_{\rm com}$ are chosen as the controlled variables in the modal space.

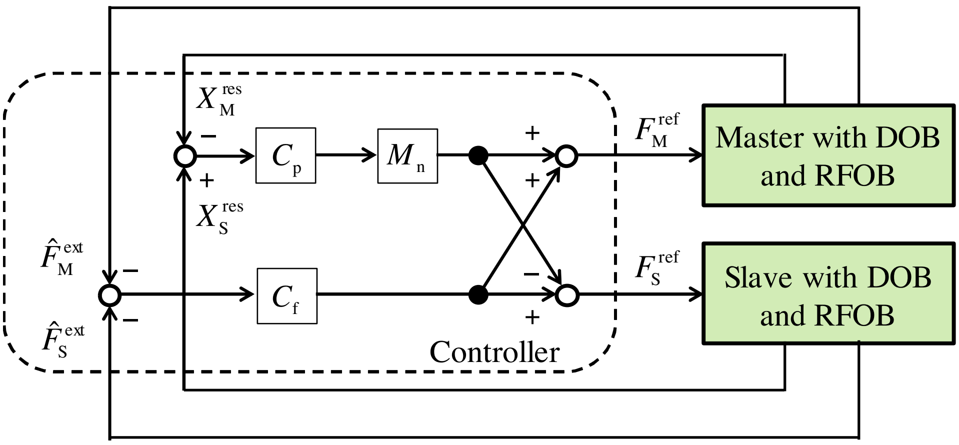

Fig. 3-2: Block diagram of the acceleration based four-channel bilateral control system constructed in motor space.

Then, the control targets given by eq. (3.1) and eq. (3.2) are rewritten as,

$$X_{\mathrm{dif}} = X_{\mathrm{M}} - X_{\mathrm{S}} \to 0, \tag{3.6}$$

$$F_{\mathrm{com}} = F_{\mathrm{M}} + F_{\mathrm{S}} \to 0. \tag{3.7}$$

Therefore, acceleration references for the differencial mode and the common mode in the modal space are given as,

$$s^2 X_{\mathrm{dif}}^{\mathrm{ref}} = C_{\mathrm{p}} \left(0 - X_{\mathrm{dif}}\right), \tag{3.8}$$

$$s^2 X_{\mathrm{com}}^{\mathrm{ref}} = C_{\mathrm{f}} \left(0 - F_{\mathrm{com}}\right). \tag{3.9}$$

A position controller C_{p} and a force controller C_{f} are used for the differential mode and the common mode, respectively. The references in the modal space are converted into the reference of each motor by the inverse of the transformation matrix $\boldsymbol{T}^{-1}$.

The block diagram of the acceleration based four-channel bilateral control system constructed in the motor space is shown in Fig. 3-2. The force references $F_{\mathrm{M}}^{\mathrm{ref}}$ and $F_{\mathrm{S}}^{\mathrm{ref}}$ are given as,

$$F_{\mathrm{M}}^{\mathrm{ref}} = -M_{\mathrm{n}} C_{\mathrm{p}} \left(X_{\mathrm{M}}^{\mathrm{res}} - X_{\mathrm{S}}^{\mathrm{res}}\right) - C_{\mathrm{f}} \left(\hat{F}_{\mathrm{M}}^{\mathrm{ext}} + \hat{F}_{\mathrm{S}}^{\mathrm{ext}}\right) \tag{3.10}$$

$$F_{\mathrm{S}}^{\mathrm{ref}} = M_{\mathrm{n}} C_{\mathrm{p}} \left(X_{\mathrm{M}}^{\mathrm{res}} - X_{\mathrm{S}}^{\mathrm{res}}\right) - C_{\mathrm{f}} \left(\hat{F}_{\mathrm{M}}^{\mathrm{ext}} + \hat{F}_{\mathrm{S}}^{\mathrm{ext}}\right). \tag{3.11}$$

A constant value $\det\boldsymbol{T}$ is included in the position controller C_{p} and the force controller C_{f}. Besides, nominal mass M_{n} is included in the force controller C_{f}.

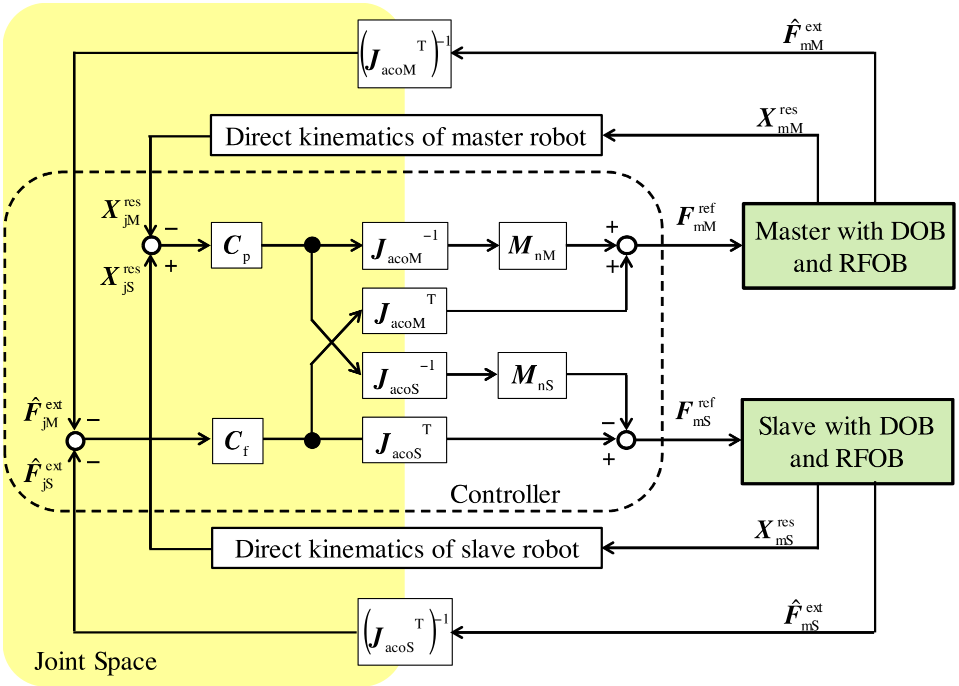

Fig. 3-3: Block diagram of the acceleration based four-channel bilateral control system constructed in joint space.

The block diagram of the acceleration based four-channel bilateral control system constructed in the joint space is shown in Fig. 3-3. Force reference vectors $\boldsymbol{F}_{\mathrm{jM}}^{\mathrm{ref}}$ and $\boldsymbol{F}_{\mathrm{jS}}^{\mathrm{ref}}$ are given as,

$$\boldsymbol{F}_{\mathrm{mM}}^{\mathrm{ref}} = -\boldsymbol{M}_{\mathrm{nM}} \left(\boldsymbol{J}_{\mathrm{acoM}}\right)^{-1} \boldsymbol{C}_{\mathrm{p}} \left(\boldsymbol{X}_{\mathrm{jM}}^{\mathrm{res}} - \boldsymbol{X}_{\mathrm{jS}}^{\mathrm{res}}\right) - \boldsymbol{J}_{\mathrm{acoM}}{}^{\mathrm{T}} \boldsymbol{C}_{\mathrm{f}} \left(\hat{\boldsymbol{F}}_{\mathrm{jM}}^{\mathrm{ext}} + \hat{\boldsymbol{F}}_{\mathrm{jS}}^{\mathrm{ext}}\right), \tag{3.12}$$

$$\boldsymbol{F}_{\mathrm{mS}}^{\mathrm{ref}} = \boldsymbol{M}_{\mathrm{nS}} \left(\boldsymbol{J}_{\mathrm{acoS}}\right)^{-1} \boldsymbol{C}_{\mathrm{p}} \left(\boldsymbol{X}_{\mathrm{jM}}^{\mathrm{res}} - \boldsymbol{X}_{\mathrm{jS}}^{\mathrm{res}}\right) - \boldsymbol{J}_{\mathrm{acoS}}{}^{\mathrm{T}} \boldsymbol{C}_{\mathrm{f}} \left(\hat{\boldsymbol{F}}_{\mathrm{jM}}^{\mathrm{ext}} + \hat{\boldsymbol{F}}_{\mathrm{jS}}^{\mathrm{ext}}\right). \tag{3.13}$$

3.3 Oblique coordinate control

In the case of the scaling bilateral control with different mass, interference deteriorates the performance of the acceleration based bilateral control. The acceleration based bilateral control system based on the oblique coordinate control can suppress the influence of the interference [43]. The block diagram of the acceleration based bilateral control using the oblique coordinate control is shown in Fig. 3-4. A position vector in the motor space $\boldsymbol{X}_{\mathrm{m}}$ is defined as,

$$\boldsymbol{X}_{\mathrm{m}} = \begin{bmatrix} X_M \\ X_S \end{bmatrix}. \tag{3.14}$$

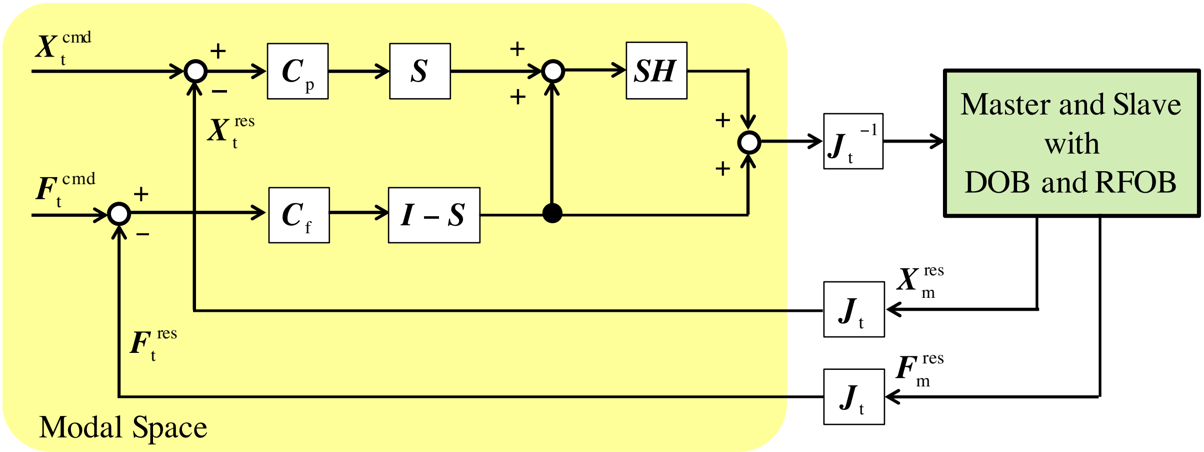

Fig. 3-4: Block diagram of the acceleration based bilateral control using the oblique coordinate control.

A force vector in the motor space $\boldsymbol{F}_{\mathrm{m}}$ is defined as,

$$\boldsymbol{F}_{\mathrm{m}} = \begin{bmatrix} F_M \\ F_S \end{bmatrix}. \tag{3.15}$$

The mass matrix in the motor space $\boldsymbol{M}$ is given as,

$$\boldsymbol{M} = \begin{bmatrix} M_{\mathrm{M}} & 0 \\ 0 & M_{\mathrm{S}} \end{bmatrix}. \tag{3.16}$$

In the case of the scaling bilateral control, the control targets of the acceleration based bilateral control are written as,

$$X_{\mathrm{M}} - \alpha X_{\mathrm{S}} = 0, \tag{3.17}$$

$$F_{\mathrm{M}} + \beta F_{\mathrm{S}} = 0. \tag{3.18}$$

α and β are the position scaling and the force scaling, respectively. The control targets given by eq. (3.17) and eq. (3.18) are expressed as a position task X_X and a force task F_F in the modal space. The control targets in the modal space are given as,

$$X_X = X_{\mathrm{M}} - \alpha X_{\mathrm{S}}, \tag{3.19}$$

$$F_F = F_{\mathrm{M}} + \beta F_{\mathrm{S}}. \tag{3.20}$$

A Jacobian matrix $\boldsymbol{J}_{\mathrm{t}}$ converts variables in the motor space into variables in the modal space. The Jacobian matrix $\boldsymbol{J}_{\mathrm{t}}$ is given as,

$$\boldsymbol{J}_{\mathrm{t}} = \begin{bmatrix} 1 & -\alpha \\ 1 & \beta \end{bmatrix}. \tag{3.21}$$

The position vector $\boldsymbol{X}_{\mathrm{m}}$ and the force vector $\boldsymbol{F}_{\mathrm{m}}$ in the motor space are converted into vectors in the modal space by the Jacobian matrix $\boldsymbol{J}_{\mathrm{t}}$. A position vector $\boldsymbol{X}_{\mathrm{t}}$ and a force vector $\boldsymbol{F}_{\mathrm{t}}$ in the modal space are given as,

$$\begin{aligned} \boldsymbol{X}_{\mathrm{t}} &= \boldsymbol{J}_{\mathrm{t}}\boldsymbol{X}_{\mathrm{m}} \\ &= \begin{bmatrix} X_X & X_F \end{bmatrix}^{\mathrm{T}}, \end{aligned} \tag{3.22}$$

$$\begin{aligned} \boldsymbol{F}_{\mathrm{t}} &= \boldsymbol{J}_{\mathrm{t}}\boldsymbol{F}_{\mathrm{m}} \\ &= \begin{bmatrix} F_X & F_F \end{bmatrix}^{\mathrm{T}}. \end{aligned} \tag{3.23}$$

A equivalent mass matrix in the modal space $\boldsymbol{M}_{\mathrm{t}}$ is given as,

$$\begin{aligned} \boldsymbol{M}_{\mathrm{t}} &= \boldsymbol{J}_{\mathrm{t}}\boldsymbol{M}\boldsymbol{J}_{\mathrm{t}}{}^{-1} \\ &= \begin{bmatrix} M_{11} & M_{12} \\ M_{21} & M_{22} \end{bmatrix}. \end{aligned} \tag{3.24}$$

In the modal space, a command value is set for each task. The command values in the modal space are given as,

$$\boldsymbol{X}_{\mathrm{t}}^{\mathrm{cmd}} = \boldsymbol{0}, \tag{3.25}$$

$$\boldsymbol{F}_{\mathrm{t}}^{\mathrm{cmd}} = \boldsymbol{0}. \tag{3.26}$$

The position controller and the force controller are given as,

$$\boldsymbol{C}_{\mathrm{p}} = C_{\mathrm{p}}\boldsymbol{I}, \tag{3.27}$$

$$\boldsymbol{C}_{\mathrm{f}} = C_{\mathrm{f}}\boldsymbol{I}. \tag{3.28}$$

$\boldsymbol{I}$ is the identity matrix of order two. Hence, the reference values derived by the position vector and the force vector are given as,

$$\boldsymbol{X}_{\mathrm{t}}^{\mathrm{ref}} = -C_{\mathrm{p}}\boldsymbol{X}_{\mathrm{t}}^{\mathrm{res}}, \tag{3.29}$$

$$\boldsymbol{F}_{\mathrm{t}}^{\mathrm{ref}} = -C_{\mathrm{f}}\boldsymbol{F}_{\mathrm{t}}^{\mathrm{res}}. \tag{3.30}$$

The force reference vector in the modal space $\boldsymbol{F}_{\mathrm{t}}^{\mathrm{ref}}$ is given as,

$$\boldsymbol{F}_{\mathrm{t}}^{\mathrm{ref}} = \boldsymbol{S}\boldsymbol{H}\begin{bmatrix} s^2 X_X \\ F_F \end{bmatrix}^{\mathrm{ref}} + (\boldsymbol{I} - \boldsymbol{S})\begin{bmatrix} 0 \\ F_F \end{bmatrix}^{\mathrm{ref}}. \tag{3.31}$$

The hybrid matrix $\boldsymbol{H}$ is given as,

$$\boldsymbol{H} = -\frac{1}{M_{22}}\begin{bmatrix} -M_{11}M_{22} + M_{12}M_{21} & -M_{12} \\ M_{21} & -1 \end{bmatrix}. \tag{3.32}$$

The selection matrix $\boldsymbol{S}$ is given as,

$$\boldsymbol{S} = \begin{bmatrix} 1 & 0 \\ 0 & 0 \end{bmatrix}. \tag{3.33}$$

The force reference vector in the motor space $\boldsymbol{F}_{\mathrm{m}}^{\mathrm{ref}}$ is given as,

$$\boldsymbol{F}_{\mathrm{m}}^{\mathrm{ref}} = \boldsymbol{J}_{\mathrm{t}}{}^{-1}\boldsymbol{F}_{\mathrm{t}}^{\mathrm{ref}}. \tag{3.34}$$

3.4 Motion reproduction system

A method to preserve and reproduce human motions as haptic information is the motion reproduction system. Procedures of the motion reproduction system can be divided into a motion saving system and a motion loading system.

3.4.1 Motion saving system

The motion saving system preserves human motions as haptic information through bilateral teleoperation. Master-slave systems implementing the acceleration based four-channel bilateral control are used to the motion saving system. In bilateral teleoperation, haptic information is obtained by the master and the slave and transmitted bidirectionaly. In parallel with the bilateral teleoperation, the haptic information obtained by the slave is saved in haptic data storage. In an ideal situation of the acceleration based bilateral control, the haptic information obtained by the master is the same with the information obtained by the slave. The block diagram of the motion saving system is shown in Fig. 3-5. The controller of the motion saving system is the same with the acceleration based bilateral control.

In this research, a FIFO (First-In First-Out) memory is used to save the haptic information. The flow of saving haptic information in the haptic data storage is shown in Fig. 3-6. In the motion saving system, the haptic information is saved in each control cycle. The saved data is loaded in order from the oldest data when the preserved motion is reproduced.

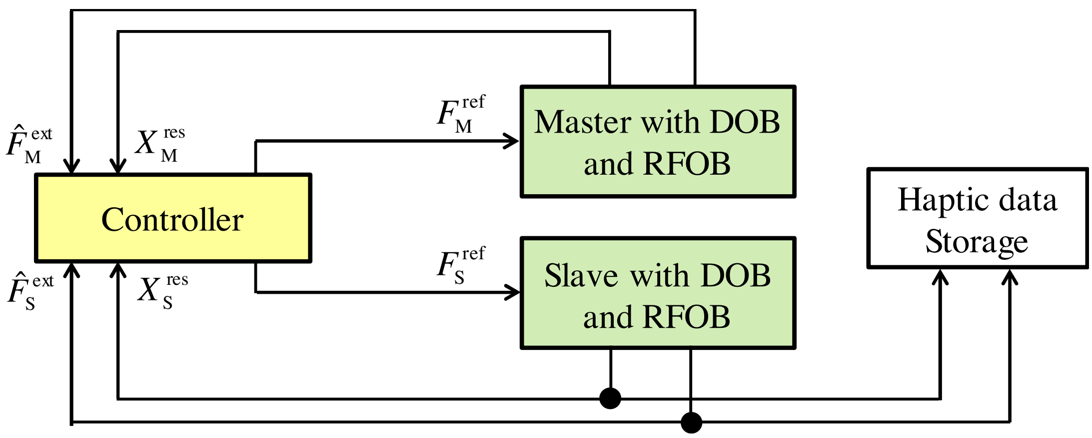

Fig. 3-5: Block diagram of the motion saving system.

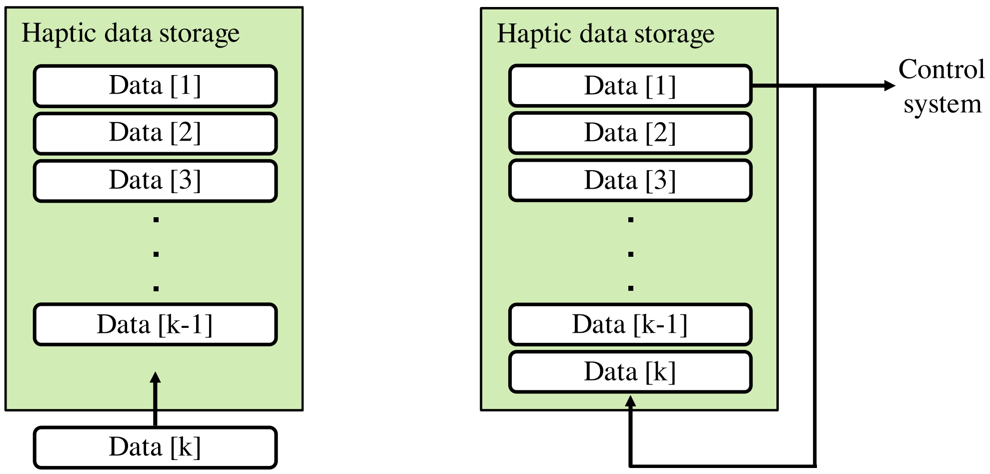

(a) Saving data

(b) Loading data

Fig. 3-6: Haptic data storage.

3.4.2 Motion loading system

The motion loading system reproduces the human motion saved in the haptic data storage. The block diagram of the motion loading system is shown in Fig. 3-7. Although the structure of the motion loading system is similar to the motion saving system, the saved haptic information is input to a controller instead of the haptic information obtained by the master. The block diagram of the controller is shown in Fig. 3-8. Control impedance of the motion loading system can be modified by adjusting gain for reproduced position C_{rp} and gain for reproduced force C_{rf}. The force reference of the slave in the motion loading

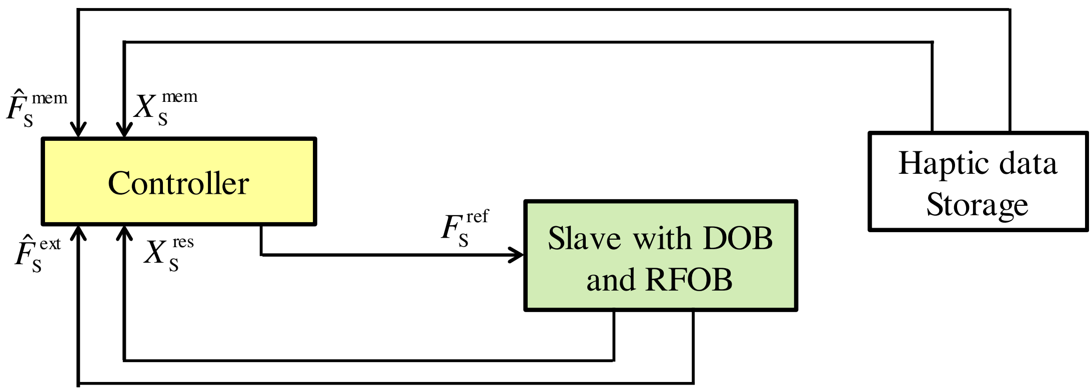

Fig. 3-7: Block diagram of the motion loading system.

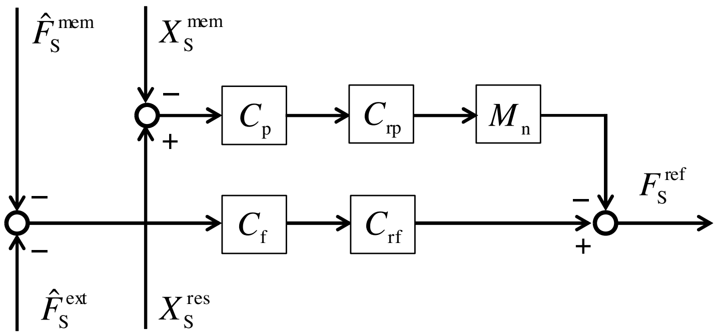

Fig. 3-8: Controller of the motion loading system.

system is given as,

$$F_S^{ref} = M_n C_p \left(X_S^{mem} - X_S^{res}\right) - C_f \left(-\hat{F}_S^{mem} + \hat{F}_S^{ext}\right). \tag{3.35}$$

X_S^{mem} and $\hat{F}_S^{mem}$ are the position information and the force information saved in the haptic data storage.

3.4.3 Compression method of haptic data

Although the motion reproduction system can be applied to multi DoF master-slave systems, size of the haptic data increases according to number of DoF, operation time, and sampling time. Therefore, the size of the haptic data is decreased by a compression method [44]. The saved haptic data is given as,

$$F_S^{mem} = K_f{}^{-1} C_{rp} K_p X_S^{res} + K_f{}^{-1} C_{rp} K_v G_{pse} X_S^{res} + C_{rf} \hat{F}_S^{ext}. \tag{3.36}$$

In the motion loading system, the force reference of the slave $F_{\mathrm{S}}^{\mathrm{ref}}$ is given as,

$$F_{\mathrm{S}}^{\mathrm{ref}} = M_{\mathrm{n}} K_{\mathrm{f}} \left(-{K_{\mathrm{f}}}^{-1} C_{\mathrm{rp}} K_{\mathrm{p}} X_{\mathrm{S}}^{\mathrm{res}} - {K_{\mathrm{f}}}^{-1} C_{\mathrm{rp}} K_{\mathrm{v}} G_{\mathrm{pse}} X_{\mathrm{S}}^{\mathrm{res}} - \left(F_{\mathrm{S}}^{\mathrm{mem}} + C_{\mathrm{rf}} \hat{F}_{\mathrm{S}}^{\mathrm{ext}} \right) \right). \qquad (3.37)$$

3.5 Summary

In this chapter, the acceleration based four-channel bilateral control, the acceleration based bilateral control using the oblique coordinate control, and the motion reproduction system were described as control systems for haptic applications The acceleration based four-channel bilateral control and the acceleration based bilateral control using the oblique coordinate control realize the transmission of clear force sensation. The motion reproduction system which has similar structure with the acceleration based bilateral control preserves and reproduces human motion as haptic information . By implementing these control systems, robotic motion utilizing haptic information can be realized.

Chapter 4

Two DoF Haptic Robot

4.1 Introduction

Structure of multi DoF robots can be divided into some modules. To improve performance of multi DoF haptic applications, performance of each module must be considered. A simple configuration of mechanical components for a module is the serial link mechanism. Actuators and links of robots are connected in series. A problem of the serial link mechanism is increase of mass and inertia which deteriorate backdrivability of the mechanism. Besides, in many cases, motion of actuators for grasping motion is converted into motion of an end-effector by some conversion mechanisms. High backdrivability and less backlash mechanism with high stiffness parts should be chosen as the conversion mechanism to obtain precise haptic information.

In this chapter, a two DoF haptic robot with the grasping motion and the translational motion as the human hand and arm motion is explained [45]. Performance of the two DoF serial link mechanism with an end-effector is validated. Structure of the two DoF haptic robot is explained in Section 4.2. Kinematics of the end-effector is described in Section 4.3. The acceleration based four-channel bilateral control and the motion reproduction system for the robot are explained in Section 4.4. Finally, experimental results to validate the performance of the two DoF haptic robot are shown in Section 4.5.

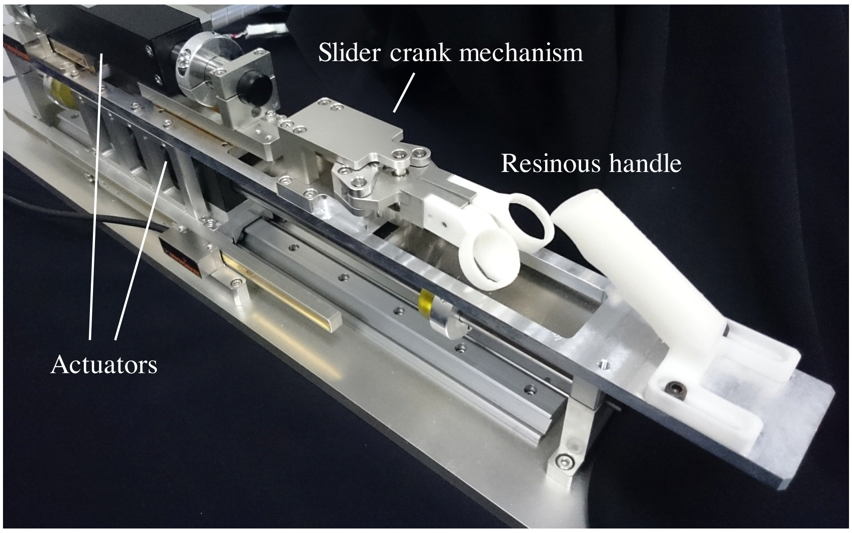

(a) The master

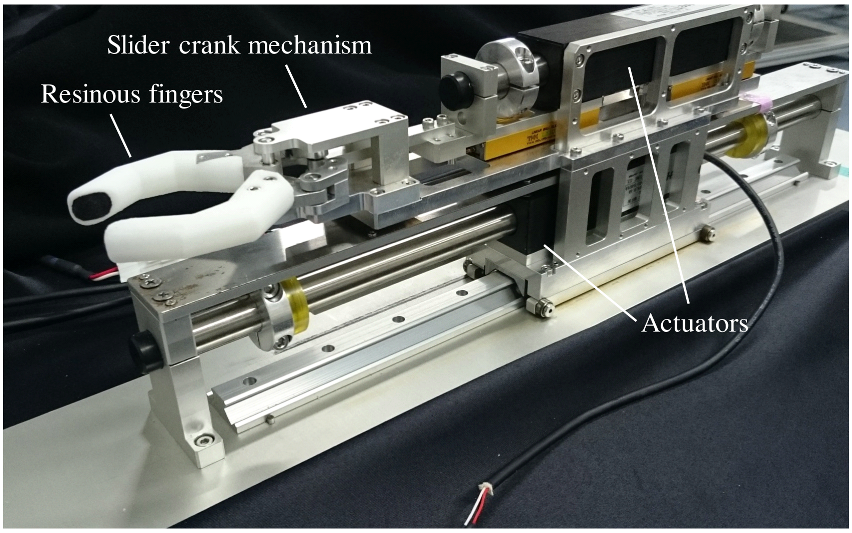

(b) The slave

Fig. 4-1: The master-slave two DoF haptic robot.

4.2 Structure

Similar structure is applied to the master and the slave of the two DoF haptic robot shown in Fig. 4-1. The serial link mechanism composed of a translational motion part and a grasping motion part is used for each robot. The translational motion part includes a linear motor which is a high backdrivability actuator. A coil moves along a shaft as a movable part of the linear motor. The grasping motion part is

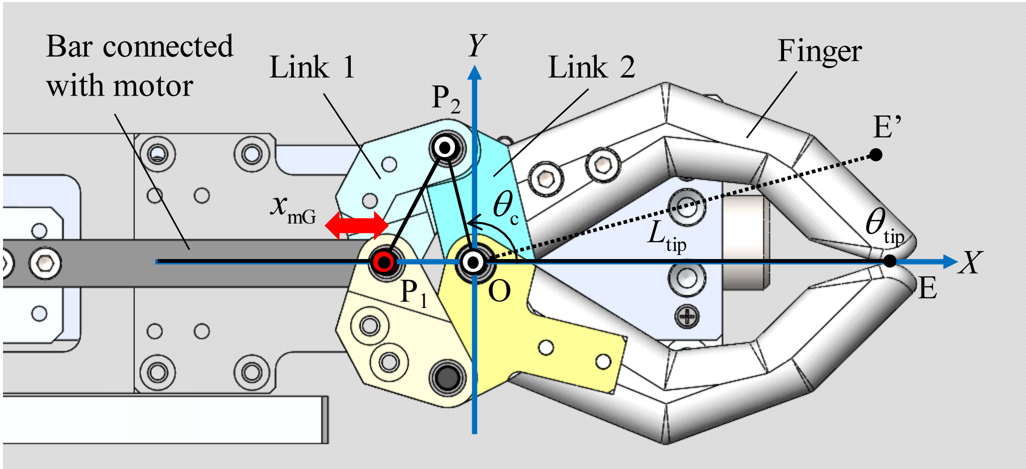

Fig. 4-2: Enlarged view of the end-effector design.

composed of a linear motor, slider crank mechanisms, and an end-effector. A shaft of the linear motor for the grasping motion moves along a shaft and transmits driving force to the slider crank mechanisms. Two sets of the slider crank mechanism convert linear motion into rotational motion of the end-effector. The grasping motion part is mounted at the movable part of the translational motion part. The same linear motor (S160Q, GMC Hillstone) is used for the grasping motion and translational motion, while stroke is different. Linear encoders (RGH24Y, Renishaw) are used to obtain position information of linear motors. Force information is estimated by RFOB. Resinous fingers made by a 3D printer are attached to the slave as the end-effector. On the other hand, the resinous handle is attached to the master. Material of the resinous parts is ABS resin.

4.3 Kinematics

An enlarged view of the end-effector with the slider crank mechanisms is shown in Fig. 4-2. Position of a rotational joint P_1 connecting the linear motor for the grasping motion and the link 1 moves according to movement of the motor x_{mG}. Position of the rotational joint O which is the center of rotation of the link 2 is fixed. The link 1 and the link 2 are connected by a rotational joint P_2. Relation between a position of the linear motor x_{mG} and a rotation angle of the end-effector θ_{tip} is given as,

$$\theta_{\mathrm{tip}} = \arccos\left(\frac{{L_1}^2 - {L_2}^2 - {x_{\mathrm{mG}}}^2}{-2L_2 x_{\mathrm{mG}}}\right) - \theta_{\mathrm{c0}}. \tag{4.1}$$

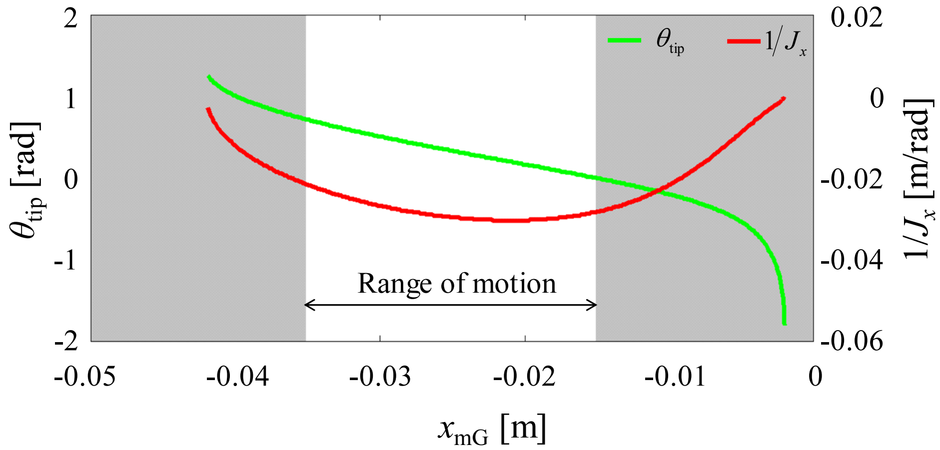

Fig. 4-3: Relation between the motor space and the joint space.

L_1 and L_2 are length of the link 1 and the link 2. $\theta_{\rm c0}$ is a constant angle made by line segments $\rm P_2O$ and OE. Relation between velocity of the linear motor $\dot{x}_{\rm mG}$ and angular velocity of the end-effector $\dot{\theta}_{\rm tip}$ is given as,

$$\dot{\theta}_{\rm tip} = J_x \dot{x}_{\rm mG}, \tag{4.2}$$

$$J_x = \frac{{x_{\rm mG}}^2 + {L_1}^2 - {L_2}^2}{x_{\rm mG}\sqrt{4{L_2}^2{x_{\rm mG}}^2 - \left({L_1}^2 - {L_2}^2 - {x_{\rm mG}}^2\right)^2}}. \tag{4.3}$$

The resinous finger is attached to the link 2. The end-effector is a double opening gripper. Therefore, an opening angle $\theta_{\rm jG}$ and output torque $\tau_{\rm jG}$ in the joint space are given as,

$$\theta_{\rm jG} = 2\theta_{\rm tip}, \tag{4.4}$$

$$\tau_{\rm jG} = \frac{1}{2J_x} f_{\rm mG}. \tag{4.5}$$

Width of the end-effector with the slider crank mechanisms must be considered to imitate human hand size and structure. The Y coordinate of $\rm P_2$ is given as,

$$y_{\rm P2} = L_2 \cos\theta_{\rm c}. \tag{4.6}$$

The doubled value of $y_{\rm P2}$ is the width of the end-effector with the slider crank mechanisms.

Dimension of the two DoF haptic robot is shown in Table 4.1. The relation between variables in the motor space and the joint space is shown in Fig. 4-3. Range of the grasping motion in the motor space is from -0.0351 m to -0.0151 m. There is no singular point in the range of the grasping motion.

Table 4.1: Dimension of the two DoF haptic robot

Descriptions	Values
Length of link 1 L_1	0.022 m
Length of link 2 L_2	0.020 m
Length of end-effector L_{tip}	0.070 m
Constant angle θ_{c0}	1.81 rad
Maximum opening angle θ_{jG}	1.432 rad

The first order approximation of a function $f(x)$ at x_0 by Taylor expansion is given as,

$$f(x) = f(x_0) + \frac{\mathrm{d}f(x_0)}{\mathrm{d}t}(x - x_0) + R. \tag{4.7}$$

R is a reminder term. From eq. (4.1), eq. (4.3), and eq. (4.7), the first order approximation of the relation between the position of the grasping motion in the motor space x_{mG} and the rotation angle of the end-effector θ_{tip} at x_{mG0} is given as,

$$\theta_{\mathrm{tip}}^{\mathrm{app}} = \theta_{\mathrm{tip}}(x_{\mathrm{mG0}}) + J_x(x_{\mathrm{mG0}})(x_{\mathrm{mG}} - x_{\mathrm{mG0}}). \tag{4.8}$$

By ignoring the first term in the right side $\theta_{\mathrm{tip}}(x_{\mathrm{mG0}})$, an approximated angle in the joint space $\theta_{\mathrm{jG}}^{\mathrm{app}}$ is give as,

$$\theta_{\mathrm{jG}}^{\mathrm{app}} = a(x_{\mathrm{mG}} - x_{\mathrm{mG0}}), \tag{4.9}$$

$$a = 2J_x(x_{\mathrm{mG0}}). \tag{4.10}$$

For the relation of force, an averaged value $\overline{J}_x$ is used as the approximation. The approximated torque in the joint space is given as,

$$\tau_{\mathrm{jG}}^{\mathrm{app}} = bf_{\mathrm{mG}}, \tag{4.11}$$

$$b = \frac{1}{2\overline{J}_x}. \tag{4.12}$$

Therefore, the relation between the motor space and the joint space can be expressed by a proportion by approximating the kinematics. The control system of the two DoF haptic robot can be simplified.

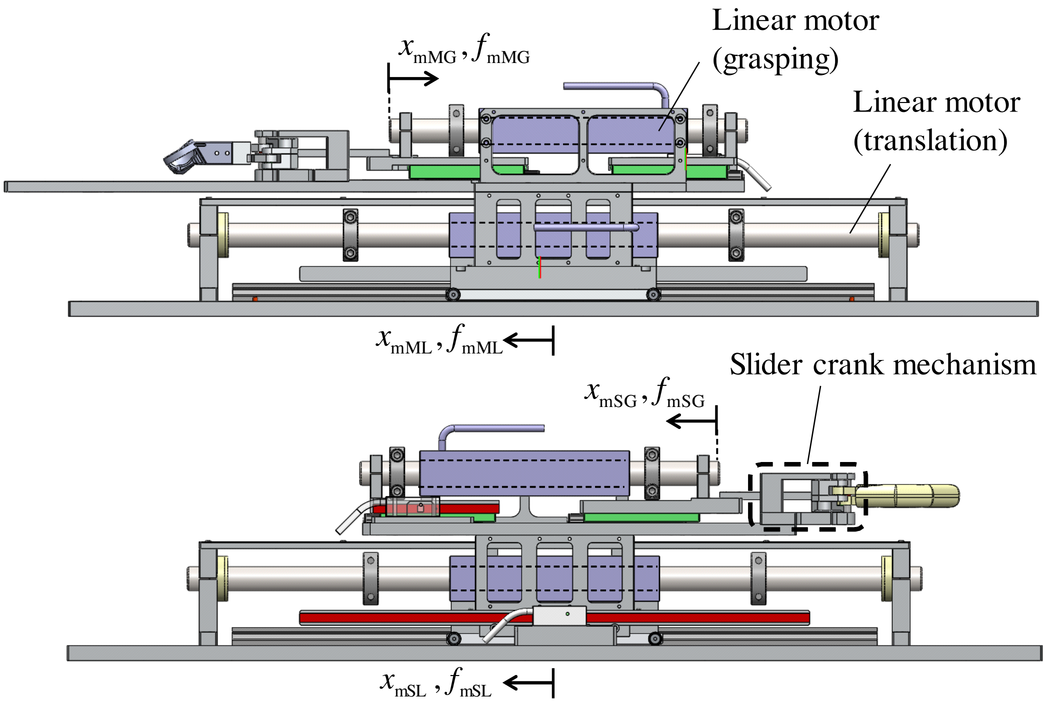

Fig. 4-4: Side view of the two DoF haptic robot.

4.4 Control system

4.4.1 Coordinate definition

A definition of the coordinate is shown in Fig. 4-4. A Laplace transformed position vector $\boldsymbol{X}_{\mathrm{m}}$ and a Laplace transformed force vector $\boldsymbol{F}_{\mathrm{m}}$ in the motor space are given as,

$$\boldsymbol{X}_{\mathrm{m}} = \begin{bmatrix} X_{\mathrm{mL}} & X_{\mathrm{mG}} \end{bmatrix}^{\mathrm{T}}, \tag{4.13}$$

$$\boldsymbol{F}_{\mathrm{m}} = \begin{bmatrix} X_{\mathrm{mL}} & X_{\mathrm{mG}} \end{bmatrix}^{\mathrm{T}}. \tag{4.14}$$

Although the similar structure is applied to the master and the slave, the definition of the coordinate for the grasping motion is different. The end-effector of the master is attached at the other side of the end-effector of the slave, while the positive direction of the translational motion is identical. Hence, the positive direction of the grasping motion at the master side is opposite from the positive direction at the slave side.

The block diagram of the linear motors with DOB and RFOB is shown in Fig. 4-5. Due to the high backdrivability mechanisms and the arrangement of the motors, inertial force generated by the

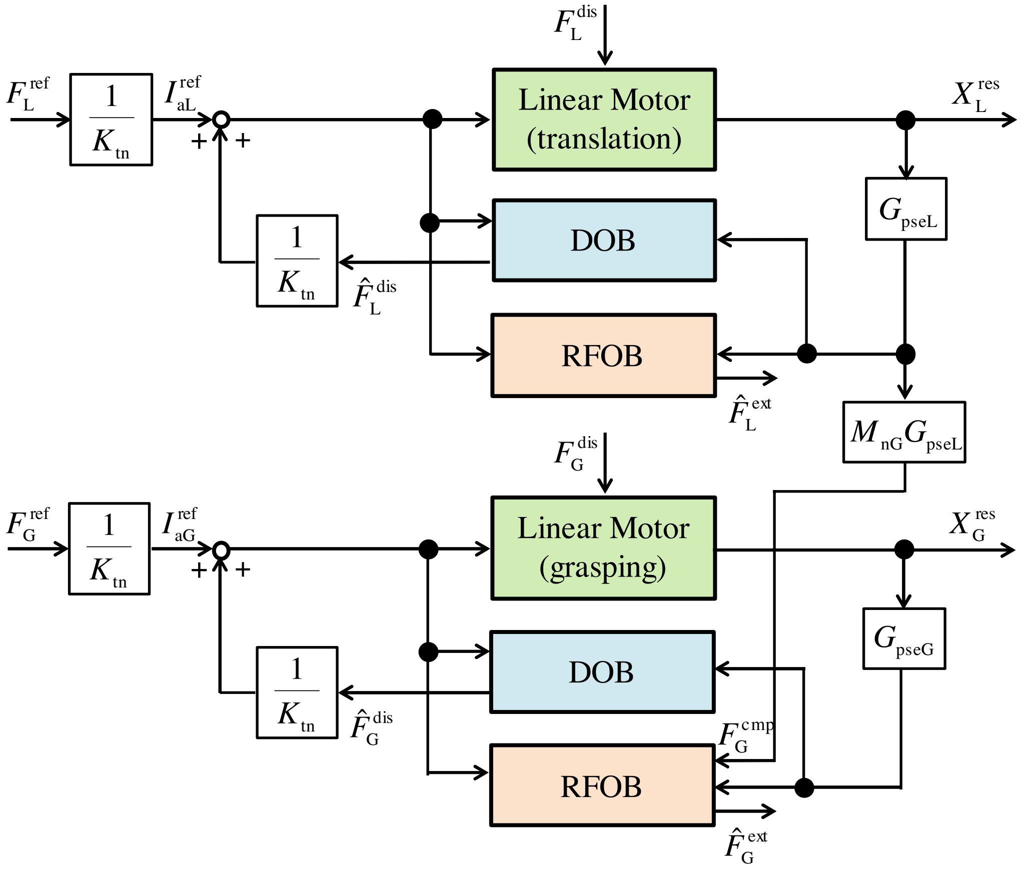

Fig. 4-5: Block diagram of motors with DOB and RFOB and inertial force compensation.

translational motion is applied to the linear motor for the grasping motion as the internal force $F^{\rm int}$. The inertial force generated by the translational motion can be calculated by the mass $M_{\rm G}$ and the acceleration $s^2X_{\rm L}$. The estimated internal force $\hat{F}^{\rm int}$ is given as,

$$\hat{F}^{\rm int} = M_{\rm nG}{G_{\rm pseL}}^2 X_{\rm L}^{\rm res}. \tag{4.15}$$

By compensating the internal force $\hat{F}^{\rm int}$, the accuracy of RFOB is improved.

4.4.2 Bilateral control and motion reproduction system

Control targets of the acceleration based bilateral control in the joint space are given as,

$$\boldsymbol{X}_{\rm jM} - \boldsymbol{X}_{\rm jS} = \boldsymbol{0}, \tag{4.16}$$

$$\boldsymbol{F}_{\rm jM} + \boldsymbol{F}_{\rm jS} = \boldsymbol{0}. \tag{4.17}$$

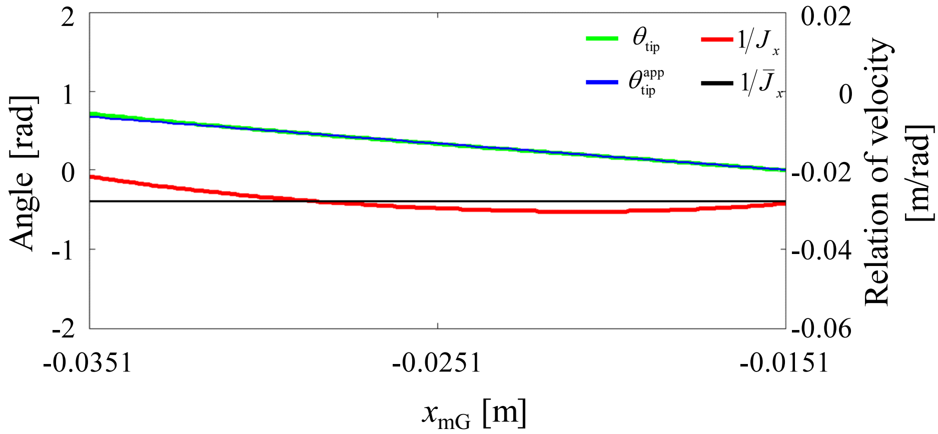

Fig. 4-6: Approximation of kinematics.

A position vector $\boldsymbol{X}_{\mathrm{j}}$ and a force vector $\boldsymbol{F}_{\mathrm{j}}$ in the joint space are given as,

$$\boldsymbol{X}_{\mathrm{j}} = \begin{bmatrix} \Theta_{\mathrm{jG}} & X_{\mathrm{jL}} \end{bmatrix}^{\mathrm{T}}, \tag{4.18}$$

$$\boldsymbol{F}_{\mathrm{j}} = \begin{bmatrix} T_{\mathrm{jG}} & F_{\mathrm{jL}} \end{bmatrix}^{\mathrm{T}}. \tag{4.19}$$

Θ and T are a Laplace transformed angle θ and torque τ. To control the variables of the grasping motion in the joint space precisely, the absolute position information is necessary. On the other hand, approximated values in the joint space are given as,

$$\Theta_{\mathrm{jMG}} \approx a_{\mathrm{M}} X_{\mathrm{mMG}}, \tag{4.20}$$

$$\Theta_{\mathrm{jSG}} \approx a_{\mathrm{S}} X_{\mathrm{mSG}}, \tag{4.21}$$

$$T_{\mathrm{jMG}} \approx b_{\mathrm{M}} F_{\mathrm{mMG}}, \tag{4.22}$$

$$T_{\mathrm{jSG}} \approx b_{\mathrm{S}} F_{\mathrm{mSG}}. \tag{4.23}$$

Hence, the control targets of the grasping motion are expressed as,

$$X_{\mathrm{mMG}} - \alpha X_{\mathrm{mSG}} = 0, \tag{4.24}$$

$$F_{\mathrm{mMG}} + \beta F_{\mathrm{mSG}} = 0, \tag{4.25}$$

$$\alpha = \frac{a_{\mathrm{S}}}{a_{\mathrm{M}}}, \tag{4.26}$$

$$\beta = \frac{b_{\mathrm{S}}}{b_{\mathrm{M}}}. \tag{4.27}$$

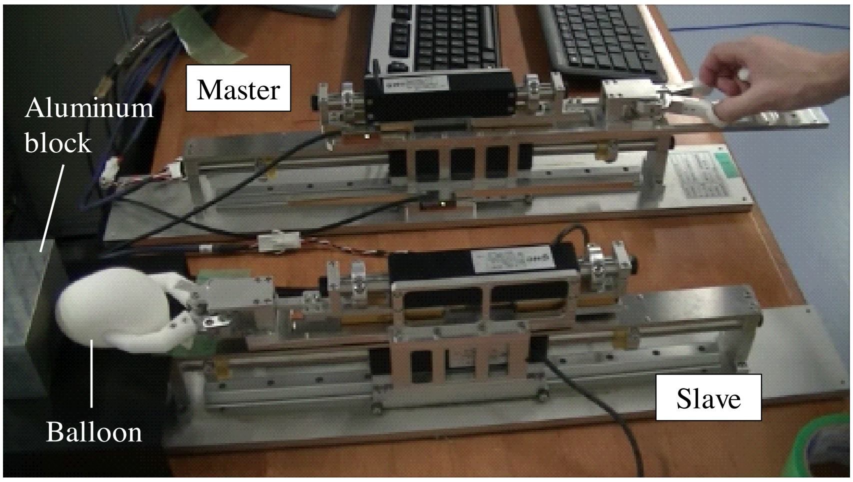

Fig. 4-7: Experimental setup of the two DoF haptic robot.

From eq. (4.24) and eq. (4.25), the control system is regarded as the scaling bilateral control constructed in the motor space. Besides, the position information in eq. (4.24) is the relative values. Since the master and the slave have the identical slider crank mechanisms, the control targets are given as,

$$\boldsymbol{X}_{\mathrm{mM}} - \boldsymbol{X}_{\mathrm{mS}} = \mathbf{0}, \tag{4.28}$$

$$\boldsymbol{F}_{\mathrm{mM}} + \boldsymbol{F}_{\mathrm{mS}} = \mathbf{0}. \tag{4.29}$$

By designing the link length properly and approximating the kinematics, the control system can be simplified. The grasping motion and the translational motion of the two DoF haptic robot are controlled in the motor space.

4.5 Experiments

The performance of the two DoF haptic robot was confirmed by experiments. The experimental setup and parameters are shown in Fig. 4-7 and Table 4.2.

4.5.1 Transmission of force sensation

The contact motion was carried out to validate the performance to transmit force sensation. A balloon and a plastic board were used as a soft object and a hard object. The acceleration based bilateral control explained in Section 3.2 was implemented to the master-slave system. Procedures of the experiment were as follows:

Table 4.2: Parameters of the two DoF haptic robot

Parameter s	Grasping	Translation
M_{n}	0.4 kg	1.8 kg
K_{tn}	33 N/A	33 N/A
K_{p}	1600.0 /s^2	2500.0 ^{2}
K_{v}	80.0 /s	100.0 /s
K_{f}	1.0	0.8
g_{dis}	300.0 rad/s	300.0 rad/s
g_{rfob}	300.0 rad/s	300.0 rad/s
g_{pse}	600.0 rad/s	600.0 rad/s
C_{rp}	$\sqrt{2}\cos\frac{1}{12}\pi$	$\sqrt{2}\cos\frac{1}{4}\pi$
C_{rf}	$\sqrt{2}\sin\frac{5}{12}\pi$	$\sqrt{2}\sin\frac{1}{4}\pi$

1) In the initial condition, the gripper was opened.

2) The soft object was held by the gripper. The grasping force was increased and decreased three times.

3) The robot was moved forward. The object was pushed on three times to the aluminum block.

4) The procedures (1) - (3) were conducted for the hard object.

The experimental results are shown in Fig. 4-8. Position responses in Fig. 4-8(a) and (c) were the relative value. When the gripper was fully closed, the position response of the grasping motion was 0 m. The object was held by the gripper for about 10 seconds. The grasping force was changed actively in blue shaded areas. Gray shaded areas denote the contact motion conducted by the translational motion. Regardless of the contacted object, the position of the slave followed the position of the master in both the grasping motion and the translational motion. Besides, Newton's third law was realized between the master and the slave. The control targets of the acceleration based bilateral control to transmit the precise haptic information were achieved. From Fig. 4-8(a) and (b), the magnitude of the reaction force from the soft object was increased according to the change of the position. On the other hand, the position was changed slightly when the action force to the hard object was increased. The manipulating force of the grasping motion and the translational motion was small and ignorable.

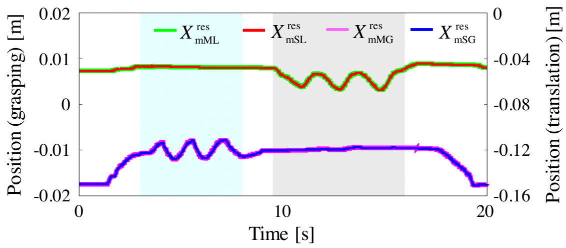

(a) Position response (soft environment)

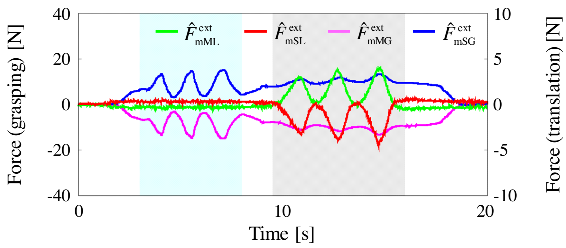

(b) Force response (soft environment)

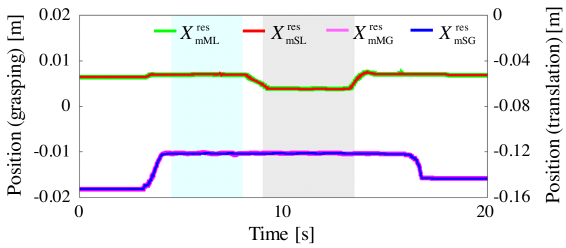

(c) Position response (hard environment)

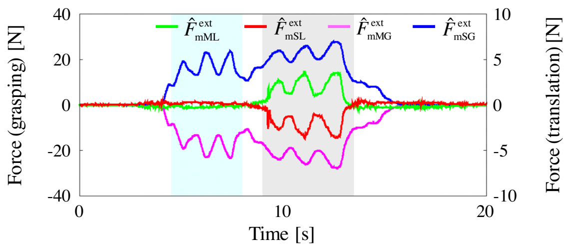

(d) Force response (hard environment)

Fig. 4-8: Experimental results of contact motion.

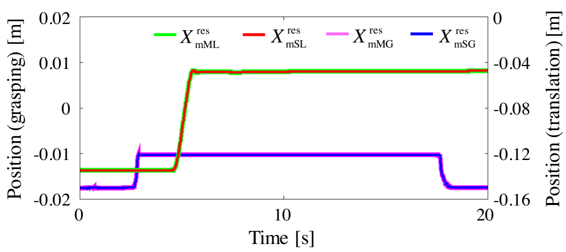

(a) Position response

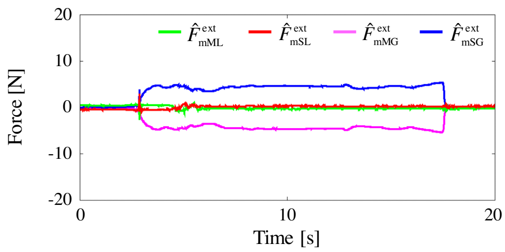

(b) Force response

Fig. 4-9: Experimental results of the motion saving system.

4.5.2 Reproduction of motion

The human motion was reproduced at the original speed and a high speed to confirm the influence of the internal force. The motion reproduction system explained in Section 3.4 was implemented to the robot. Hybrid angles were used to adjust the ratio of the position control and the force control in the motion loading system [18]. To adapt the size variation of contacted objects, the hybrid angle for the grasping motion was set at a large value. Procedures of the experiment was as follows:

1) In the initial condition, the gripper was opened.

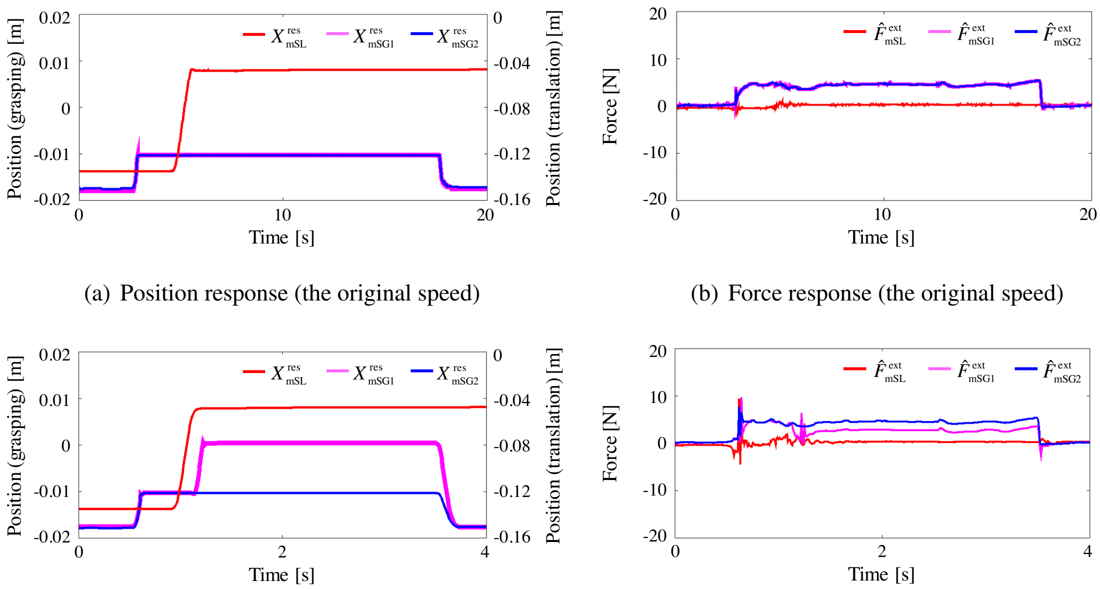

(a) Position response (the original speed)

(b) Force response (the original speed)

(c) Position response (the five times speed)

(d) Force response (the five times speed)

Fig. 4-10: Experimental results of the motion loading system.

2) The object was held by the gripper. Then, the robot was moved backward.

3) The object was held by the gripper for few seconds, while the position of the gripper was not moved. Then, the gripper was opened to put down the object.

4) The motion loading system with the inertial force compensation was implemented. The motion in procedures (1) - (3) was reproduced at the original speed and the five times speed.

5) The motion loading system without the inertial force compensation was implemented. The motion in procedures (1) - (3) was reproduced at the original speed and the five times speed.

In the motion saving system, the force information was estimated by RFOB with the inertial force compensation. The plastic board was used as the contacted object.

The experimental results of the saved motion is shown in Fig. 4-9. The control targets of the acceleration based bilateral control was realized. The object was held by the gripper from about 3 seconds after the start to about 18 seconds. The gripper was moved backward at about 5 seconds after the start. While the object was held by the gripper, the grasping force in the saved motion shown in Fig. 4-9(b) was almost constant.

The experimental results of the reproduced motion are shown in Fig. 4-10. Subscripts 1 and 2 denote the motion loading system without the compensation of the inertial force and with the compensation. In the reproduction at the original speed, the saved motion was reproduced regardless of the compensation. The influence of the internal force was ignorable at the original speed. On the other hand, the motion loading system without the compensation failed to conduct tasks at the five times speed. The large inertial force was generated by the rapid translational motion. The gripper was opened by the large inertial force and dropped the object.

4.6 Summary

In this chapter, the two DoF haptic robot for the grasping motion and the translational motion was described. The serial link mechanism composed of high backdrivability and less backlash mechanisms with high stiffness mechanical parts was applied to the robot. The kinematics of the slider crank mechanism used for the end-effector was approximated to simplify the control system. The design of the slider crank mechanisms were decided to decrease the approximation error. The acceleration based four-channel bilateral control and the motion reproduction system constructed in the motor space were implemented to validate the performance of the two DoF haptic robot. As the result of the experiments, the force sensation was transmitted by the two DoF serial link robot. In the reproduction phase, the saved motion was reproduced precisely at the original speed regardless of the compensation of the internal force caused by the serial link mechanism.

Chapter 5

Flexible Haptic Forceps Robot

5.1 Introduction

The flexible endoscopic robot is a master-slave system to support surgeons in minimally invasive surgery. A schematic view of the flexible endoscopic robot is shown in Fig. 5-1. A tip of the slave inserted into a body of patients is composed of a flexible endoscope, some flexible multi DoF forceps, and a flexible outer tube as passages of the endoscope and the forceps. Surgeons teleoperate the slave by manipulating the master placed at a console. A target of the flexible endoscopic robot is the Natural Orifice Transluminal Endoscopic Surgery (NOTES). In the NOTES, a tip of the robot is inserted into a natural orifice of patients such as a mouth and an anus and reaches affected parts. By using the natural orifices instead of incisions, burden to patients can be reduced. Therefore, the tip part of the robot must be flexible and thin adequately. Besides, force sensation is necessary for safer operation, since excessive grasping force injures tissues and organs.

In specific situations such as the NOTES, mechanisms which can be applied to robots are limited. Size of the robot is limited, since the flexible endoscopic robot passes through narrow space. It is difficult to mount actuators and sensors for multi DoF motion at the tip part of the slave. Although driving force can be transmitted from the outside of the body, flexible structure of the robot deteriorates the performance to transmit haptic information. Motion of the robot depends on the posture of the flexible part.

In this chapter, an one DoF miniature haptic forceps robot is developed to realize the grasping motion with force sensation as the end-effector of the flexible endoscopic robot [46]. A high reduction ratio mechanism is implemented to the miniature haptic forceps robot to increase grasping force. Performance

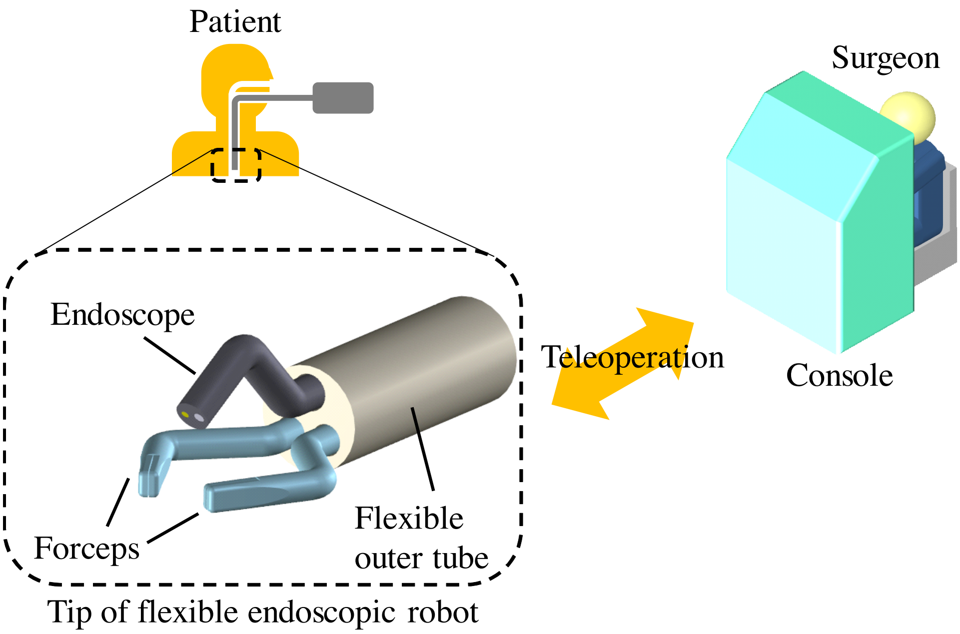

Fig. 5-1: Schematic view of flexible endoscopic robot.

of the robot with mechanical components which deteriorate the backdrivability is validated. First, a master-slave flexible haptic forceps robot is described in Section 5.2. Second, a control system for the robot is explained in Section 5.3. Finally, experiments are described in Section 5.4.

5.2 Flexible haptic forceps robot

The one DoF flexible haptic forceps robot is a master-slave system to realize the grasping motion with force sensation for flexible endoscopic robots. The miniature haptic forceps robot is used as the slave of the flexible haptic forceps robot. Due to contact time with objects, magnitude of applied force, and frequency in use, implementation of the haptic technology to the grasping motion of multi DoF flexible forceps robots is the most highest priority. By arranging electrical components for the grasping motion at the tip of the flexible part, the grasping motion of the forceps not depending upon the posture of the flexible part can be realized, while suppressing the increase of the size. To manipulate the slave, a simple one DoF robot with a handle is developed as the master.

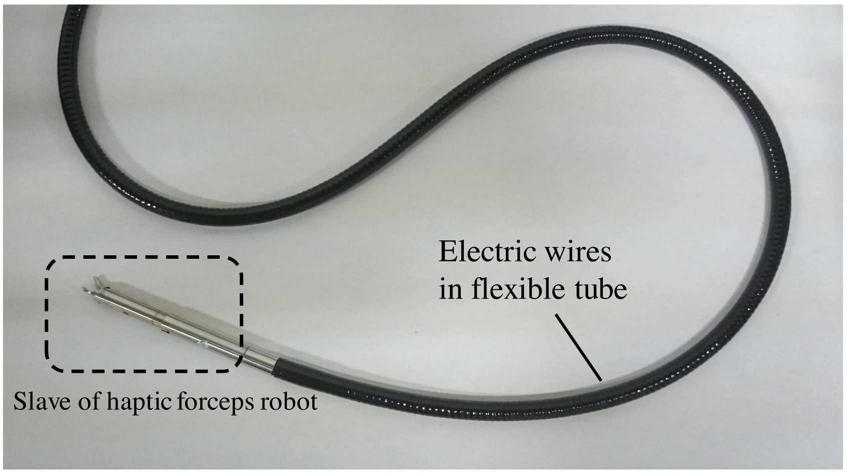

Fig. 5-2: The miniature haptic forceps robot mounted at flexible tube with electric wires.

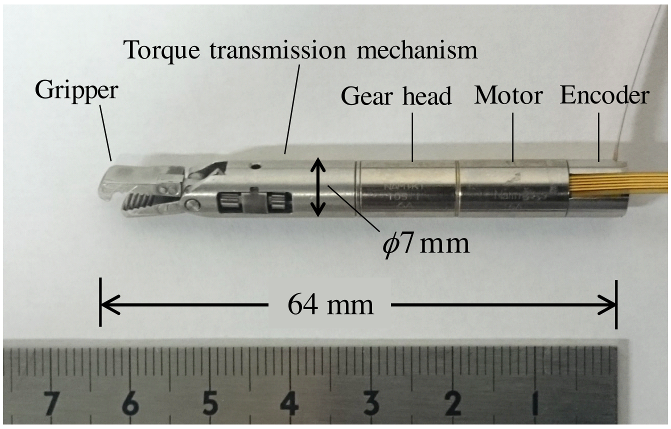

Fig. 5-3: Dimension of the miniature haptic forceps robot.

5.2.1 Miniature haptic forceps robot

The slave of the flexible haptic forceps robot is shown in Fig. 5-2. The miniature haptic forceps robot is mounted at the tip of a flexible tube. The input to a motor and signals of a encoder are transmitted by electric wires in the flexible tube. A prototype of the miniature haptic forceps robot is shown in Fig. 5-3. Specifications of the miniature haptic forceps robot is shown in Table 5.1. The miniature haptic forceps robot can be divided into a driving unit and a tip part.

Table 5.1: Specifications of the miniature haptic forceps robot

Descriptions	Values
Diameter of the slave	7 mm
Mass of the robot	12 g
Range of motion (double opening)	90 degrees
Reduction ratio of mechanism G_{fmech}	4.0

Table 5.2: Specifications of the driving unit

Descriptions	Values
Torque coefficient of rotary motor K_{tnS}	2.03 mNm/A
Rated torque of rotary motor	0.49 mNm
Reduction ratio of gear head G_{h}	105
Efficiency of gear head e_{fh}	0.61
Resolution of rotary encoder	256 P/R

Driving unit

The driving unit of the miniature haptic forceps robot is composed of a planetary geared brushless DC rotary motor and an incremental optical rotary encoder. Both the geared motor and the encoder are made by Namiki Precision Jewel Co., Ltd. Specifications of the driving unit is shown in Table 5.2. The diameter of all components is 7 mm.

Tip part

The tip part of the slave is composed of a gripper with two jaws and a torque transmission mechanism. The shape of the gripper depends on the purpose of tasks using the flexible endoscopic robot. Hence, the tip part can be changed to various types of grippers. The developed grippers are shown in Fig. 5-4. The maximum opening angle of a double opening forceps is about 90 degrees. In this chapter, the double opening forceps shown in Fig. 5-3 is explained.

The rotation axis of the geared motor is orthogonal to the rotation axis of the gripper. The torque generated by the geared motor is transmitted by the torque transmission mechanism composed of pinion gears and face gears. Each jaw of the gripper is connected with a face gear. Therefore, rotational motion of the face gears becomes opening and closing motion of the gripper. The diameter of the torque

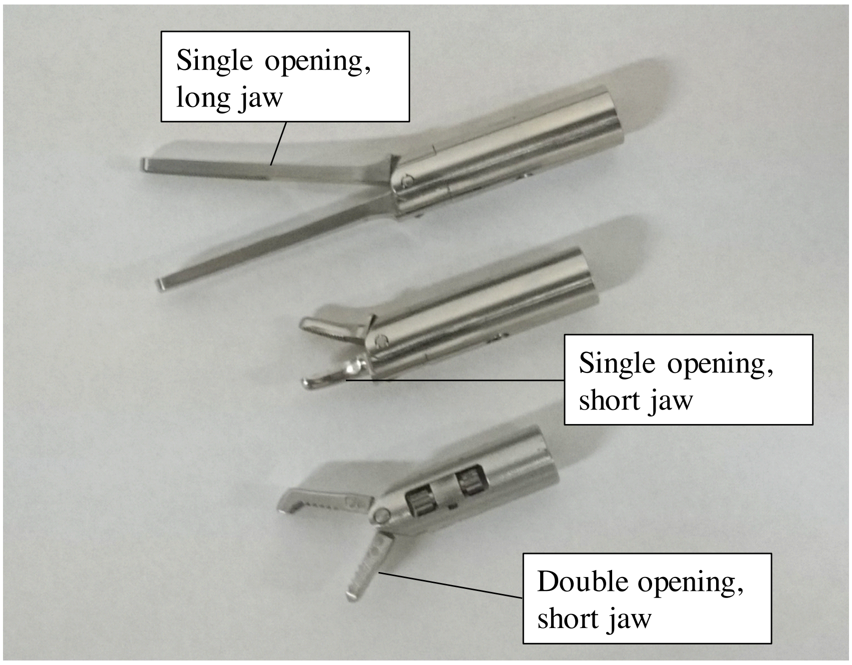

Fig. 5-4: Various types of grippers for the miniature haptic forceps robot.

transmission mechanism is 7 mm.

5.2.2 Master of flexible haptic forceps robot

The master of the flexible haptic forceps robot is shown in Fig. 5-5. A linear motor (S160Q, GMC Hillstone) and an optical linear encoder (RGH24Y, Renishaw) are used for the master. The rated force and the rated current of the linear motor are 20 N and 0.62 A. The resolution of the linear encoder is 0.1 μm. A handle is attached to the tip of the linear motor as an end-effector. Therefore, the grasping force of the human operator is directly transmitted to the linear motor.

5.3 Control system

The acceleration based four-channel bilateral control using the oblique coordinate control described in Section 3.3 is applied to the flexible haptic forceps robot. The robot is controlled in the joint space.

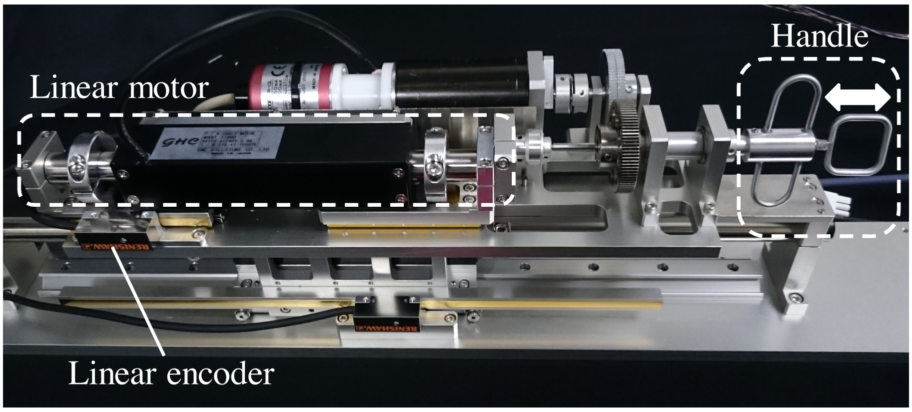

Fig. 5-5: The master of the flexible haptic forceps robot.

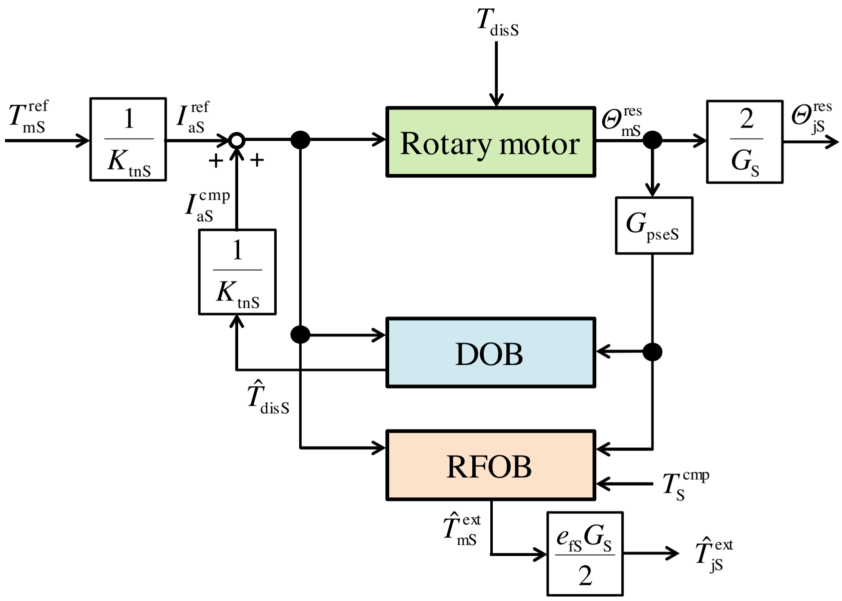

Fig. 5-6: Block diagram of the slave with DOB and RFOB.

5.3.1 Joint space of slave

The planetary gear head with high reduction ratio is implemented to the rotary motor of the slave to increase the output torque. Relation between a rotation angle of the motor θ_{mS} and the rotary shaft of the gear head θ_{gS} is given as,

$$\theta_{\mathrm{gS}} = \frac{1}{G_{\mathrm{h}}}\theta_{\mathrm{mS}}. \tag{5.1}$$

$G_{\rm h}$ is the reduction ratio of the planetary gear head. Although the output torque of the motor $\tau_{\rm mS}$ is increased by the gear head, the efficiency of the torque transmission is decreased by friction force between gears and shafts. Hence, relation between the motor torque $\tau_{\rm mS}$ and the output torque of the gear head $\tau_{\rm gS}$ is given as,

$$\tau_{\rm gS} = e_{\rm fh} G_{\rm h} \tau_{\rm mS}. \tag{5.2}$$

$e_{\rm fh}$ is the torque transmission efficiency of the gear head. In the same manner, relation between variables of the output axis of the gear head and the rotation axis of the double opening gripper is given as,

$$\theta_{\rm jS} = \frac{2}{G_{\rm mech}} \theta_{\rm gS}, \tag{5.3}$$

$$\tau_{\rm jS} = \frac{1}{2} e_{\rm fmech} G_{\rm mech} \tau_{\rm gS}. \tag{5.4}$$

$\theta_{\rm jS}$ and $\tau_{\rm jS}$ are the opening angle and the output torque of the gripper in the joint space, respectively. $G_{\rm mech}$ and $e_{\rm fmech}$ are the reduction ratio and the efficiency of the torque transmission mechanism, respectively. The reduction ratio $G_{\rm S}$ and the efficiency $e_{\rm fS}$ of the slave are defined as,

$$G_{\rm S} = G_{\rm h} G_{\rm mech}, \tag{5.5}$$

$$e_{\rm fS} = e_{\rm fh} e_{\rm fmech}. \tag{5.6}$$

Therefore, relation between the motor space and the joint space is given as,

$$\theta_{\rm jS} = \frac{2}{G_{\rm S}} \theta_{\rm mS}, \tag{5.7}$$

$$\tau_{\rm jS} = \frac{1}{2} e_{\rm fS} G_{\rm S} \tau_{\rm mS}. \tag{5.8}$$

The block diagram of the slave with the double opening gripper is shown in Fig. 5-6. The output torque estimated by RFOB $\hat{T}^{\rm ext}_{\rm mS}$ is corrected by the efficiency of the mechanical components to transmit driving torque.

5.3.2 Efficiency of torque transmission mechanism

The efficiency of the torque transmission mechanism $e_{\rm fmech}$ can be obtained by the driving torque of the motor $\tau_{\rm aS}$ and the torque measured by a force sensor $\tau^{\rm sen}_{\rm S}$. The torque information can be obtained by dividing force information obtained by the force sensor by the radius. When the force sensor contact

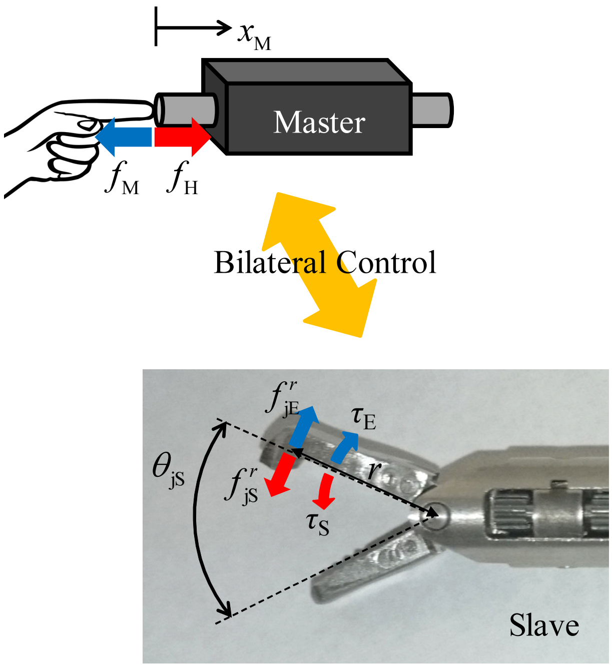

Fig. 5-7: Bilateral control system for the flexible haptic forceps robot.

with a jaw of the gripper, the output torque of the gripper is regarded as the same as one of a single opening gripper. Hence, the efficiency of the torque transmission mechanism e_{fmech} is given as,

$$e_{\mathrm{fmech}} = \frac{\tau_{\mathrm{S}}^{\mathrm{sen}}}{G_{\mathrm{S}} e_{\mathrm{fh}} \tau_{\mathrm{aS}}}. \tag{5.9}$$

The driving torque τ_{aS} is calculated by the constant current input to the rotary motor and the torque coefficient K_{tn}.

5.3.3 Bilateral control

The composition of the master-slave system is shown in Fig. 5-7. To construct the acceleration based four-channel bilateral control for the flexible haptic forceps robot, the rotation angle θ_{jS} and the output torque τ_{jS} of the slave are converted into position information and force information. The position of a point on a contact surface of the gripper x^r_{S} is given as,

$$x^r_{\mathrm{jS}} = r\theta_{\mathrm{jS}}. \tag{5.10}$$

r is the distance from the rotation axis of the jaw and the point on the contact surface. The force along a tangential direction of the contact surface f^r_{S} is given as,

$$f^r_{\mathrm{jS}} = \frac{\tau_{\mathrm{jS}}}{r}. \tag{5.11}$$

The position of the point on the contact surface with scaling αx^r_{jS} follows the position of the master x_{jM}. Newton's third law is realized between the force along a tangential direction of the contact surface with scaling βf^r_{jS} and the force of the master f_{jM}. The variables of the master in the joint space is the same with the variables in the motor space. Therefore, the control targets of the acceleration based bilateral control for the flexible haptic forceps robot are given as,

$$x_{\mathrm{jM}} - \alpha x^r_{\mathrm{jS}} = 0, \tag{5.12}$$

$$f_{\mathrm{jM}} + \beta f^r_{\mathrm{jS}} = 0. \tag{5.13}$$

These control targets can be expressed as,

$$\begin{aligned} x_{\mathrm{jM}} - \alpha x^r_{\mathrm{jS}} &= x_{\mathrm{jM}} - \alpha r \frac{2}{G_{\mathrm{mech}}} \frac{1}{G_{\mathrm{h}}} \theta_{\mathrm{mS}} \\ &= x_{\mathrm{jM}} - \alpha_{\mathrm{m}} \theta_{\mathrm{mS}}, \end{aligned} \tag{5.14}$$

$$\begin{aligned} f_{\mathrm{jM}} + \beta f^r_{\mathrm{jS}} &= f_{\mathrm{jM}} + \beta \frac{1}{r} \frac{1}{2} e_{\mathrm{fS}} G_{\mathrm{S}} \tau_{\mathrm{mS}} \\ &= f_{\mathrm{jM}} + \beta_{\mathrm{m}} \tau_{\mathrm{mS}}. \end{aligned} \tag{5.15}$$

Therefore, the control system of the flexible haptic forceps robot can be expressed by the scaling bilateral control in the motor space.

5.4 Experiments

To construct the bilateral control system, the efficiency of the torque transmission mechanism was decided by a preliminary experiment. Then, the bilateral teleoperation was conducted by the flexible haptic forceps robot.

5.4.1 Efficiency of torque transmission mechanism

The efficiency of the torque transmission mechanism was decided by a preliminary experiment. The constant current I_{a} was input to the rotary motor of the miniature haptic forceps robot. The output force of the jaw was measured by a force sensor (LUR-A-200NSA1, Kyowa Electronic Instruments) and a

Table 5.3: Relation between constant current and output force

Contents	Constant current				
	0.04 A	0.12 A	0.20 A	0.28 A	0.36 A
Average of measured grasping force	0.36 N	1.62 N	2.27 N	3.50 N	4.77 N
Calculated grasping force	0 N	6.82 N	13.64 N	20.46 N	27.28 N
Efficiency e_{S}	–	0.238	0.166	0.171	0.175
Efficiency e_{fmech}	–	0.390	0.272	0.281	0.287

strain amplifier (DPM-711B M10, Kyowa Electronic Instruments). An analog value of the force sensor was converted into a digital value by a linux computer with PCI board for AD conversion (PCI-3135, Interface). The rotary motor was driven by a motor driver (ESCON Module 24/2, maxon motor ag). The input constant current was 0.04 A, 0.12 A, 0.20 A, 0.28 A, and 0.36 A. 0.04 A and 0.28 A are the no-load current and the rated current of the motor. The output force was measured five times for each constant current value.

Relation between the input current and the averaged value of the measured force is shown in Table 5.3. The maximum output force within the range of the rated current was about 3.5 N. Since the no-load current of the motor was about 0.04 A, the efficiency of the torque transmission mechanism was calculated by the result that the current value was 0.12 A, 0.20 A, and 0.28 A. As the result, the averaged efficiency of the slave e_{fS} was 0.192. From Table 5.2, the efficiency of the planetary gear head G_{h} is 0.61. Therefore, the efficiency of the torque transmission mechanism was decided at 0.314.

5.4.2 Bilateral teleoperation

The acceleration based four-channel bilateral control using the oblique coordinate control was implemented to the flexible haptic forceps robot. The efficiency of the torque transmission mechanism decided in Section 5.4.1 was used to correct the estimated value of RFOB.

Experimental setup

The slave was driven by the same experimental setup with the preliminary experiment described in Section 5.4.1. The linear motor of the master was driven by a motor driver (SVFM1-H3-DSP, Servoland). A microcomputer was used to implement the acceleration based bilateral control. Parameters of the bilateral control for the flexible haptic forceps robot are shown in Table 5.4. The sampling time of the

Table 5.4: Parameters of the flexible haptic forceps robot

Parameters	Values
M_{nM}	0.5 kg
J_{nS}	0.012 gcm^2
K_{tnM}	33 N/A
K_{p}	6400.0 s^{-2}
K_{v}	160.0 s^{-1}
K_{f}	1.0
$g_{\mathrm{dis}}, g_{\mathrm{rfob}}, g_{\mathrm{pse}}$	628.3 rad/s
α	1.2
β	5.12

control was 0.2 ms. In the construction of RFOB, the internal force F_{int} was not considered, since both the master and the slave were the one DoF robot. Besides, the moving direction of the master was perpendicular to the direction of gravity force for the master $F_{g\mathrm{M}}$. Therefore, the gravity force $F_{g\mathrm{M}}$ was not considered. Friction force F_{fric} and gravity force for the slave $F_{g\mathrm{S}}$ were ignored.

In the experiment, the gripper of the slave held a soft object and a hard object. A sponge rubber and a metal rod of 4 mm in diameter were used as the soft object and the hard object contacted by the slave. Each object was held by the slave twice.

Experimental result

The position response and the force response are shown in Fig. 5-8. The green line and the red line denote the response of the master and the slave, respectively. The contact motion was conducted in gray shaded areas. When the robot contacted with the soft object, the reaction force was gradually increased. On the other hand, the reaction force was increased rapidly when contacting with the hard object. The difference of the object can be distinguished by these results.

The position error and the force error between the master and the slave are shown in Fig. 5-9. In the almost time period, the magnitude of the errors was small and ignorable. Both errors were increased by the transient response at the moment when contacting with the object. Therefore, the position tracking and Newton's third law between the master and the slave were realized.

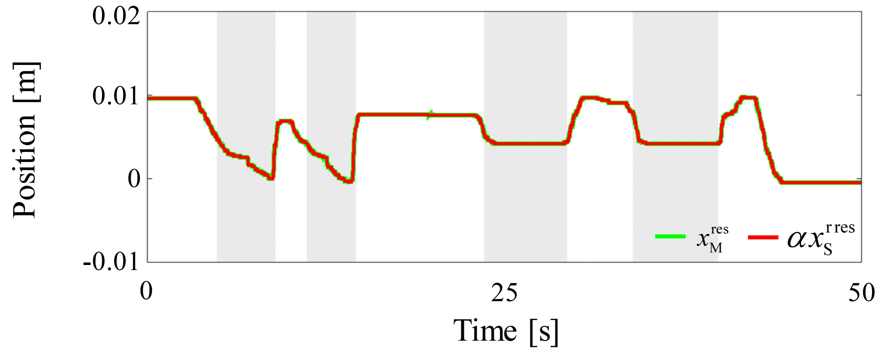

(a) Position response

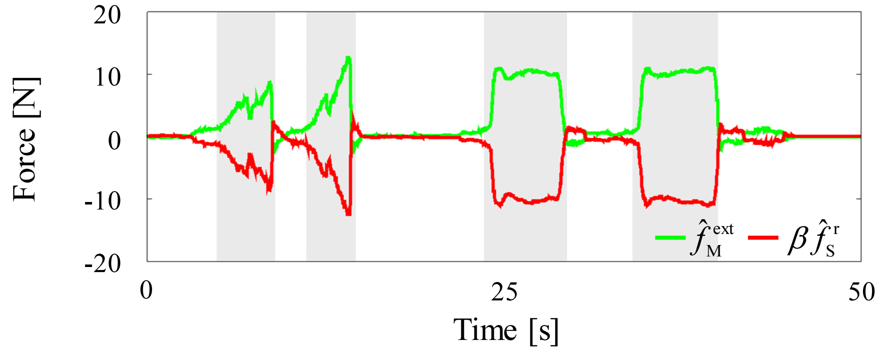

(b) Force response

Fig. 5-8: Experimental results.

5.5 Summary

In this chapter, the flexible haptic forceps robot to realize the grasping motion with force sensation for the flexible endoscopic robot was described. The miniature haptic forceps robot with the high reduction ratio mechanism which is the slave of the flexible haptic forceps robot was developed. The efficiency of the torque transmission mechanism was decided by the preliminary experiment to correct the estimation of force information deteriorated by mechanical components. Besides, the motion of the robot with the gear mechanism was expressed by the scaling bilateral control in the motor space. In the experiment, the acceleration based four-channel bilateral control system using the oblique coordinate control was constructed in the joint space. The experimental results showed that the control targets of the bilateral control were achieved. Besides, the contacted object can be distinguished from the change of the position response and the force response.

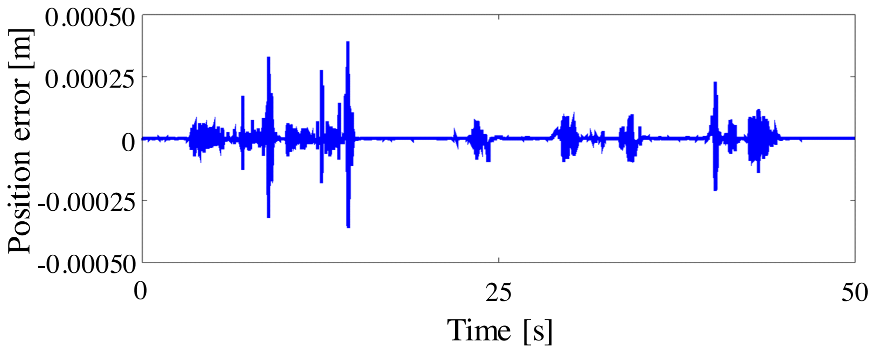

(a) Position error

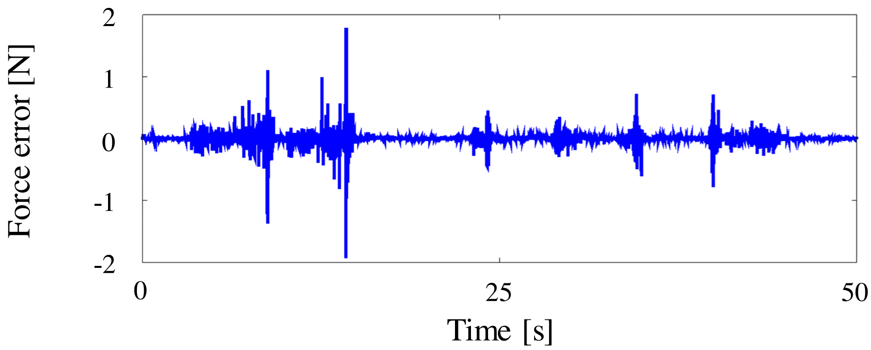

(b) Force error

Fig. 5-9: Errors between the master and the slave.

Chapter 6

Five DoF HEM^2

6.1 Introduction

Motion of the upper limb is important to conduct complex tasks requiring human skill such as surgical procedures and manufacturing tasks. To support human workers , multi DoF robots for medical treatments and manufacturing must reproduce the upper limb motion. However, large number of DoF increases complexity of mechanisms and deteriorates performance to obtain haptic information.

The five DoF HEM^2 is a master-slave system developed to achieve complex tasks by bilateral teleoperation. The motion of the five DoF HEM^2 corresponds to human upper limb motion which can realize complex tasks. The grasping motion is a simplified human hand motion. The roll motion, the pitch motion, and the yaw motion correspond to the human wrist motion. The translational motion is used to move the position of the end-effector as a simplified human arm motion. Two prototypes of the five DoF HEM^2 have been developed [47][48]. The parallel drive mechanism is applied to both prototypes, since the serial link mechanism increases mass and inertia of movable parts and deteriorates the backdrivability. A joint driven by the parallel link mechanism realizes human wrist motion mechanically.

In this chapter, structure, kinematics, and performance of systems using the five DoF HEM^2 are described. First, the structure and the kinematics of the first prototype are described in Section 6.2. Second, the structure, the kinematics, and the performance of the second prototype are described in Section 6.3. Finally, a ten DoF double arm teleoperation robot composed of two prototypes of the five DoF HEM^2 is explained in Section 6.4.

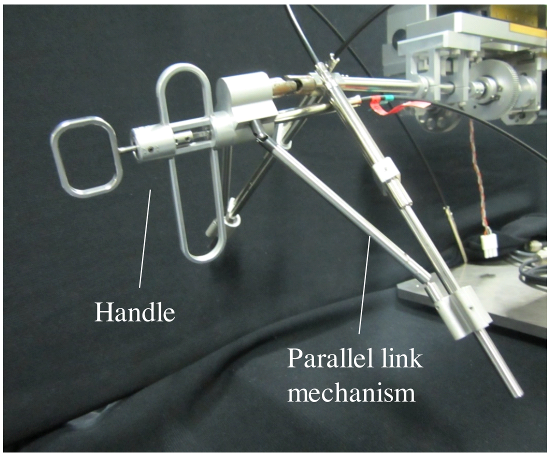

(a) The tip part of the master

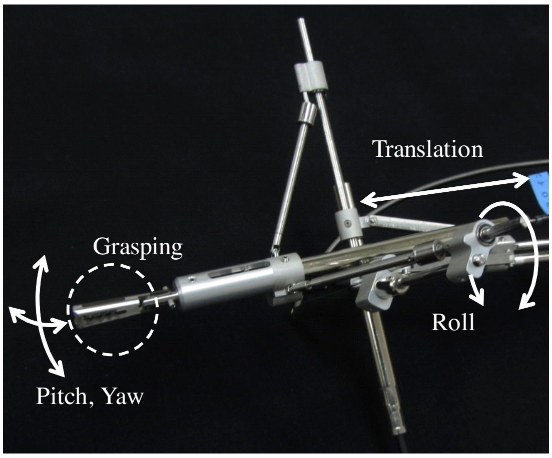

(b) The tip part of the slave

Fig. 6-1: The first prototype of the five DoF HEM^2.

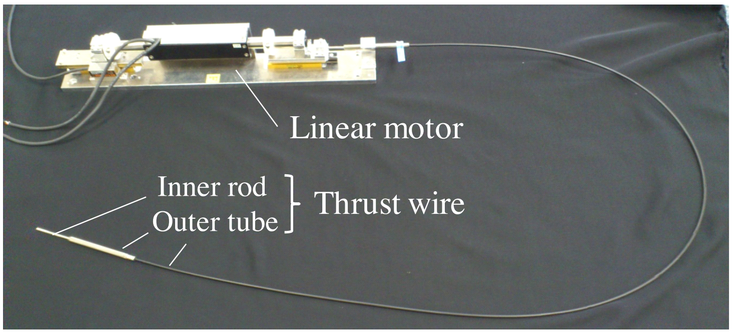

Fig. 6-2: The flexible actuator.

6.2 First prototype

6.2.1 Structure

The structure of the master and the slave is divided into a tip part and a base part. Actuators and sensors are placed at the base part. The driving power is transmitted from the base part to the tip part by mechanical components. The tip part of the first prototype shown in Fig. 6-1 is connected with the base part by a shaft. A linear motor mounted at the base part transmits the driving force to the tip part through the shaft. The tip part moves along the center axis of the shaft as the translational motion. Besides, the driving torque for the roll motion generated by a rotary motor mounted at the base part is transmitted by the shaft. The tip part rotates on the center axis of the shaft as the roll motion. The linear motor and the

Table 6.1: Range of motion of the first prototype

Motion	Range
Grasping	Open and close
Translation	about 0.03 m
Roll	about - π/4 rad – π/4 rad
Pitch	about 0 rad – π/4 rad
Yaw	about 0 rad – π/4 rad

rotary motor mounted at the base part are moved independently.

The base part includes three flexible actuators [49] shown in Fig. 6-2. Flexible actuators composed of a linear motor and a thrust wire can transmit both pushing force and pulling force, while the thrust wire bends flexibly. A flexible actuator is connected with the gripper or the handle for the grasping motion. The others are used to provide the driving force to the parallel link mechanism for the pitch motion and the yaw motion. The outer tube of thrust wires are connected with the tip part directly. Therefore, the grasping motion, the translational motion, the roll motion, and the remaining rotational motion are driven independently. A position of the linear motors (S160Q, GMC Hillstone) and an angle of the rotary motor (RE40, maxon motor ag) are measured by linear encoders (RGH24Y, Renishaw) and a rotary encoder (R-1SL, Canon), respectively.

The parallel link mechanism at the tip part converts the linear motion of the flexible actuators into the pitch motion and the yaw motion. A universal joint is used as the center of the pitch motion and the yaw motion and placed at the center axis of the roll motion to imitate the structure of the human wrist for intuitive operation. The range of each motion on the design is shown in Table 6.1.

6.2.2 Kinematics

A position vector $\boldsymbol{x}_{1\mathrm{m}}$ and a force vector $\boldsymbol{f}_{1\mathrm{m}}$ of the first prototype in the motor space are given as,

$$\boldsymbol{x}_{1\mathrm{m}} = \begin{bmatrix} x_{1\mathrm{mG}} & x_{1\mathrm{mL}} & q_{1\mathrm{mR}} & x_{1\mathrm{mP}} & x_{1\mathrm{mY}} \end{bmatrix}^{\mathrm{T}}, \tag{6.1}$$

$$\boldsymbol{f}_{1\mathrm{m}} = \begin{bmatrix} f_{1\mathrm{mG}} & f_{1\mathrm{mL}} & \tau_{1\mathrm{mR}} & f_{1\mathrm{mP}} & f_{1\mathrm{mY}} \end{bmatrix}^{\mathrm{T}}. \tag{6.2}$$

The subscripts G, L, R, P, and Y denote the grasping motion, the translational motion, the roll motion, the pitch motion, and the yaw motion, respectively. The subscript 1 denotes the variables of the first prototype. A position vector $\boldsymbol{x}_{1\mathrm{j}}$ and a force vector $\boldsymbol{f}_{1\mathrm{j}}$ of the first prototype in the joint space are given

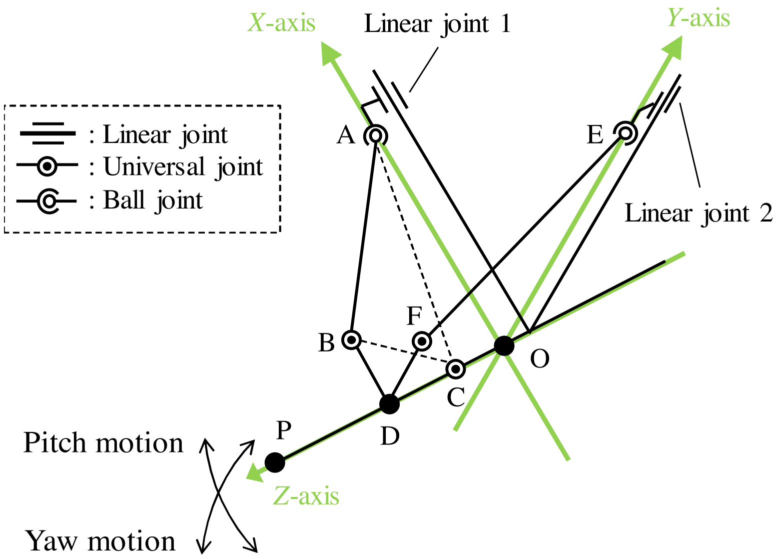

Fig. 6-3: Schematic drawing of the tip part of the first prototype in three dimensional space.

as,

$$\boldsymbol{x}_{1\mathrm{j}} = \begin{bmatrix} x_{1\mathrm{jG}} & x_{1\mathrm{jL}} & \phi_{1\mathrm{jR}} & \theta_{1\mathrm{jP}} & \psi_{1\mathrm{jY}} \end{bmatrix}^{\mathrm{T}}, \tag{6.3}$$

$$\boldsymbol{f}_{\mathrm{j}} = \begin{bmatrix} f_{1\mathrm{jG}} & f_{1\mathrm{jL}} & \tau_{1\mathrm{jR}} & \tau_{1\mathrm{jP}} & \tau_{1\mathrm{jY}} \end{bmatrix}^{\mathrm{T}}. \tag{6.4}$$

In the case of the grasping motion, the translational motion, and the roll motion, the variables in the motor space coincide with the variables in the joint space. On the other hand, the kinematics of the parallel link mechanism must be considered to control the variables of the pitch motion and the yaw motion in the joint space [50].

Schematic drawings of the tip part including the parallel link mechanism are shown in Fig. 6-3 and Fig. 6-4. L denotes the link length or the distance between two points. The flexible actuators for the parallel link mechanism are connected with the linear joint 1 and the linear joint 2. The rotational motion obtained by the motion of the linear joint 1 is defined as the pitch motion. On the other hand, the rotational motion by the motion of the linear joint 2 is defined as the yaw motion. Relation between the

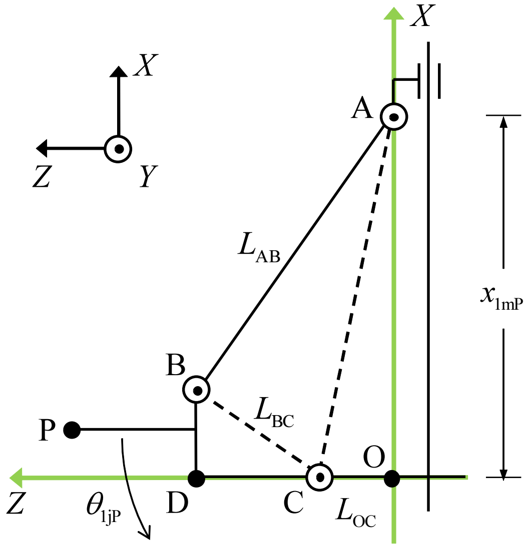

Fig. 6-4: Schematic drawing of the tip part of the first prototype in two dimensional space.

pitch angle θ_{1jP} and the position of the flexible actuator x_{1mP} is given as,

$$x_{1mP} = -L_{1BC} \sin \theta_{1jPe} + \sqrt{N_{1P}}, \tag{6.5}$$

$$N_{1P} = L_{1AB}{}^2 - L_{1OC}{}^2 - 2L_{1OC}L_{1BC} \cos \psi_{1jY} \cos \theta_{1jPe} - L_{1BC}{}^2 \cos{}^2\theta_{1jPe}, \tag{6.6}$$

$$\theta_{1jPe} = \theta_{1jP} - \theta_{1j0}. \tag{6.7}$$

θ_{1j0} is a constant angle formed by line segments BC and DC. As with the pitch motion, relation between the yaw angle ψ_{1jY} and the position of the flexible actuator x_{1mY} is given as,

$$y_{1mY} = -L_{1FC} \sin \psi_{1jYe} + \sqrt{N_{1Y}}, \tag{6.8}$$

$$N_{1Y} = L_{1EF}{}^2 - L_{1OC}{}^2 - 2L_{1OC}L_{1FC} \cos \theta_{1jP} \cos \psi_{1jYe} - L_{1FC}{}^2 \cos{}^2\psi_{1jYe}, \tag{6.9}$$

$$\psi_{1jYe} = \psi_{1jY} - \psi_{1j0}. \tag{6.10}$$

ψ_{1j0} is a constant angle formed by line segments BC and DC.

Relation between the velocity in the motor space and the angular velocity in the joint space is expressed by the Jacobian matrix. The inverse kinematics of the parallel link mechanism is used to derive

Table 6.2: Link length of the first prototype

Link	Master	Slave
Initial value of x_{1mP} and x_{1mY}	0.1207 m	0.059 m
L_{AB}, L_{EF}	0.1039 m	0.0535 m
L_{BC}, L_{FC}	0.0381 m	0.0205 m
L_{OC}	0.0155 m	0.0095 m

the Jacobian matrix for the pitch motion and the yaw motion $\boldsymbol{J}_{\mathrm{v1}}$ given as,

$$\boldsymbol{J}_{\mathrm{v1}} = \begin{bmatrix} \dfrac{\partial x_{\mathrm{1mP}}}{\partial \theta_{\mathrm{1jP}}} & \dfrac{\partial x_{\mathrm{1mP}}}{\partial \psi_{\mathrm{1jY}}} \\ \dfrac{\partial y_{\mathrm{1mY}}}{\partial \theta_{\mathrm{1jP}}} & \dfrac{\partial y_{\mathrm{1mY}}}{\partial \psi_{\mathrm{1jY}}} \end{bmatrix}. \tag{6.11}$$

The components of the Jacobian matrix $\boldsymbol{J}_{\mathrm{v1}}$ are given as,

$$\frac{\partial x_{\mathrm{1mP}}}{\partial \theta_{\mathrm{1jP}}} = -L_{\mathrm{1BC}} \cos\theta_{\mathrm{1jPe}} + \frac{L_{\mathrm{1BC}} \sin\theta_{\mathrm{1jPe}} \left(L_{\mathrm{1OC}} \cos\psi_{\mathrm{1jY}} + L_{\mathrm{1BC}} \cos\theta_{\mathrm{1jPe}}\right)}{\sqrt{N_{\mathrm{1P}}}}, \tag{6.12}$$

$$\frac{\partial x_{\mathrm{1mP}}}{\partial \psi_{\mathrm{1jY}}} = \frac{L_{\mathrm{1OC}} L_{\mathrm{1BC}} \sin\psi_{\mathrm{1jY}} \cos\theta_{\mathrm{1jPe}}}{\sqrt{N_{\mathrm{1P}}}}, \tag{6.13}$$

$$\frac{\partial y_{\mathrm{1mY}}}{\partial \theta_{\mathrm{1jP}}} = \frac{L_{\mathrm{1OC}} L_{\mathrm{1FC}} \sin\theta_{\mathrm{1jP}} \cos\psi_{\mathrm{1jYe}}}{\sqrt{N_{\mathrm{1Y}}}}, \tag{6.14}$$

$$\frac{\partial y_{\mathrm{1mY}}}{\partial \psi_{\mathrm{1jY}}} = -L_{\mathrm{1FC}} \cos\psi_{\mathrm{1jYe}} + \frac{L_{\mathrm{1FC}} \sin\psi_{\mathrm{1jYe}} \left(L_{\mathrm{1OC}} \cos\theta_{\mathrm{1jP}} + L_{\mathrm{1FC}} \cos\psi_{\mathrm{1jYe}}\right)}{\sqrt{N_{\mathrm{1Y}}}}. \tag{6.15}$$

The Jacobian matrix between the motor space and the joint space $\boldsymbol{J}_{\mathrm{aco1}}$ is given as,

$$\boldsymbol{J}_{\mathrm{aco1}} = \begin{bmatrix} \boldsymbol{I}_3 & \mathbf{0} \\ \mathbf{0} & \boldsymbol{J}_{\mathrm{v1}} \end{bmatrix}. \tag{6.16}$$

$\boldsymbol{I}_3$ is the identity matrix of order three. The length of each link is shown in Table 6.2. The kinematics of the first prototype is used to the acceleration based bilateral control explained in Section 3.2. Since the inverse kinematics is used, the Jacobian matrix $\boldsymbol{J}_{\mathrm{aco}}$ in Fig. 3-3 is given as,

$$\boldsymbol{J}_{\mathrm{aco}} = {\boldsymbol{J}_{\mathrm{aco1}}}^{-1}. \tag{6.17}$$

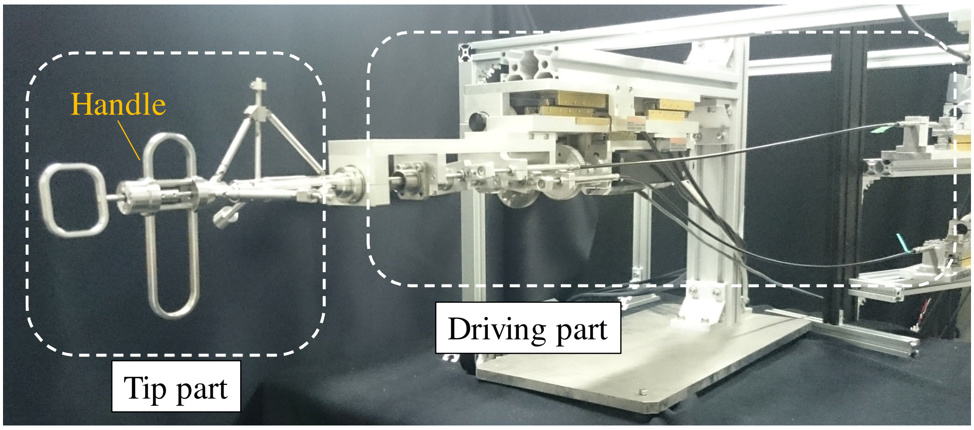

(a) The master

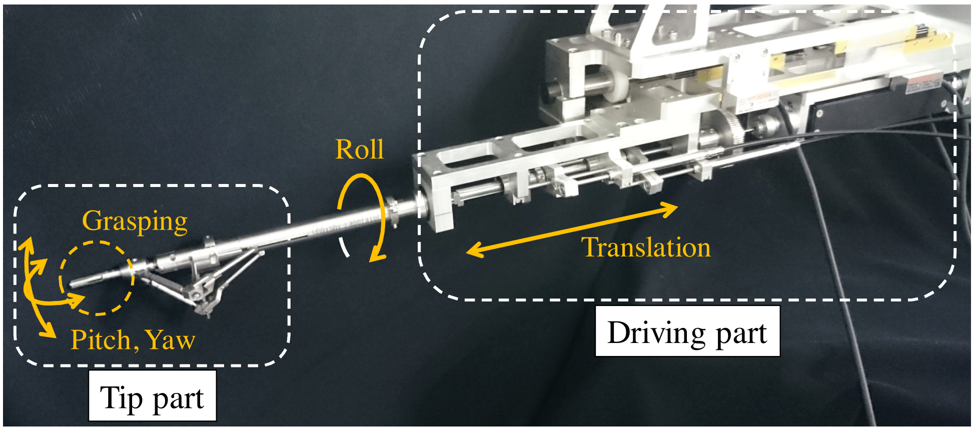

(b) The slave

Fig. 6-5: The second prototype of the five DoF HEM^2.

6.3 Second prototype

6.3.1 Structure

The second prototype of the five DoF HEM^2 is shown in Fig. 6-5. The structure of the second prototype is based on the design of the first prototype explained in Section 6.2 and the two DoF haptic robot explained in Section 4. The tip part is connected with the base part by a shaft and rods. As with the first prototype of the five DoF HEM^2, a linear motor and a rotary motor mounted at the base part provide the driving force of the translational and roll motion to the tip part by the shaft. Besides, a linear motor mounted at the movable part of the linear motor for the translational motion is used for the grasping

Table 6.3: Range of motion of the second prototype

Motion	Range
Grasping	Open and close
Translation	about 0.05 m
Roll	about - π rad – π rad
Pitch	about -π/6 rad – π/6 rad
Yaw	about -π/6 rad – π/6 rad

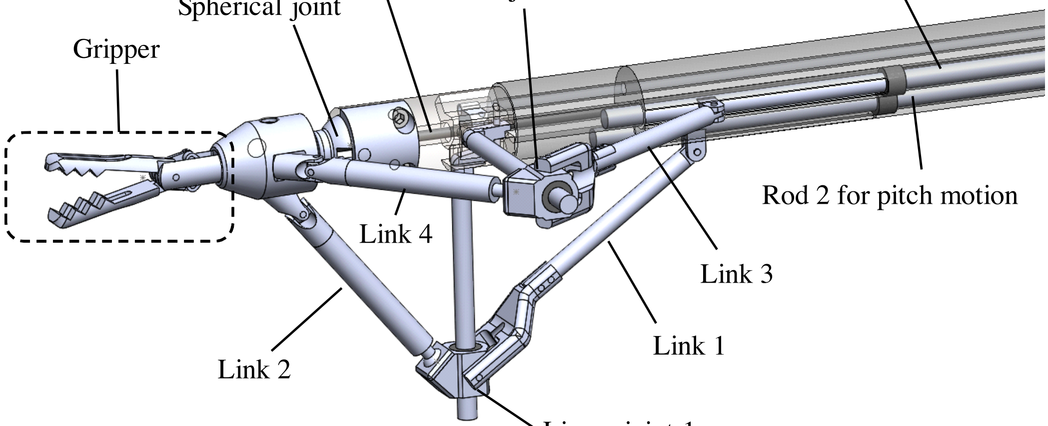

Fig. 6-6: Detailed structure of the tip part of the slave.

motion. These linear motors configure the two DoF serial link mechanism.

Two flexible actuators for the pitch motion and the yaw motion of the end-effector are connected with the base part. The driving force for the parallel link mechanism and the grasping motion is transmitted from the base part to the tip part through rods in the shaft. The parallel link mechanism, the serial link part, and the roll motion are driven independently. Therefore, the deterioration of the backdrivability according to the increasing number of DoF is suppressed.

The structure of the tip part of the slave is shown in Fig. 6-6. A gripper composed of slider crank mechanisms is attached to the end-effector. The driving force of the grasping motion is provided by the rod 1. The gripper and the rod 1 are connected by a thrust wire in the spherical joint to bend the end-effector flexibly. The parallel link mechanism is driven by the rod 2 and the rod 3. The linear motion of

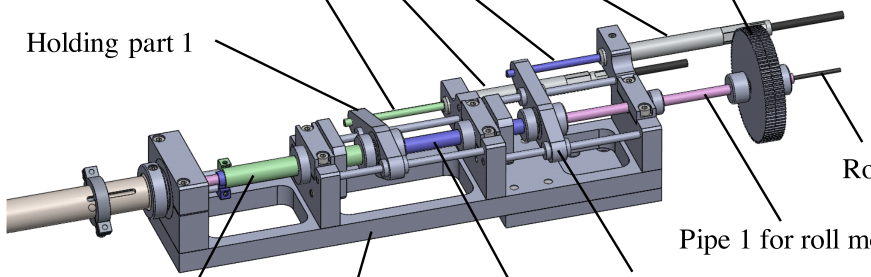

Fig. 6-7: Coaxial mechanism to transmit driving force.

the rod 2 and the rod 3 is transmitted to the linear joint 1 and the linear joint 2 by link mechanisms. Then, the motion of the linear joint 1 and the linear joint 2 is converted into the two DoF rotational motion of the end-effector. The spherical joint for the two DoF rotational motion is placed on the center axis of the shaft. In general, a spherical joint has three DoF rotational motion. Therefore, the remaining rotational motion of the spherical joint is constrained by a pin and a groove.

The detailed structure of the parallel drive mechanism in the base part is shown in Fig. 6-7. The coaxial mechanism to transmit the driving force is constructed as the parallel drive mechanism. By arranging the mechanical parts concentrically, rotational motions and translational motions can be driven in parallel [51]. The pipe 1, the pipe 2, the pipe 3, the rod 1, and the shaft connecting the tip part and the base part are arranged coaxially. One end of the rod 1 is connected with the linear motor for the grasping motion. The other end of the rod 1 goes through in the shaft. The driving torque for the roll motion is provided to the pipe 1 by a no-backlash gear. The pipe 1 surrounding the rod 1 is connected with the shaft and transmits the driving torque. The inner rods of flexible actuators are connected with the pipe 2 and the pipe 3 via the holding part 1 and the holding part 2. These pipes are connected with the rod 2 and 3. The base plate of the coaxial mechanism is moved by the translational motion.

The rod 1, the pipe 2, and the pipe 3 moves along the moving direction of the translational motion independently. On the other hand, ball bearings placed at the holding part 1, the holding part 2, the linear

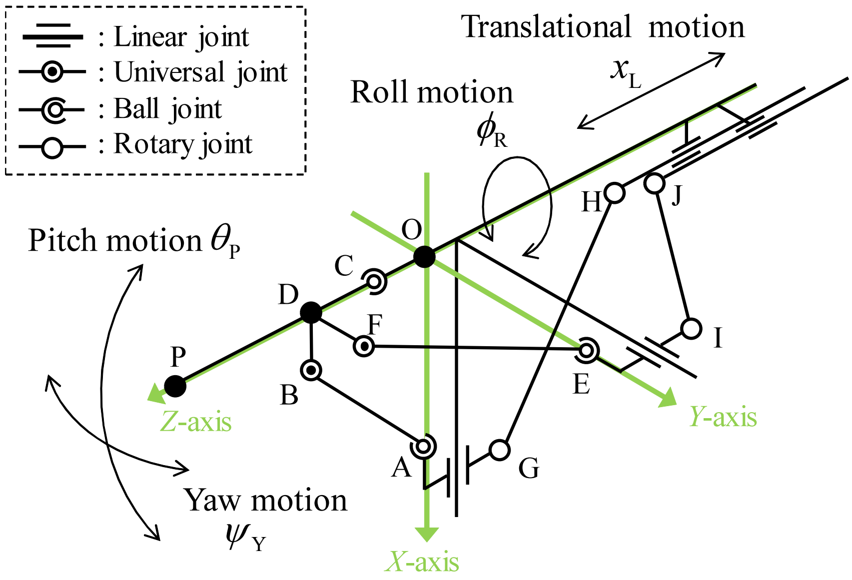

Fig. 6-8: Schematic drawing of the tip part of the second prototype in three dimensional space.

motor for the grasping motion, and the base plate allow the rotation of the pipe 2 and the pipe 3, the rod 1, and the shaft passively according to the rotation of the pipe 1. The range of each motion on the design is shown in Table 6.3.

6.3.2 Kinematics

The position vector $\boldsymbol{x}_{2\mathrm{m}}$ and the force vector $\boldsymbol{f}_{2\mathrm{m}}$ of the second prototype in the motor space are given as,

$$\boldsymbol{x}_{2\mathrm{m}} = \begin{bmatrix} x_{2\mathrm{mG}} & x_{2\mathrm{mL}} & q_{2\mathrm{mR}} & x_{2\mathrm{mP}} & x_{2\mathrm{mY}} \end{bmatrix}^{\mathrm{T}}, \tag{6.18}$$

$$\boldsymbol{f}_{2\mathrm{m}} = \begin{bmatrix} f_{2\mathrm{mG}} & f_{2\mathrm{mL}} & \tau_{2\mathrm{mR}} & f_{2\mathrm{mP}} & f_{2\mathrm{mY}} \end{bmatrix}^{\mathrm{T}}. \tag{6.19}$$

The position vector $\boldsymbol{x}_{2\mathrm{j}}$ and the force vector $\boldsymbol{f}_{2\mathrm{j}}$ of the second prototype in the joint space are given as,

$$\boldsymbol{x}_{2\mathrm{j}} = \begin{bmatrix} x_{2\mathrm{jG}} & x_{2\mathrm{jL}} & \phi_{2\mathrm{jR}} & \theta_{2\mathrm{jP}} & \psi_{2\mathrm{jY}} \end{bmatrix}^{\mathrm{T}}, \tag{6.20}$$

$$\boldsymbol{f}_{2\mathrm{j}} = \begin{bmatrix} f_{2\mathrm{jG}} & f_{2\mathrm{jL}} & \tau_{2\mathrm{jR}} & \tau_{2\mathrm{jP}} & \tau_{2\mathrm{jY}} \end{bmatrix}^{\mathrm{T}}. \tag{6.21}$$

As with the first prototype, the kinematics of the parallel link mechanism is necessary to control the motion in the joint space. The schematic drawing of the tip part including the parallel link mechanism is

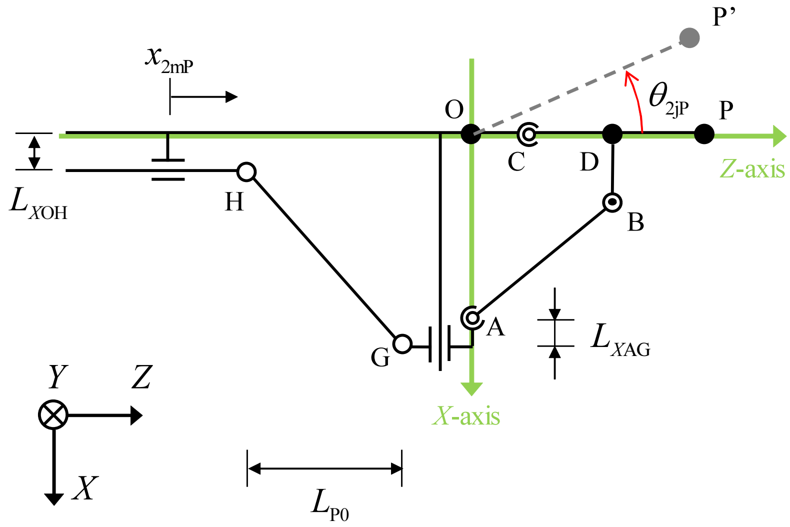

Fig. 6-9: Schematic drawing of the tip part of the second prototype in two dimensional space.

shown in Fig. 6-8 and Fig. 6-9. The transformation matrix from the motor space to the joint space $\boldsymbol{T}$ is given as,

$$\boldsymbol{T} = \begin{bmatrix} & \boldsymbol{R} & & \boldsymbol{x}_{\mathrm{D}} \\ 0 & 0 & 0 & 1 \end{bmatrix}. \tag{6.22}$$

The rotation matrix from the motor space to the joint space $\boldsymbol{R}$ is given as,

$$\boldsymbol{R} = \begin{bmatrix} \cos\theta_{2\mathrm{jP}} & -\sin\theta_{2\mathrm{jP}}\sin\psi_{2\mathrm{jY}} & \sin\theta_{2\mathrm{jP}}\cos\psi_{2\mathrm{jY}} \\ 0 & \cos\psi_{2\mathrm{jY}} & \sin\psi_{2\mathrm{jY}} \\ \sin\theta_{2\mathrm{jP}} & \cos\theta_{2\mathrm{jP}}\sin\psi_{2\mathrm{jY}} & \cos\theta_{\mathrm{P}}\cos\psi_{2\mathrm{jY}} \end{bmatrix}. \tag{6.23}$$

The position of the point D in the three dimensional cartesian coordinate system is given as,

$$\begin{aligned} \boldsymbol{x}_{\mathrm{D}} &= \begin{bmatrix} x_{\mathrm{D}} & y_{\mathrm{D}} & z_{\mathrm{D}} \end{bmatrix}^{\mathrm{T}} \\ &= \begin{bmatrix} -L_{2\mathrm{CD}}\sin\theta_{2\mathrm{jP}}\cos\psi_{2\mathrm{jY}} \\ -L_{2\mathrm{CD}}\sin\psi_{2\mathrm{jY}} \\ L_{2\mathrm{CD}}\cos\theta_{2\mathrm{jP}}\cos\psi_{2\mathrm{jY}} + L_{2\mathrm{OC}} \end{bmatrix}. \end{aligned} \tag{6.24}$$

The link 2 and the link 3 are connected with the end-effector by universal joints placed at a point B and a point F. The center of the rotation of the universal joint $\boldsymbol{x}_{\mathrm{B}}$ and $\boldsymbol{x}_{\mathrm{F}}$ is given as,

$$\begin{aligned}\boldsymbol{x}_{\mathrm{B}} &= \begin{bmatrix} x_{\mathrm{B}} & y_{\mathrm{B}} & z_{\mathrm{B}} \end{bmatrix}^{\mathrm{T}} \\ &= \boldsymbol{x}_{\mathrm{D}} + \boldsymbol{R} \begin{bmatrix} L_{2\mathrm{BD}} & 0 & 0 \end{bmatrix}^{\mathrm{T}}, \end{aligned} \tag{6.25}$$

$$\begin{aligned}\boldsymbol{x}_{\mathrm{F}} &= \begin{bmatrix} x_{\mathrm{F}} & y_{\mathrm{F}} & z_{\mathrm{F}} \end{bmatrix}^{\mathrm{T}} \\ &= \boldsymbol{x}_{\mathrm{D}} + \boldsymbol{R} \begin{bmatrix} 0 & L_{2\mathrm{FD}} & 0 \end{bmatrix}^{\mathrm{T}}. \end{aligned} \tag{6.26}$$

The position of the linear joint 1 is given as,

$$L_{2\mathrm{OA}} = x_{\mathrm{B}} + \sqrt{{L_{2\mathrm{AB}}}^2 - {y_{\mathrm{B}}}^2 - {z_{\mathrm{B}}}^2}. \tag{6.27}$$

The position of the linear joint 2 is given as,

$$L_{2\mathrm{OE}} = y_{\mathrm{F}} + \sqrt{{L_{2\mathrm{EF}}}^2 - {x_{\mathrm{F}}}^2 - {z_{\mathrm{F}}}^2}. \tag{6.28}$$

The linear joint 1 and the linear joint 2 are moved by the link mechanism composed of the link 1 and the link 3. The relation between the position of the linear joints and linear motors is given as,

$$x_{2\mathrm{mP}} = -\sqrt{{L_{2\mathrm{GH}}}^2 - (L_{2\mathrm{OA}} - L_{X2\mathrm{OH}} + L_{2X\mathrm{AG}})^2} + L_{2\mathrm{P0}}, \tag{6.29}$$

$$x_{2\mathrm{mY}} = -\sqrt{{L_{2\mathrm{IJ}}}^2 - (L_{2\mathrm{OE}} - L_{Y2\mathrm{OJ}} + L_{2Y\mathrm{EI}})^2} + L_{2\mathrm{Y0}}. \tag{6.30}$$

The relation between the velocity vector in the motor space and the joint space is given as,

$$\dot{\boldsymbol{x}}_{2\mathrm{m}} = \boldsymbol{J}_{\mathrm{aco2}} \dot{\boldsymbol{x}}_{2\mathrm{j}}, \tag{6.31}$$

$$\boldsymbol{J}_{\mathrm{aco2}} = \begin{bmatrix} \boldsymbol{I}_3 & \boldsymbol{0} \\ \boldsymbol{0} & \boldsymbol{J}_{\mathrm{v2}} \end{bmatrix}. \tag{6.32}$$

The inverse kinematics is used to derive the Jacobian matrix $\boldsymbol{J}_{\mathrm{aco2}}$. The Jacobian matrix for the pitch and yaw motion $\boldsymbol{J}_{\mathrm{v2}}$ is given as,

$$\begin{aligned}\boldsymbol{J}_{\mathrm{v2}} &= \boldsymbol{J}_{\mathrm{v2sl}} \boldsymbol{J}_{\mathrm{v2pl}} \\ &= \begin{bmatrix} \dfrac{\partial x_{2\mathrm{mP}}}{\partial L_{2\mathrm{OA}}} & 0 \\ 0 & \dfrac{\partial x_{2\mathrm{mY}}}{\partial L_{2\mathrm{OE}}} \end{bmatrix} \begin{bmatrix} \dfrac{\partial L_{2\mathrm{OA}}}{\partial \theta_{2\mathrm{jP}}} & \dfrac{\partial L_{2\mathrm{OA}}}{\partial \psi_{2\mathrm{jY}}} \\ \dfrac{\partial L_{2\mathrm{OE}}}{\partial \theta_{2\mathrm{jP}}} & \dfrac{\partial L_{2\mathrm{OE}}}{\partial \psi_{2\mathrm{jY}}} \end{bmatrix}. \end{aligned} \tag{6.33}$$

$\boldsymbol{J}_{\mathrm{v2sl}}$ and $\boldsymbol{J}_{\mathrm{v2pl}}$ are the Jacobian matrix of the link mechanism to move the linear joints and the parallel link mechanism. The components of the Jacobian matrices are given as,

$$\frac{\partial L_{2\mathrm{OA}}}{\partial \theta_{2\mathrm{jP}}} = -L_{2\mathrm{e}} \cos\theta_{2\mathrm{eB}} + \frac{z_{\mathrm{B}} L_{2\mathrm{e}} \cos\theta_{2\mathrm{eC}}}{\sqrt{{L_{2\mathrm{EF}}}^2 - {x_{\mathrm{F}}}^2 - {z_{\mathrm{F}}}^2}}, \tag{6.34}$$

$$\begin{aligned}\frac{\partial L_{2\mathrm{OA}}}{\partial \psi_{2\mathrm{jY}}} &= L_{2\mathrm{CD}} \sin\theta_{2\mathrm{jP}} \sin\psi_{2\mathrm{jY}} + \frac{{L_{2\mathrm{CD}}}^2 \sin\psi_{2\mathrm{jY}} \cos\psi_{2\mathrm{jY}}}{\sqrt{{L_{2\mathrm{EF}}}^2 - {x_{\mathrm{F}}}^2 - {z_{\mathrm{F}}}^2}} \\ &\quad + \frac{(L_{2\mathrm{CD}} \sin\psi_{2\mathrm{jY}} \left(L_{2\mathrm{OC}} + L_{2\mathrm{e}} \sin\theta_{2\mathrm{eC}}\right) \sin\theta_{2\mathrm{jP}})}{\sqrt{{L_{2\mathrm{EF}}}^2 - {x_{\mathrm{F}}}^2 - {z_{\mathrm{F}}}^2}},\end{aligned} \tag{6.35}$$

$$\frac{\partial L_{2\mathrm{OE}}}{\partial \theta_{2\mathrm{jP}}} = \frac{L_{2\mathrm{OC}} L_{2\mathrm{FC}} \sin\theta_{2\mathrm{jP}} \cos\psi_{2\mathrm{eF}}}{\sqrt{{L_{2\mathrm{EF}}}^2 - {x_{\mathrm{F}}}^2 - {z_{\mathrm{F}}}^2}}, \tag{6.36}$$

$$\frac{\partial L_{2\mathrm{OE}}}{\partial \psi_{2\mathrm{jY}}} = -L_{2\mathrm{FC}} \cos\psi_{2\mathrm{eF}} + \frac{L_{2\mathrm{FC}} \sin\psi_{2\mathrm{eF}} \left(L_{2\mathrm{FC}} \sin\psi_{2\mathrm{eF}} + L_{2\mathrm{OC}} \cos\theta_{2\mathrm{jP}}\right)}{\sqrt{{L_{2\mathrm{EF}}}^2 - {x_{\mathrm{F}}}^2 - {z_{\mathrm{F}}}^2}}, \tag{6.37}$$

$$\frac{\partial x_{2\mathrm{mP}}}{\partial L_{2\mathrm{OA}}} = \frac{L_{2\mathrm{OA}} - L_{2X\mathrm{OH}} + L_{2X\mathrm{AG}}}{\sqrt{{L_{2\mathrm{GH}}}^2 - \left(L_{2\mathrm{OA}} - L_{2X\mathrm{OH}} + L_{2X\mathrm{AG}}\right)^2}}, \tag{6.38}$$

$$\frac{\partial x_{2\mathrm{mY}}}{\partial L_{2\mathrm{OE}}} = \frac{L_{2\mathrm{OE}} - L_{2Y\mathrm{OJ}} + L_{2Y\mathrm{EI}}}{\sqrt{{L_{2\mathrm{IJ}}}^2 - \left(L_{2\mathrm{OE}} - L_{2Y\mathrm{OJ}} + L_{2Y\mathrm{EI}}\right)^2}}. \tag{6.39}$$

$L_{2\mathrm{e}}$, $\theta_{2\mathrm{eB}}$, $\theta_{2\mathrm{eC}}$, and $\psi_{2\mathrm{eF}}$ are given as,

$$L_{2\mathrm{e}} = \sqrt{{L_{2\mathrm{BD}}}^2 + {L_{2\mathrm{CD}}}^2 \cos^2\psi_{2\mathrm{jY}}}, \tag{6.40}$$

$$\theta_{2\mathrm{eB}} = \theta_{2\mathrm{jP}} - \arcsin\left(\frac{L_{2\mathrm{BD}}}{L_{2\mathrm{e}}}\right), \tag{6.41}$$

$$\theta_{2\mathrm{eC}} = \theta_{2\mathrm{jP}} + \arcsin\left(\frac{L_{2\mathrm{CD}} \cos\psi_{2\mathrm{jY}}}{L_{2\mathrm{e}}}\right), \tag{6.42}$$

$$\psi_{2\mathrm{eF}} = \psi_{2\mathrm{jY}} - \arcsin\left(\frac{L_{2\mathrm{FD}}}{L_{2\mathrm{FC}}}\right). \tag{6.43}$$

The relation between the force vector in the motor space and the joint space is given as,

$$\boldsymbol{f}_{\mathrm{j2}} = {\boldsymbol{J}_{\mathrm{aco2}}}^{\mathrm{T}} \boldsymbol{f}_{\mathrm{m2}}. \tag{6.44}$$

A measure of the manipulating ability of robot manipulators is the manipulability [52]. The manipulability of the second prototype is shown in Fig. 6-10. The length of each link is shown in Table 6.4. There is no singular point in the range of the motion.

The kinematics of the second prototype is used to the bilateral control explained in Section 3.2. Since the inverse kinematics is used, the Jacobian matrix $\boldsymbol{J}_{\mathrm{aco}}$ in Fig. 3-3 is given as,

$$\boldsymbol{J}_{\mathrm{aco}} = {\boldsymbol{J}_{\mathrm{aco2}}}^{-1}. \tag{6.45}$$

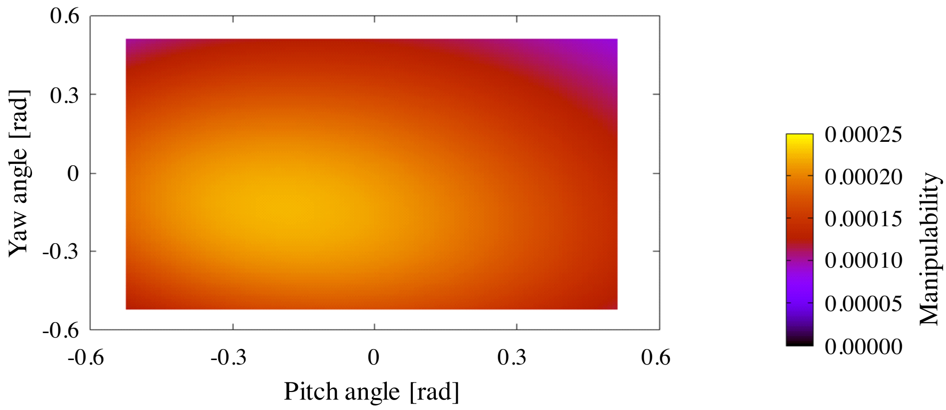

(a) The master

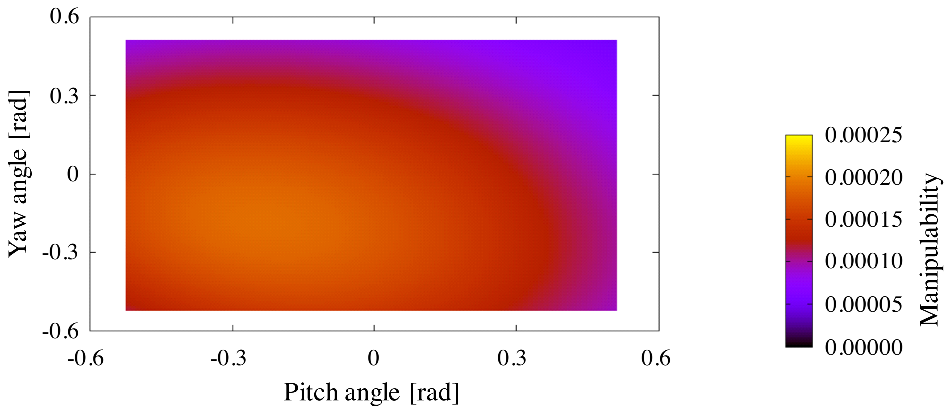

(b) The slave

Fig. 6-10: Manipulability at pitch and yaw angle of the second prototype.

6.3.3 Experiments

The performance of the second prototype as a multi DoF haptic device was validated by two experiments. First, the free motion and the contact motion was conducted to validate the performance of the robot. Second, a peg-in-hole task was conducted. Third, a screw was fastened by the robot.

The acceleration based four-channel bilateral control was implemented to the second prototype of the five DoF HEM^2. The block diagram of the bilateral control for the second prototype is shown in Fig. 6-11. The parameters of the bilateral control and the friction compensation are shown in Table 6.5. The friction force was compensated in the estimation of the force information. In the peg-in-hole task and the screw fastening task, $F_{\mathrm{MG}}^{\mathrm{const}}$ and $F_{\mathrm{SL}}^{\mathrm{const}}$ were set to 0.0 N. Besides, the efficiency of the mechanism

Table 6.4: Link length of the second prototype

Link	Master	Slave
L	0.0411 m	0.0358 m
L_{AB}, L_{EF}	0.0376 m	0.0346 m
L_{BC}, L_{FC}	0.0134 m	0.0132 m
L_{BD}, L_{FD}	0.0088 m	0.0088 m
L_{CD}	0.0101 m	0.0098 m
L_{OC}	0.0092 m	0.0127 m
L_{GH}, L_{IJ}	0.0510 m	0.0486 m
$L_{X\mathrm{AG}}$, $L_{Y\mathrm{EI}}$	0.0017 m	0.0017 m
$L_{X\mathrm{OH}}$, $L_{Y\mathrm{OJ}}$	0.0080 m	0.0080 m
L_{P0}, L_{Y0}	0.0373 m	0.0386 m

Table 6.5: Parameters of the second prototype

Parameters	Grasping	Translation	Roll	Pitch & Yaw
M_{n}	0.3 kg	2.4 kg	0.0837 gm^2	0.6 kg
K_{tn}	33 N/A	33 N/A	0.0603 Nm/A	33 N/A
K_{p}	1600.0 s^{-2}	400.0 s^{-2}	1600.0 s^{-2}	3600.0 s^{-2}
K_{v}	80.0 s^{-1}	40.0 s^{-1}	100.0 s^{-1}	120.0 s^{-1}
K_{f}	0.8	0.8	0.2	0.2
g_{dis}, g_{rfob}	450.0 rad/s	450.0 rad/s	400.0 rad/s	450.0 rad/s
g_{pse}	900.0 rad/s	900.0 rad/s	800.0 rad/s	900.0 rad/s
$F_{\mathrm{M}}^{\mathrm{const}}$	0.5 N	0.0 N	6.0 mNm	1.0 N
$F_{\mathrm{S}}^{\mathrm{const}}$	0.5 N	0.5 N	6.0 mNm	1.0 N
V_{thresh}	2.0 mm/s	4.0 mm/s	0.15 rad/s	4.0 mm/s

$\boldsymbol{e}_{\mathrm{f}}$ was used to correct the force information estimated by RFOB, since complex structure of multi DoF robots causes the deterioration of the estimation accuracy. The efficiency of the mechanism of the slave $\boldsymbol{e}_{\mathrm{fS}}$ measured in the preliminary experiment is given as,

$$\boldsymbol{e}_{\mathrm{fS}} = \begin{bmatrix} 0.897 & 1.0 & 1.0 & 0.697 & 0.747 \end{bmatrix}. \tag{6.46}$$

The robot was controlled by RTAI 3.8.1 on CentOS 5.8. PCI boards (PCI-6205C and PCI-3340, Interface) were used for the pulse count of the encoders and the DA conversion of command signals.

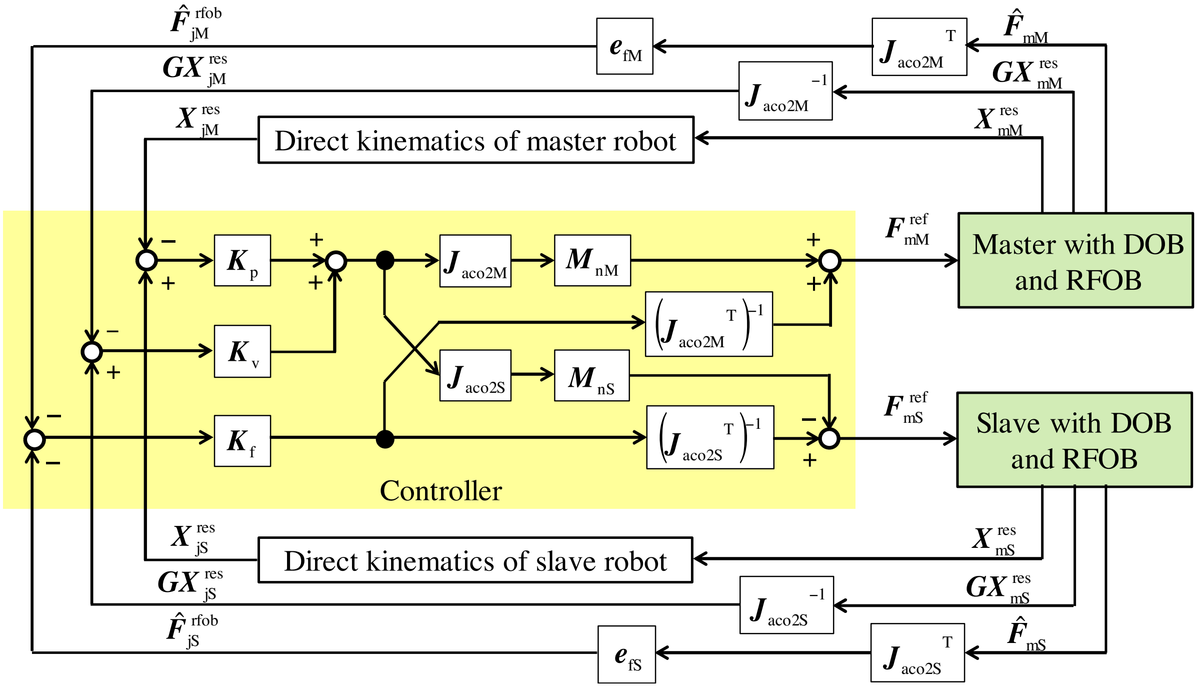

Fig. 6-11: Block diagram of the bilateral control for the second prototype.

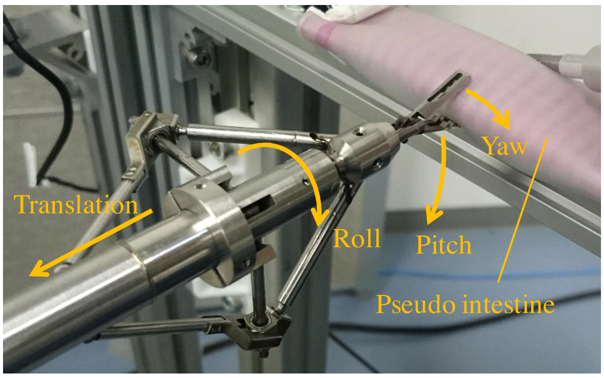

Fig. 6-12: Experimental setup to validate the performance of the second prototype.

Free motion and contact motion

In the first experiment, free motion and contact motion were conducted. In the free motion, the master was manipulated in the order of the grasping motion, the translational motion, the roll motion, the pitch motion, and the yaw motion. In the contact motion, a pseudo small intestine was used as a contacted object. The slave contacted with the object is shown in Fig. 6-12. First, the pseudo small intestine was

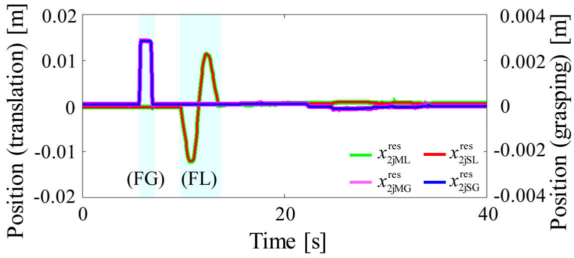

(a) Position response of grasping motion and translational motion

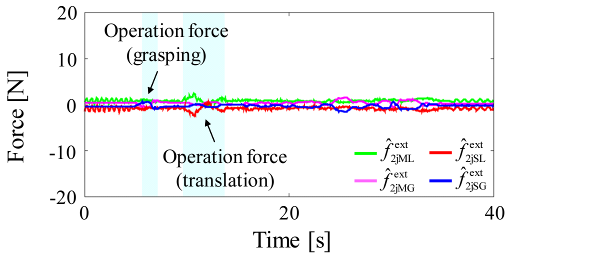

(b) Force response of grasping motion and translational motion

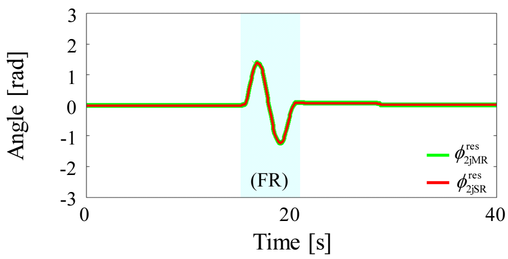

(c) Angle response of roll motion

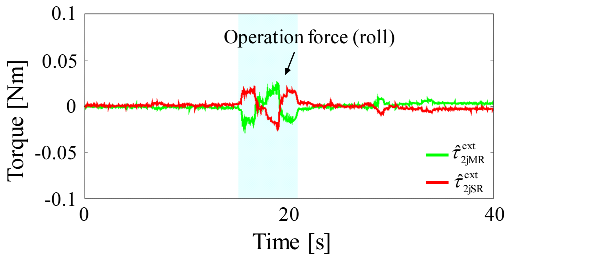

(d) Torque response of roll motion

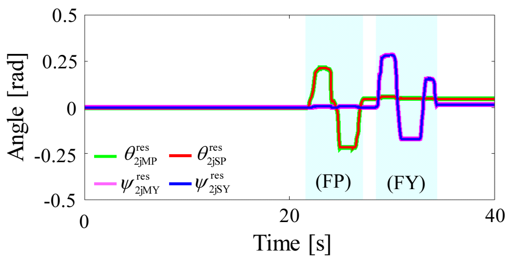

(e) Angle response of pitch motion and yaw motion

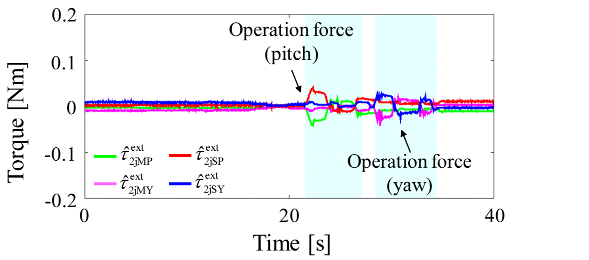

(f) Torque response of pitch motion and yaw motion

Fig. 6-13: Experimental results of free motion.

held by the gripper. Second, the master was manipulated in the order of the translational motion, the roll motion, the pitch motion, and the yaw motion, while the gripper kept holding the object.

The experimental results are shown in Fig. 6-13 and Fig. 6-14. (F·) and (C·) denote the motion manipulated by the operator. The blue shaded areas, the gray shaded areas, and the areas indicated by an arrow denote the time that the master was manipulated. In the free motion, the operation force of the master-slave system was small. In the contact motion, the large grasping force was kept, and the pseudo intestine was held till the end of the contact motion. The reaction force from the pseudo intestine was transmitted to the operator by the master. It can be confirmed that the magnitude of the force and

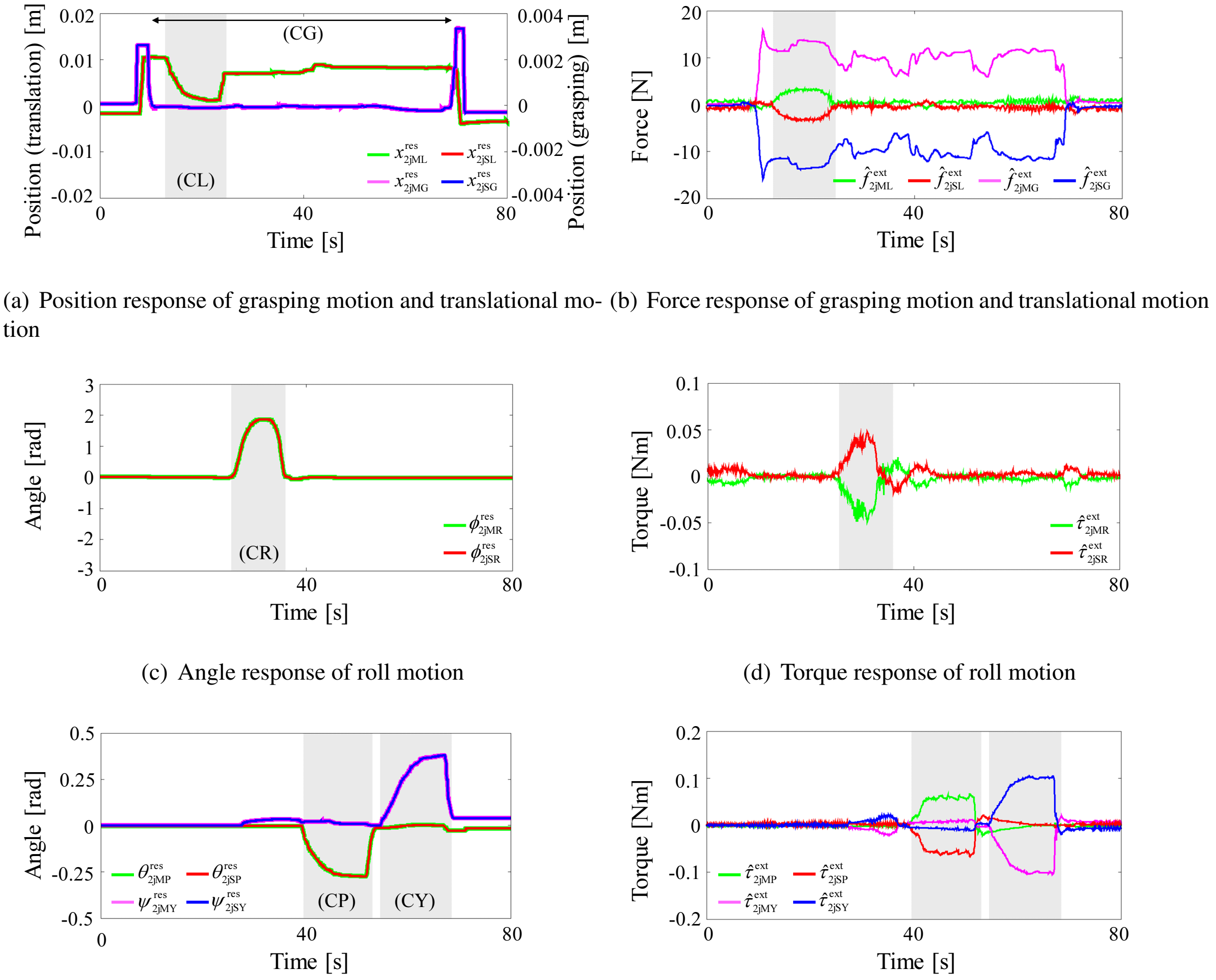

(a) Position response of grasping motion and translational motion

(b) Force response of grasping motion and translational motion

(c) Angle response of roll motion

(d) Torque response of roll motion

(e) Angle response of pitch motion and yaw motion

(f) Torque response of pitch motion and yaw motion

Fig. 6-14: Experimental results of contact motion.

the torque was increased according to the change of the position and the angle in each motion. The position of the slave followed the position of the master in each motion. Besides, Newton's third law was realized. Therefore, the control targets of the bilateral control were achieved, and the force sensation was transmitted.

Peg-in-hole task

In the second experiment, a peg-in-hole task and a screw fastening task were conducted. The experimental setup is shown in Fig. 6-15. In the peg-in-hole task, a nickel plated steel dowel and a aluminum

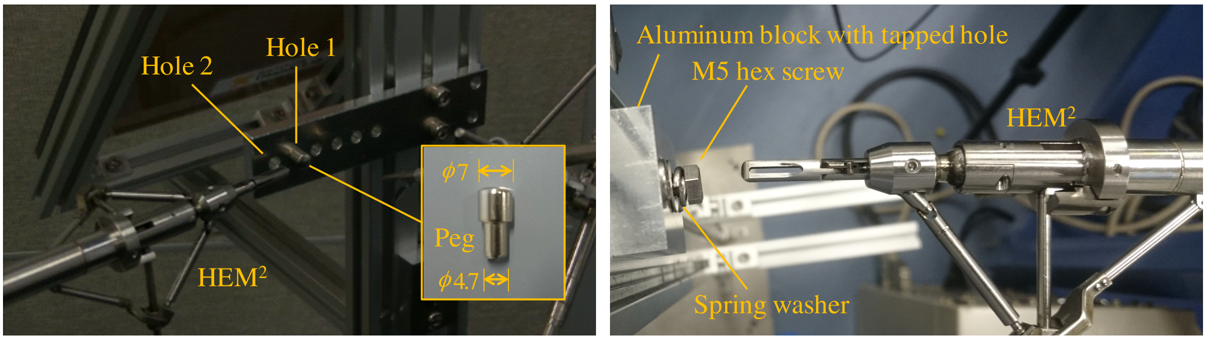

(a) Peg-in-hole task (b) Screw fastening task

Fig. 6-15: Experimental setup of peg-in-hole task and screw fastening task.

plate with holes were used as the peg and the holes. The diameter of the holes was about 4.7 mm. The peg was completely inserted into the hole 1 initially. As the procedure 1, the robot extracted the peg from the hole 1. As the procedure 2, the robot inserted the peg into the hole 2. As the procedure 3, the robot changed the grasped point and inserted the peg into the hole 2 completely.

The experimental results of the peg-in-hole task was shown in Fig. 6-16. The gray shaded areas denote the time which the procedure was conducted. In the procedure 1, the peg was grasped by the slave and the large grasping force was generated. The yaw motion of the robot was mainly used to extract the peg. In contrast with the rotational motion of the yaw motion, the peg was moved along the center axis of the hole. Therefore, the large torque was generated until the peg was completely extracted. Although the large torque was generated for the same reason in the procedure 2 and the procedure 3, the task was achieved by the robot.

Screw fastening task

A M5 stainless steel hex screw was fastened by the robot. A spring washer and a washer were arranged between the hex screw and a aluminum block with a tapped hole. The rotation axis of the screw and the roll motion was different. The screw was rotated by about 60 degrees five times.

The experimental results of the screw fastening task was shown in Fig. 6-17. The gray shaded areas denote the time which the screw was rotated. The spring washer increased the torque required to rotate the screw after the fourth rotation. From the torque response of the roll motion in Fig. 6-17(d), the estimated torque in the fifth rotation was larger than the results before the third rotation.

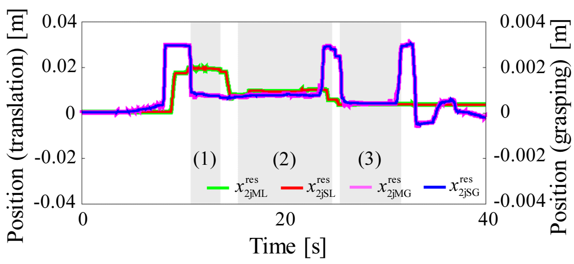

(a) Position response of grasping motion and translational motion

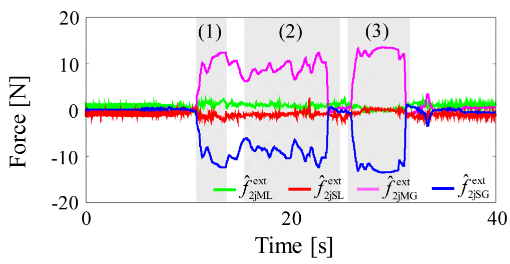

(b) Force response of grasping motion and translational motion

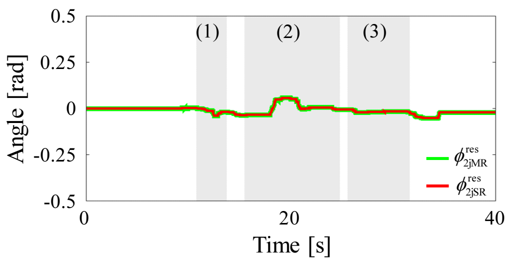

(c) Angle response of roll motion

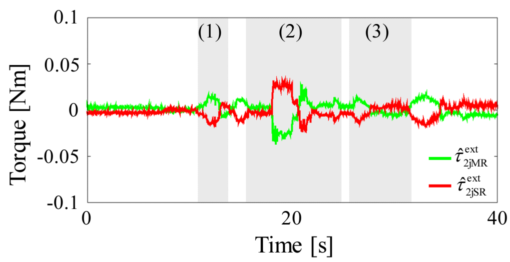

(d) Torque response of roll motion

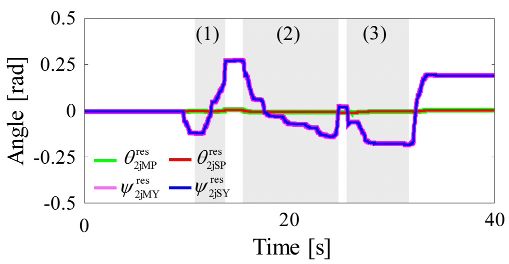

(e) Angle response of pitch motion and yaw motion

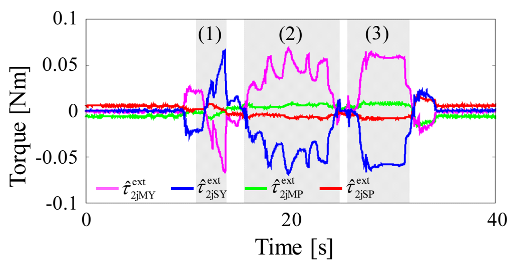

(f) Torque response of pitch motion and yaw motion

Fig. 6-16: Experimental results of peg-in-hole task.

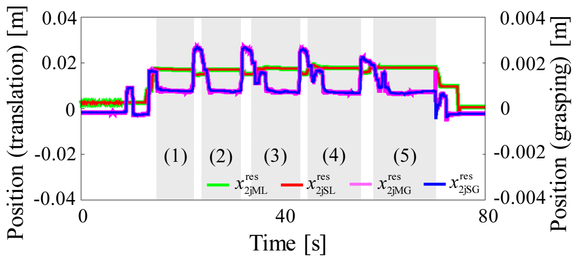

(a) Position response of grasping motion and translational motion

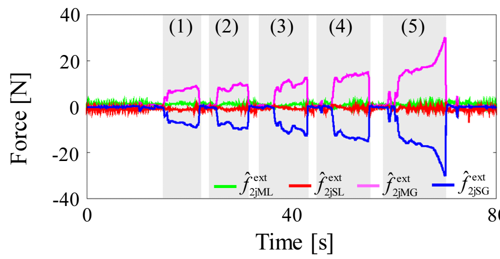

(b) Force response of grasping motion and translational motion

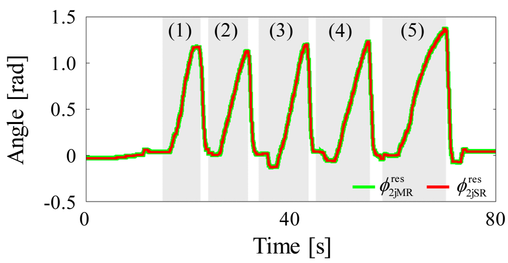

(c) Angle response of roll motion

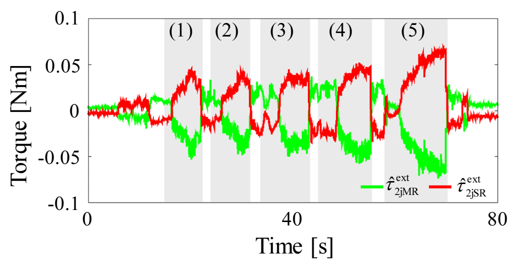

(d) Torque response of roll motion

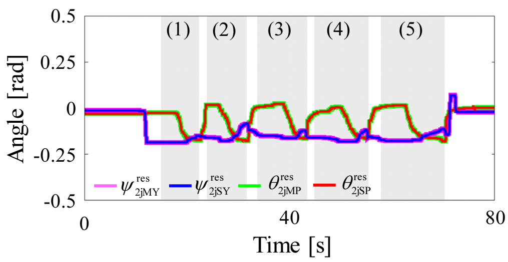

(e) Angle response of pitch motion and yaw motion

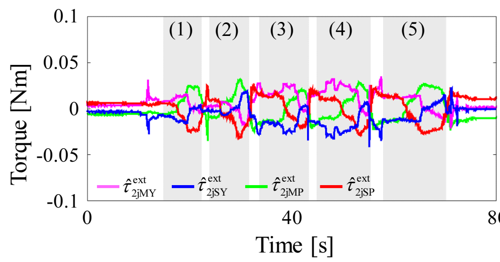

(f) Torque response of pitch motion and yaw motion

Fig. 6-17: Experimental results of screw fastening task.

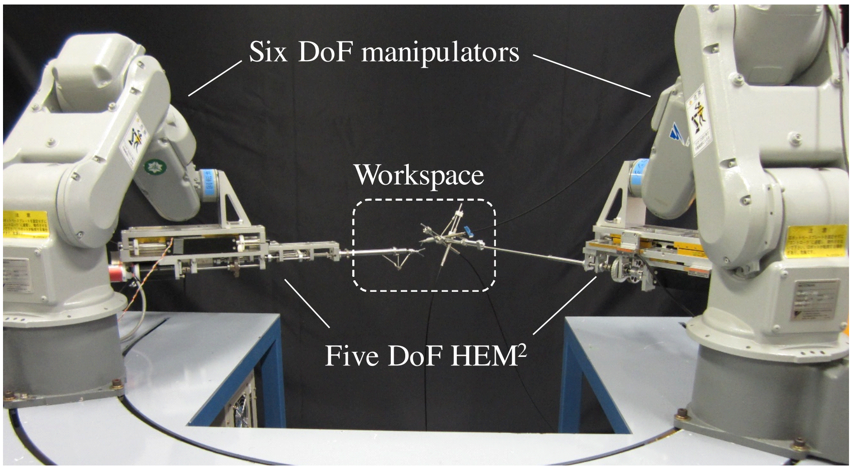

Fig. 6-18: The slave side of the double arm teleoperation system with six DoF manipulators.

6.4 Double hands manipulation

A ten DoF double arm teleoperation system is constructed by two prototypes of the five DoF HEM^2. Complex tasks realized by both hands of human operator can be achieved by bilateral teleoperation and automatic motion based on the motion reproduction system [53][54].

6.4.1 Teleoperation system

The slave side of the double arm teleoperation system is shown in Fig. 6-18. The first prototype and the second prototype of the five DoF HEM^2 are mounted on six DoF serial link manipulators. The first prototype is placed at the left hand side of an operator. The second prototype is the right hand side. The whole teleoperation system including a camera and a display is shown in Fig. 6-19. The visual information is obtained by the camera at the slave side and provided to the operator by the display at the master side. Bilateral teleoperation is realized by implementing the acceleration four-channel bilateral control to both prototypes. Motion of operators in bilateral teleoperation can be saved and reproduced by the motion reproduction system. To decrease size of haptic information, the compression method is used.

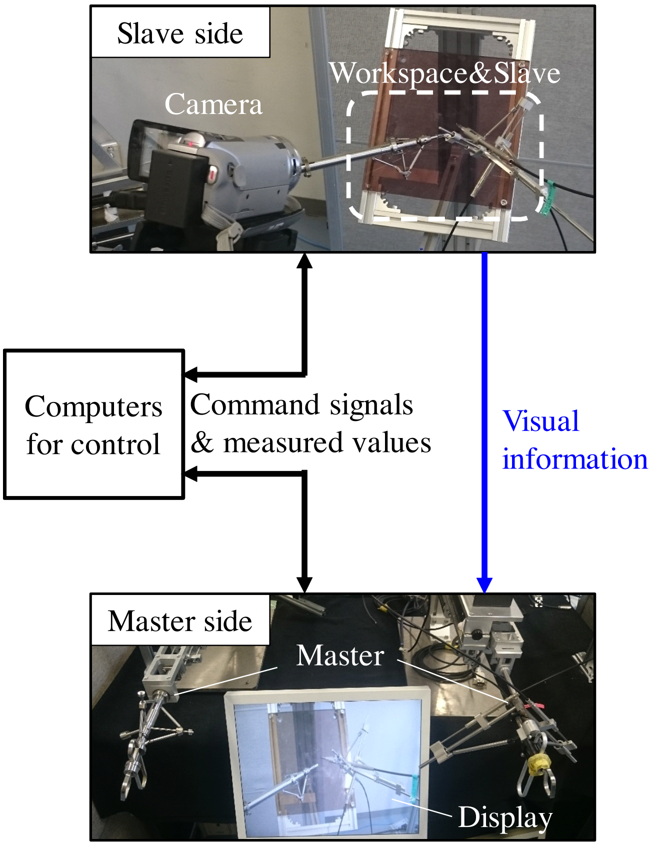

Fig. 6-19: The double arm teleoperation system.

6.4.2 Tip position of robot

Trajectories of the end-effector is useful information to evaluate the motion of robots. The tip position of the end-effector moved by the translational motion, the roll motion, the pitch motion, and the yaw motion can be derived by coordinate transformation. The coordinate definition of the first prototype is shown in Fig. 6-20. The origin of the reference cartesian coordinate system Σ_{R} is the center of rotation of the universal joint for the pitch motion and the yaw motion. The Z_{R}-axis accords with the center axis of the shaft connecting the tip part and the base part. The X_{R}-axis is parallel with the horizontal plane. The origin of the end-effector coordinate system Σ_{E} is the tip of the end-effector. Coordinate systems of the second prototype are defined as with the first prototype. Procedures of the coordinate transformation are shown in Fig. 6-21. L_{tip} is the length between the tip of the end-effector and the center of the pitch motion and the yaw rotation. The position of the end-effector coordinate system Σ_{E} is transformed to

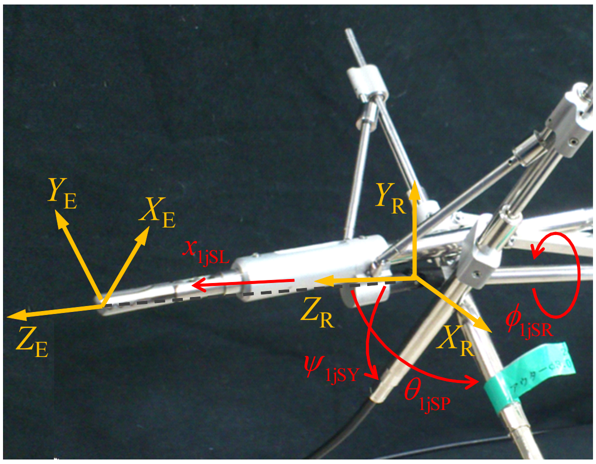

Fig. 6-20: Coordinate definition of the first prototype.

the position of the reference coordinate system Σ_{R}. The tip position of the first prototype $\boldsymbol{x}_{\mathrm{tip1}}$ on the reference coordinate system Σ_{R} is given as,

$$
\begin{aligned}
\boldsymbol{x}_{\mathrm{tip1}} &= \begin{bmatrix} x_{\mathrm{tip1}} & y_{\mathrm{tip1}} & z_{\mathrm{tip1}} \end{bmatrix}^{\mathrm{T}} \\
&= \begin{bmatrix} L_{\mathrm{tip1}} \left(\sin\phi_{\mathrm{1wR}} \sin\theta_{\mathrm{1wP}} \cos\psi_{\mathrm{1wY}} - \cos\phi_{\mathrm{1wR}} \sin\psi_{\mathrm{1wY}} \right) \\ L_{\mathrm{tip1}} \left(-\cos\phi_{\mathrm{1wR}} \sin\theta_{\mathrm{1wP}} \cos\psi_{\mathrm{1wY}} - \sin\phi_{\mathrm{1wR}} \sin\psi_{\mathrm{1wY}} \right) \\ L_{\mathrm{tip1}} \cos\theta_{\mathrm{1wP}} \cos\psi_{\mathrm{1wY}} + x_{\mathrm{1jL}} \end{bmatrix}
\end{aligned}
\tag{6.47}
$$

The tip position of the second prototype $\boldsymbol{x}_{\mathrm{tip2}}$ on the reference coordinate Σ_{R} is given as,

$$
\begin{aligned}
\boldsymbol{x}_{\mathrm{tip2}} &= \begin{bmatrix} x_{\mathrm{tip2}} & y_{\mathrm{tip2}} & z_{\mathrm{tip2}} \end{bmatrix}^{\mathrm{T}} \\
&= \begin{bmatrix} L_{\mathrm{tip2}} \left(\cos\phi_{\mathrm{2wR}} \sin\theta_{\mathrm{2jP}} \cos\psi_{\mathrm{2jY}} - \sin\phi_{\mathrm{2wR}} \sin\psi_{\mathrm{2jY}} \right) \\ L_{\mathrm{tip2}} \left(\sin\phi_{\mathrm{2wR}} \sin\theta_{\mathrm{2jP}} \cos\psi_{\mathrm{2jY}} + \cos\phi_{\mathrm{2wR}} \sin\psi_{\mathrm{2jY}} \right) \\ L_{\mathrm{tip2}} \cos\theta_{\mathrm{2jP}} \cos\psi_{\mathrm{2jY}} + x_{\mathrm{2jL}} \end{bmatrix}.
\end{aligned}
\tag{6.48}
$$

ϕ_{1wR}, θ_{1wP}, ψ_{1wY}, and ϕ_{2wR} are given as,

$$\phi_{\mathrm{1wR}} = \phi_{\mathrm{1jR}} + \phi_{\mathrm{1we}} \tag{6.49}$$

$$\theta_{\mathrm{1wP}} = \theta_{\mathrm{1jP}} + \theta_{\mathrm{1we}} \tag{6.50}$$

$$\psi_{\mathrm{1wY}} = \psi_{\mathrm{1jY}} + \psi_{\mathrm{1we}} \tag{6.51}$$

$$\phi_{\mathrm{2wR}} = \phi_{\mathrm{2jR}} + \phi_{\mathrm{2we}}. \tag{6.52}$$

The value of the link length L_{tip} and the constant offset terms ϕ_{1we}, θ_{1we}, ψ_{1we}, and ϕ_{2we} are shown in Table 6.6.

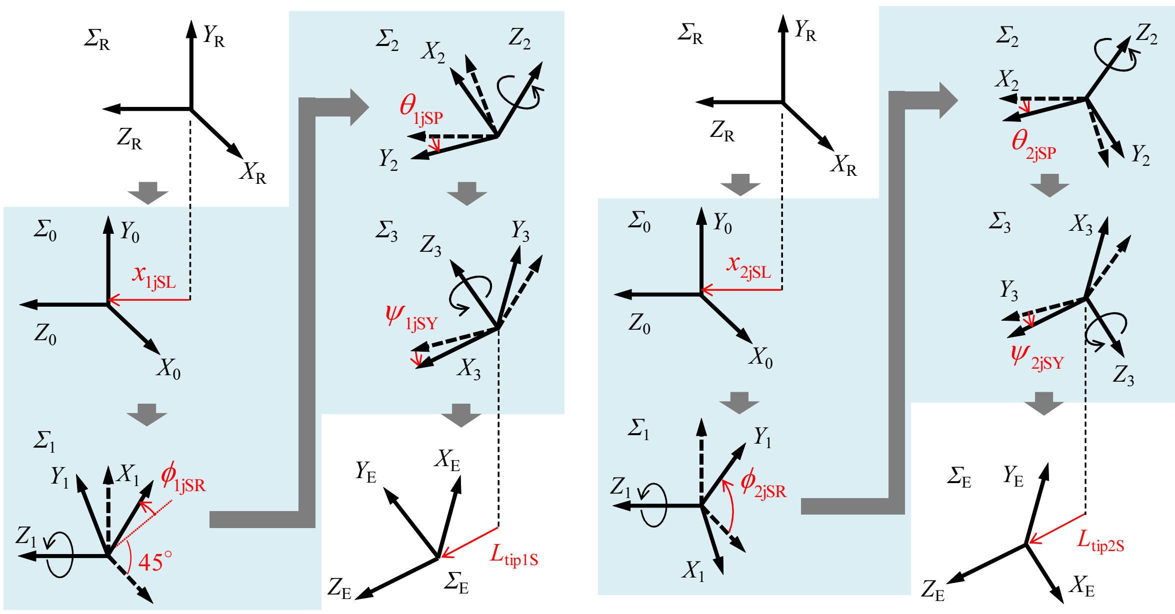

(a) The first prototype (b) The second prototype

Fig. 6-21: Coordinate transformation for the five DoF HEM^2.

6.4.3 Experiment

A complex task in surgical procedures is the ligation task. In the experiment, the ligation task was conducted by bilateral teleoperation and automatic motion based on the motion reproduction system.

Experimental setup

Procedures of the ligation task are shown in Fig. 6-22. The detailed procedures are as follows:

(1) Both robots were set at the initial position and posture. The thread was attached to a training pad for suturing tasks. One end of the thread with a needle was held by the second prototype. The length of the thread between the needle and the training pad was long, while the other side was short.

(2) The loop of the long side thread was made by the forceps. Then, the second prototype went through the loop.

(3) The second prototype held the short side thread and went through the loop of the thread.

Table 6.6: Link length and offset values

Variables	Values
L_{tip1}	0.0808 m
L_{tip2}	0.048 m
ϕ_{1we}	$\frac{\pi}{4}$
θ_{1we}	0.100 rad
ψ_{1we}	0.100 rad
ϕ_{2we}	$-\frac{\pi}{2}$

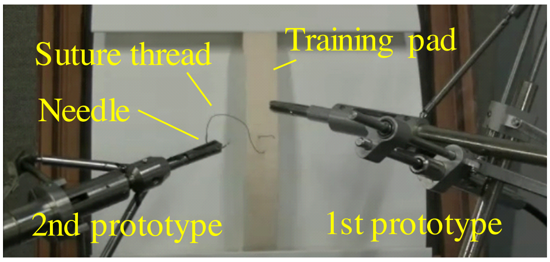

(a) The procedure 1

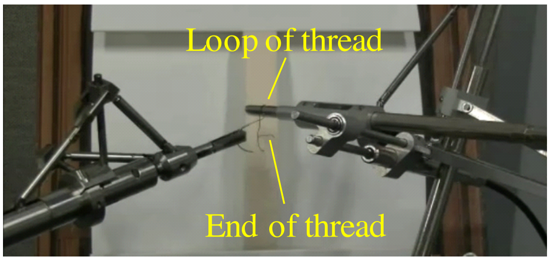

(b) The procedure 2

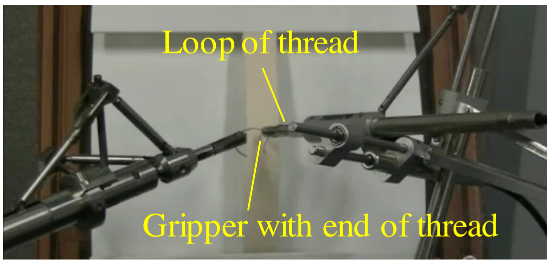

(c) The procedure 3

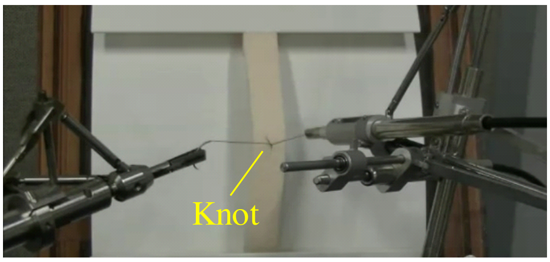

(d) The procedure 4

Fig. 6-22: Procedures of ligation task.

(4) A knot was tightened by both forceps. Then, the position and the posture of the robots were returned to the initial condition.

By returning the position and the posture to the initial condition, rapid motion of the robot can be avoided when starting reproduction of the saved motion. The suture thread and the training pad was arranged so that the conditions in the motion saving phase and the motion loading phase was the same, although it is difficult to set the flexible suture thread to the same position. In the motion saving phase, the bilateral

Table 6.7: Parameters of the first prototype for ligation task

Parameter	Grasping	Translation	Roll	Pitch & Yaw
$M_{\rm n}$	0.6 kg	1.7 kg	0.0837 gm^2	0.6 kg
$K_{\rm tn}$	33 N/A	33 N/A	0.0603 Nm/A	33 N/A
$K_{\rm p}$	1600.0 s^{-2}	400.0 s^{-2}	1600.0 s^{-2}	1600.0 s^{-2}
$K_{\rm v}$	80.0 s^{-1}	40.0 s^{-1}	100.0 s^{-1}	80.0 s^{-1}
$K_{\rm f}$	0.8	0.8	0.2	0.2
$g_{\rm dis}$, $g_{\rm rfob}$	450.0 rad/s	450.0 rad/s	400.0 rad/s	450.0 rad/s
$g_{\rm pse}$	900.0 rad/s	900.0 rad/s	800.0 rad/s	900.0 rad/s
$C_{\rm rp}$	1.0	1.5	1.5	1.5
$C_{\rm rf}$	1.0	0.5	0.5	0.5

Table 6.8: Parameters of the second prototype for ligation task

Parameters	Grasping	Translation	Roll	Pitch & Yaw
$M_{\rm n}$	0.3 kg	2.4 kg	0.0837 gm^2	0.6 kg
$K_{\rm tn}$	33 N/A	33 N/A	0.0603 Nm/A	33 N/A
$K_{\rm p}$	1600.0 s^{-2}	400.0 s^{-2}	1600.0 s^{-2}	3600.0 s^{-2}
$K_{\rm v}$	80.0 s^{-1}	40.0 s^{-1}	100.0 s^{-1}	120.0 s^{-1}
$K_{\rm f}$	0.8	0.8	0.2	0.2
$g_{\rm dis}$, $g_{\rm rfob}$	450.0 rad/s	450.0 rad/s	400.0 rad/s	450.0 rad/s
$g_{\rm pse}$	900.0 rad/s	900.0 rad/s	800.0 rad/s	900.0 rad/s
$F_{\rm M}^{\rm const}$	0.0 N	0.0 N	6.0 mNm	1.0 N
$F_{\rm S}^{\rm const}$	0.5 N	0.0 N	6.0 mNm	1.0 N
$V_{\rm thresh}$	2.0 mm/s	4.0 mm/s	0.15 rad/s	4.0 mm/s
$C_{\rm rp}$	1.0	1.5	1.5	1.5
$C_{\rm rf}$	1.0	0.5	0.5	0.5

control in joint space was implemented both prototypes. In the motion loading phase, the slave of both prototypes was controlled in the motor space. The parameters are shown in Table 6.7 and Table 6.8.

Experimental result

The ligation task was realized by both bilateral teleoperation and automatic motion based on the motion reproduction system. The experimental results are shown in Fig. 6-23, Fig. 6-24, Fig. 6-25, Fig. 6-26, and Fig. 6-27. The required time to achieve the ligation task was about 50 seconds. The

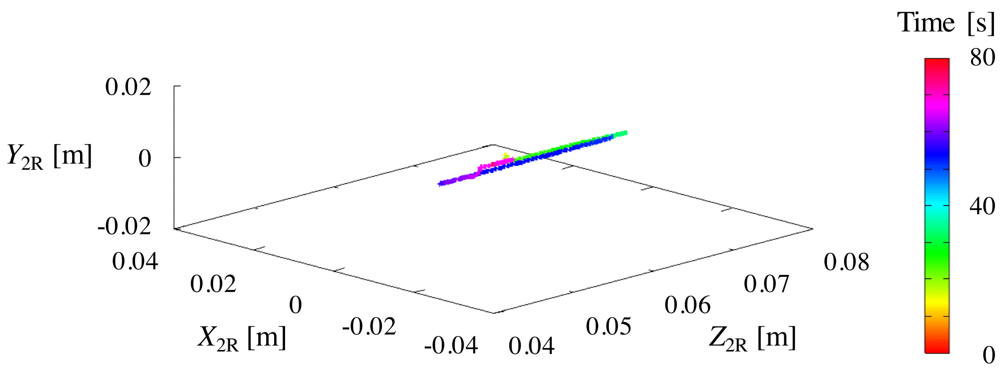

(a) Trajectory in the saved motion

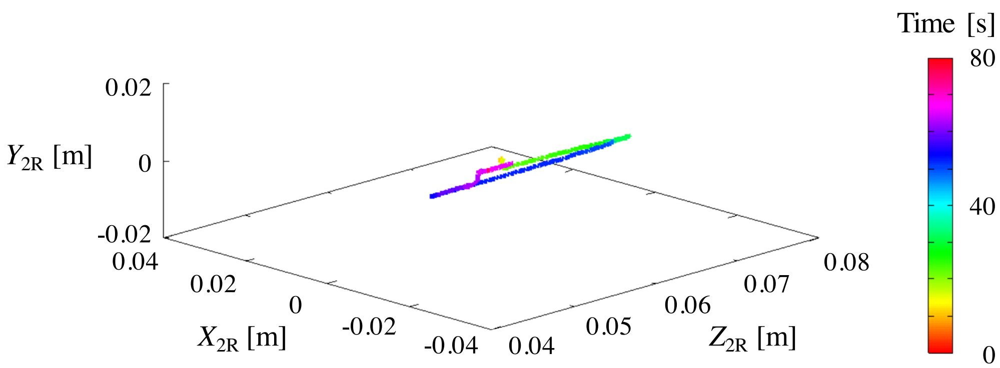

(b) Trajectory in the reproduced motion

Fig. 6-23: Trajectories of the tip position (the left hand side).

procedure 2, the procedure 3, and the procedure 4 were conducted for about 18 seconds, 17 seconds, and 15 seconds, respectively. Since the procedure 1 is the initial condition, it is not included in the required time. The required time in the reproduction phase was also about 50 seconds. In the motion saving phase, both the position tracking and Newton's third law between the master and the slave were realized.

The trajectories of the tip position of the slave calculated by eq. (6.47) and eq. (6.48) is shown in Fig. 6-23 and Fig. 6-24. The tip of the second prototype used as the left forceps was moved along the Z_2-axis in the motion saving phase. The reproduced motion of the second prototype was the almost same with the saved motion. On the other hand, the reproduced motion of the first prototype was slightly different from the saved motion. The control system and the hardware can be mentioned as the reasons of the trajectory error between the saved motion and the reproduced motion. The motion loading system

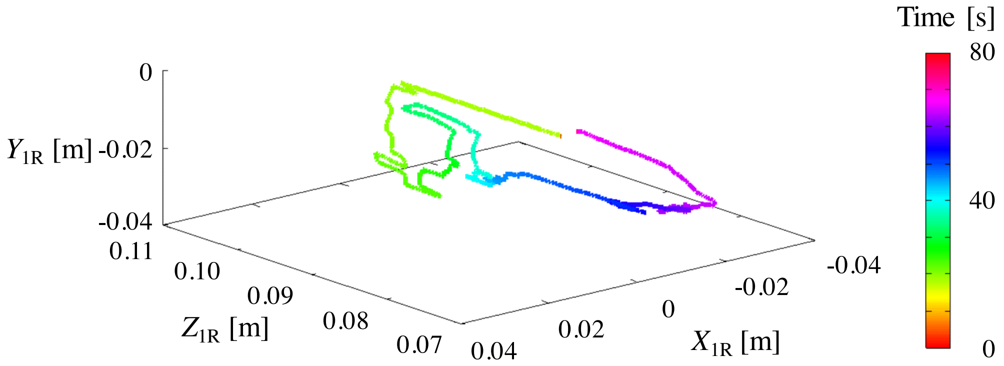

(a) Trajectory in the saved motion

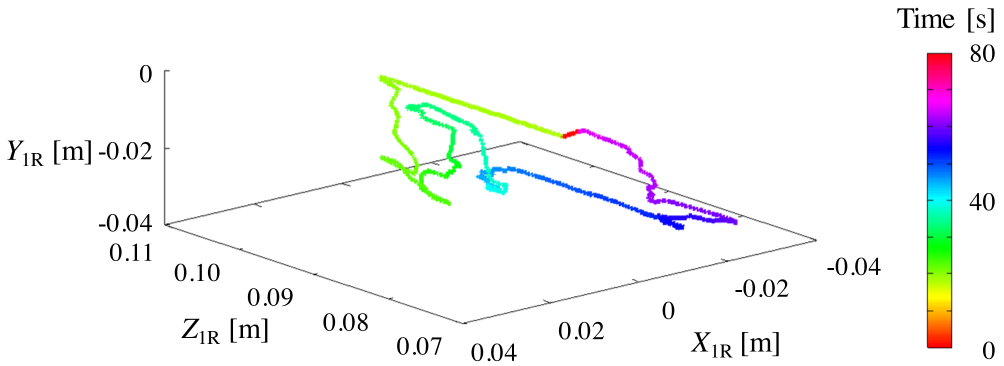

(b) Trajectory in the reproduced motion

Fig. 6-24: Trajectories of the tip position (the right hand side).

has the adaptability to the change of the environment. The reaction force which is larger or smaller than the saved force information changes the trajectory of the robot. There were many factors to change the reaction force such as the arrangement and the length of the suture thread. In this experiment, the task was achieved by the reproduced motion, even if the trajectory was automatically changed. Besides, the robot was controlled by four linux computers due to the hardware limitation. Although the realtime OS was implemented to each computer, there was a possibility that small time lag between computers influenced the reproduced motion.

The position and angle response of each motion except the grasping motion which is used to calculate the trajectories in Fig. 6-23 and Fig. 6-24 is shown in Fig. 6-25. The position and angle response of the reproduced translational and roll motion were the almost same with the saved motion. On the other hand, the angle response of the reproduced pitch and yaw motion was slightly different from the saved motion, although the shape of the graph was similar. The force and torque response of motions except the grasping motion is shown in Fig. 6-26. The large reaction force and torque were not generated by the translational motion and the roll motion. The torque generated by the roll motion of the first prototype in the procedure (4) was generated by thrust wires connected to the tip part. In the motion saving phase, large torque was generated by the yaw motion of the first prototype when tightening the knot. The knot was tightened by both forceps from about 55 seconds to 60 seconds. The torque reproduced by the yaw motion of the first prototype was the almost same with the saved motion. On the other hand, the reproduced torque for the yaw motion of the second prototype in the procedure (4) was larger than the saved motion. The position response and the force response of the grasping motion are shown in Fig. 6-27. The reproduced grasping force was larger than the saved grasping force, while the position response was the almost same.

The results can be classified into three cases. First, both the reproduced position and force were the almost same with the saved motion. Second, the reproduced position was the almost same with the saved motion, while the force was different (the grasping motion). Finally, the reproduced force was the almost same with the saved motion, while the position was different (the yaw motion). There are some differences between the grasping motion and the other motions. The force gain for the reproduced grasping motion C_{rfG} was a large value. Besides, the change of the position according to the magnitude of the grasping force was small, since the objects held by the gripper were the thin thread and the rigid needle. From Fig. 6-27, the force was generated by the motor for the grasping motion when the gripper was closed. Therefore, the reproduced position was the almost same with the saved motion.

The difference between the yaw motion and the other motion was variation of the environment. The force generated by the translational motion and the roll motion was small in both the motion saving phase and the motion loading phase. Namely, there was no object to cause variation of the environment. The motion loading system reproduced the motion mainly based on the saved position. On the other hand, there was the variation such as the length of the short side thread with needle and the held position of the long side thread. The length of thread between a knot and the tip of the end-effector affects magnitude of force. To improve the quality of tasks, these factors must be considered.

6.5 Summary

In this chapter, the systems using the five DoF HEM^2 were explained. Two prototypes of the five DoF HEM^2 were developed to realize the simplified upper limb motion. The design of the second prototype was based on the two DoF serial link mechanism with the end-effector explained in Chapter 4 and the first prototype of the five DoF HEM^2. The efficiency of the second prototype was decided by the preliminary experiment. The performance of the second prototype was validated by the free motion and the contact motion in the experiment. Besides, the peg-in-hole task and the screw fastening task were achieved by the second prototype.

The ten DoF double arm teleoperation system composed of the two prototypes, the camera, and the display was constructed. In the experiment, the ligation task was conducted by the teleoperation system as a complex task. The ligation task was realized by both bilateral teleoperation and automatic motion based on the motion reproduction system, although the trajectories of the tip position in the motion loading phase was slightly different from the saved motion. Besides, the reproduced grasping force was larger than the saved motion. To achieve tasks with better quality, not only the adaptation to variation of the environment, but also the trajectory and the magnitude of force applied to objects must be considered.

The tasks in the experiments required robotic motion in small working places. The five DoF HEM^2 realized the simplified motion of upper limbs with the transmission of haptic information in small working areas.

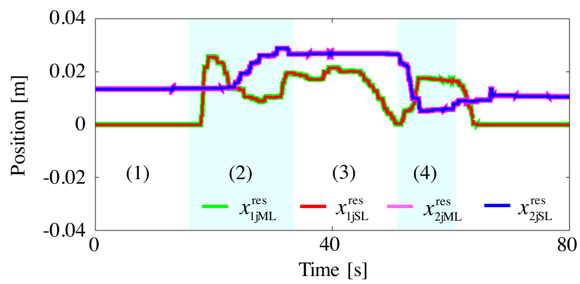

(a) The saved translational motion

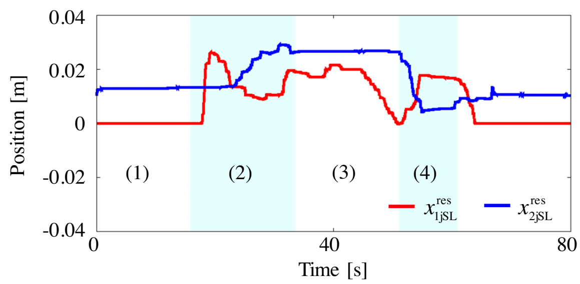

(b) The reproduced translational motion

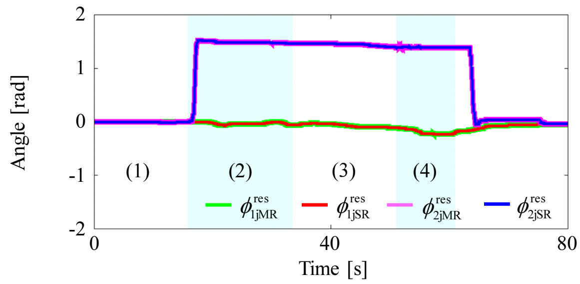

(c) The saved roll motion

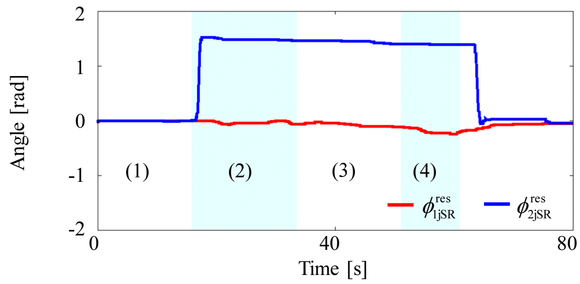

(d) The reproduced roll motion

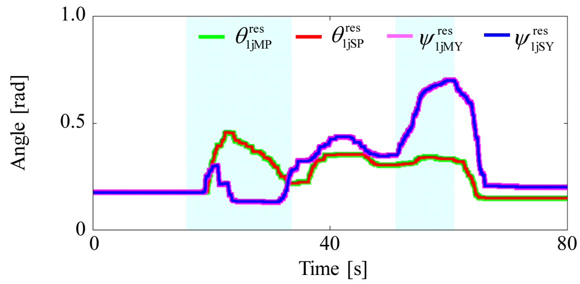

(e) The saved pitch and yaw motion of the first prototype

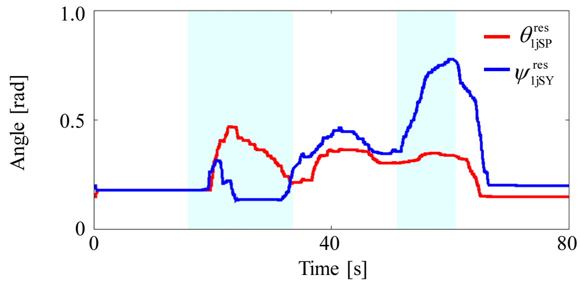

(f) The reproduced pitch and yaw motion of the second prototype

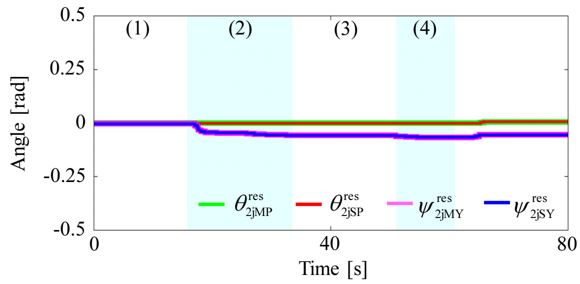

(g) The saved pitch and yaw motion of the first prototype

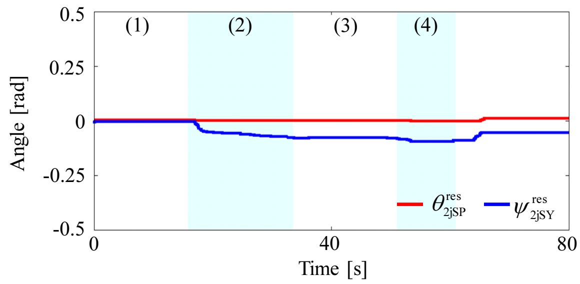

(h) The reproduced pitch and yaw motion of the second prototype

Fig. 6-25: Position and angle response.

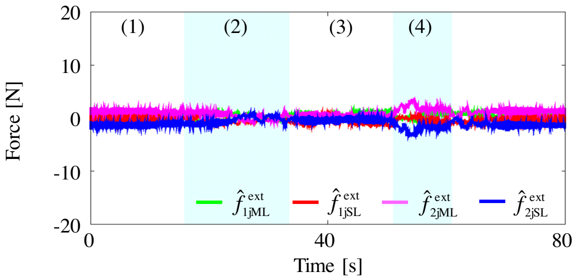

(a) The saved translational motion

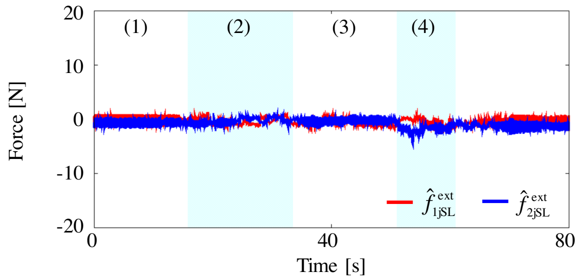

(b) The reproduced translational motion

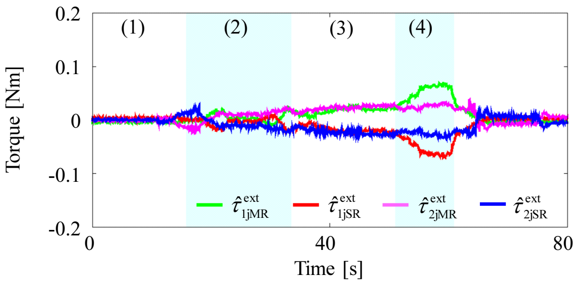

(c) The saved roll motion

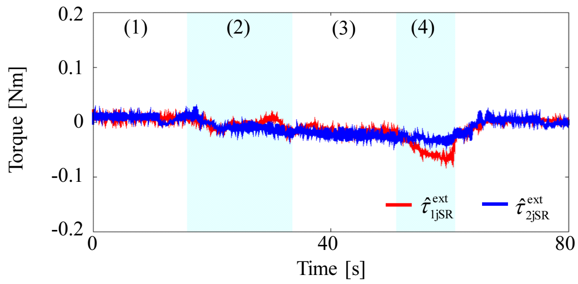

(d) The reproduced roll motion

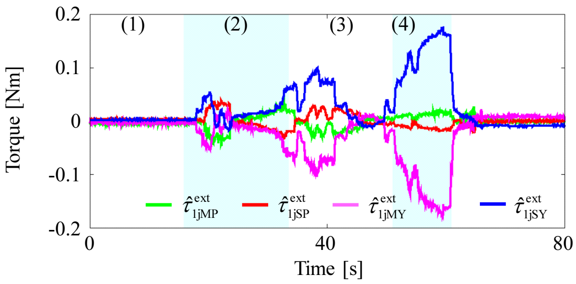

(e) The saved pitch and yaw motion of the first prototype

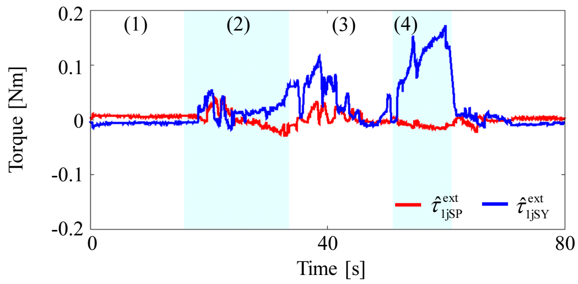

(f) The reproduced pitch and yaw motion of the second prototype

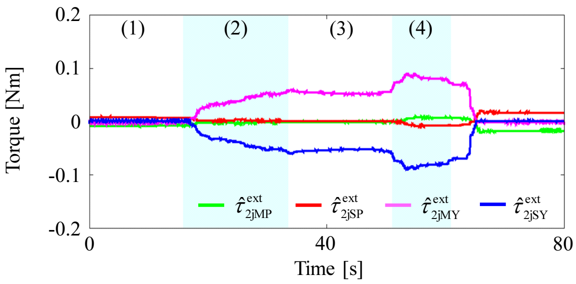

(g) The saved pitch and yaw motion of the first prototype

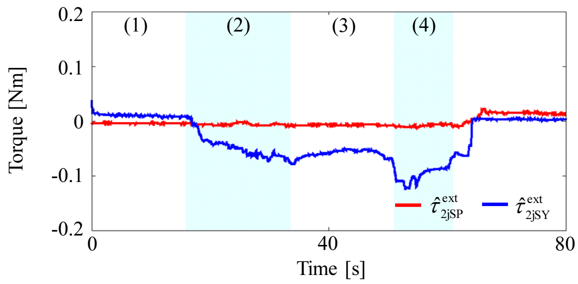

(h) The reproduced pitch and yaw motion of the second prototype

Fig. 6-26: Estimated force and torque information.

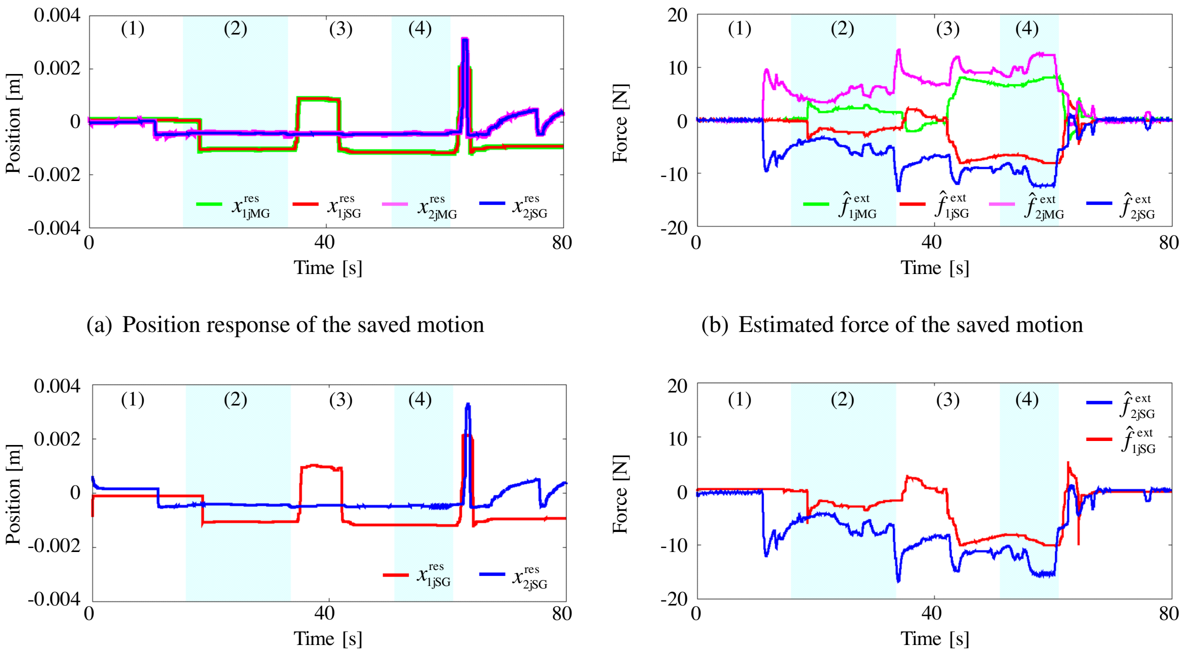

(a) Position response of the saved motion

(b) Estimated force of the saved motion

(c) Position response of the reproduced motion

(d) Estimated force of the reproduced motion

Fig. 6-27: Experimental results of grasping motion.

Chapter 7

Conclusions

In this dissertation, the master-slave five DoF HEM^2 was developed to realize motion of an upper limb by bilateral teleoperation and reproduce human motion by preserved haptic information was developed.

First, the control systems for HEM^2 were explained.The robust acceleration control to realize desired motion of robots was described in Chapter 2. DOB was implemented to realize the robust acceleration control. To obtain force information without using force sensors. RFOB was utilized. The control systems for haptic applications based on the robust acceleration control were described in Chapter 3. The acceleration based four-channel bilateral control was explained as the method to transmit haptic information. For the master-slave system with different mass, the bilateral control using oblique coordinate control was implemented. As the method to preserve and reproduce human motion, the motion reproduction system was explained.

Second, the prototypes to develop the five DoF HEM^2 were described. The two DoF haptic robot was described in Chapter 4. The two DoF serial link mechanism with the end-effector composed of the slider crank mechanisms was applied to both the master and the slave. The performance of the robot was validated by the bilateral control and the motion reproduction system. The one DoF flexible haptic forceps robot was described in Chapter 5. The slave of the flexible haptic forceps robot was composed of the end-effector, the torque transmission mechanism, and the driving unit with high reduction ratio. The efficiency of the torque transmission mechanism was decided by the preliminary experiment and used to correct estimated force information. The performance of the robot was validated by the bilateral control using the oblique coordinate control. In addition, the bilateral control system with the kinematics implemented to these robots were expressed by the scaling bilateral control.

Finally, the five DoF HEM^2 was described in Chapter 6. Two prototypes of the five DoF HEM^2 were developed. The five DoF motion composed of one DoF grasping motion, three DoF wrist motion, and one DoF translational motion was realized by the first prototype. The parallel link mechanism was implemented to the tip part of the first prototype to realize the wrist motion. The design of the second prototype was based on the first prototype. The parallel drive mechanism was constructed to implement the two DoF serial link mechanism, the parallel link mechanism, and the gear mechanism to the second prototype. The efficiency of the slave was decided by the preliminary experiment. The performance of the second prototype was validated by the bilateral teleoperation. Besides, the double arm teleoperation system was constructed by the two prototypes. The ligation task was achieved by both bilateral teleoperation and automatic motion based on the motion reproduction system. The five DoF HEM^2 realized the simplified motion of upper limbs with the utilization of haptic information in small working areas.

Robotic technologies are useful to solve problems in the modern society such as the shortage of labor force and the execution of dangerous tasks requiring human skill. More safer robotic motion in medical treatments and manufacturing tasks can be expected by using the five DoF HEM^2.

References

[1] T. Goto and K. Sugiyama, "Industrial applications of robots", *Journal of the Robotics Society of Japan*, Vol. 1, No. 1, pp. 31–37, 1983.

[2] T. B. Sheridan, "Telerobotics", *Automatica*, Vol. 25, No. 4, pp. 487–507, Jul. 1989.

[3] R. H. Taylor and D. Stoianovici, "Medical robotics in computer-integrated surgery", *IEEE Transactions on Robotics and Automation*, Vol. 19, No. 5, pp. 765–781, Oct. 2003.

[4] G. S. Guthart and J. K. Salisbury Jr., "The intuitive$^{\mathrm{TM}}$ telesurgery system: Overview and application", In *Proceedings of 17th IEEE International Conference of Robotics and Automation*, pp. 618–621, Apr. 2000.

[5] M. Ghodoussi, S. E. Butner, and Y. Wang, "Robotic surgery – the transatlantic case", In *Proceedings of 19th IEEE International Conference of Robotics and Automation*, pp. 1882–1888, May 2002.

[6] M. Mitsuishi, A. Morita, N. Sugita, S. Sora, R. Mochizuki, K. Tanimoto, Y. M. Baek, H. Takahashi, and K. Harada, "Master-slave robotic platform and its feasibility study for micro-neurosurgery", *The International Journal of Medical Robotics and Computer Assisted Surgery*, Vol. 9, No. 2, pp. 180–189, Jun. 2013.

[7] M. Nambi, P. S. Bernstein, and J. J. Abbott, "Effect of haptic-interface virtual kinematics on the performance and preference of novice users in telemanipulated retinal surgery", *IEEE Robotics and Automation Letters*, Vol. 2, No. 1, pp. 64–71, Jan. 2017.

[8] B. Bardou, F. Nageotte, P. Zanne, and M. de Mathelin, "Design of a telemanipulated system for transluminal surgery", In *Proceedings of 2009 Annual International Conference of the IEEE Engineering in Medicine and Biology Society*, pp. 5577–5582, Sep. 2009.

[9] J. Zhao, X. Zheng, M. Zheng, A. J. Shih, and K. Xu, "An endoscopic continuum testbed for finalizing system characteristics of a surgical robot for notes procedures", In *Proceedings of 2013 IEEE/ASME International Conference on Advanced Intelligent Mechatronics*, pp. 63–70, Jul. 2013.

[10] M. Tavakoli, R. V. Patel, M. Moallem, and A. Aziminejad, "Haptics for teleoperated surgical robotic systems (new frontiers in robotics sereies)", World Scientific Publishing Company, 2008.

[11] A. M. Okamura, "Methods for haptic feedback in teleoperated robot-assisted surgery", *The Industrial Robot*, Vol. 31, No. 6, pp. 499–508, Dec. 2004.

[12] P. F. Hokayem and M. W. Spong, "Bilateral teleoperation: An historical survey", *Automatica*, Vol. 42, No. 12, pp. 2035–2057, Dec. 2006.

[13] B. Hannaford, "A design framework for teleoperators with kinesthetic feedback", *IEEE Transaction on Robotics and Automation*, Vol. 5, No. 4, pp. 426–434, Aug. 1989.

[14] D. A. Lawrence, "Stability and transparency in bilateral teleoperation", *IEEE Transactions on Robotics and Automation*, Vol. 9, No. 5, pp. 624–637, Oct. 1993.

[15] W. Iida and K. Ohnishi, "Reproducibility and operationality in bilateral teleoperation", In *Proceedings of 8th IEEE International Workshop on Advanced Motion Control*, pp. 217–222, Mar 2004.

[16] F. Duan, T. Zhang, N. Pongthanya, K. Watanabe, H. Yokoi, and T. Arai, "Analyzing human skill through control trajectories and motion capture data", In *Proceedings of 4th IEEE International Conference on Automation Science and Engineering*, pp. 454–459, Aug. 2008.

[17] Y. Yokokura, S. Katsura, and K. Ohishi, "Stability analysis and experimental validation of a motion-copying system", *IEEE Transactions on Industrial Electronics*, Vol. 56, No. 10, pp. 3906–3913, Oct. 2009.

[18] T. Nozaki, T. Mizoguchi, and K. Ohnishi, "Motion expression by elemental separation of haptic information", *IEEE Transactions on Industrial Electronics*, Vol. 61, No. 11, pp. 6192–6201, Nov. 2014.

[19] T. Ishida and A. Takanishi, "A robot actuator development with high backdrivability", In *Proceedings of 2006 IEEE Conference on Robotics, Automation and Mechatronics*, pp. 1–6, Jun. 2006.

[20] S. Yamada and H. Fujimoto, "Proposal of high backdrivable control using load-side encoder and backlash", In *Proceedings of 42nd Annual Conference of the IEEE Industrial Electronics Society*, pp. 6429–6434, Oct. 2016.

[21] Y. Suzuki, H. Kuwahara, M. Sato, K. Mikami, and K. Ohnishi, "Force sensation transmission with same-structured master-slave robot hands using flexible actuators", *Journal of the Japan Society for Precision Engineering*, Vol. 76, No. 8, pp. 938–944, 2010.

[22] T. Nozaki, Y. Suzuki, and K. Ohnishi, “Transmission of force sensations by hand of multi-dof master-slave robot using tendon-driven mechanism”, *IEEJ Transactions on Industry Applications*, Vol. 131, No. 3, pp. 297–303, 2011.

[23] B. Hannaford, J. Rosen, D. W. Friedman, H. King, P. Roan, L. Cheng, D. Glozman, J. Ma, S. N. Kosari, and L. White, “Raven-II: An open platform for surgical robotics research”, *IEEE Transactions on Biomedical Engineering*, Vol. 60, No. 4, pp. 954–959, Apr. 2013.

[24] K. Sugawara and K. Ohnishi, “Development of actively-controllable endoscopic forceps”, In *Proceedings of 12th IEEE International Workshop on Advanced Motion Control*, pp. 1–6, Mar. 2012.

[25] D. J. Abbott, C. Becke, R. I. Rothstein, and W. J. Peine, “Design of an endoluminal notes robotic system”, In *Proceedings of 2007 IEEE/RSJ International Conference on Intelligent Robots and Systems*, pp. 410–416, Oct. 2007.

[26] K. Yang, Z. L. Sun, A. P. Kencana, V. A. Huynh, M. Rasouli, S. J. Phee, D. Lomanto, and K. Y. Ho, “Enhancement of spatial orientation and haptic perception for master-slave robotic natural orifice transluminal endoscopic surgery (notes)”, In *Proceedings of 2010 IEEE Conference on Robotics, Automation and Mechatronics*, pp. 15–18, Jun. 2010.

[27] H. Li, K. Kawashima, K. Tadano, S. Ganguly, and S. Nakano, “Achieving haptic perception in forceps’ manipulator using pneumatic artificial muscle”, *IEEE/ASME Transactions on Mechatronics*, Vol. 18, No. 1, pp. 74–85, Feb. 2013.

[28] T. Sasaki, K. Kokubo, and H. Sakai, “Hydraulically driven joint for a force feedback manipulator”, *Precision Engineering*, Vol. 47, pp. 445–451, Jan. 2017.

[29] K. Ibrahim, A. Ramadan, M. Fanni, Y. Kobayashi, A. Abo-Ismail, and M. G. Fujie, “Screw theory based-design and tracking control of an endoscopic parallel manipulator for laparoscopic surgery”, In *Proceedings of 2013 IEEE International Conference on Robotics and Automation*, pp. 2491–2496, May 2013.

[30] K. Kishi, M. G. Fujie, M. Hashizume, I. Sakuma, and T. Dohi, “MR-compatible surgical support manipulator system with rod-driven instruments”, *Journal of the Robotics Society of Japan*, Vol. 27, No. 6, pp. 652–660, Jul. 2009.

[31] J. Arata, M. Mitsuishi, S. Warisawa, K. Tanaka, T. Yoshizawa, and M. Hashizume, “Development of a dexterous minimally-invasive surgical system with augmented force feedback capability”, In *Proceedings of 2005 IEEE/RSJ International Conference on Intelligent Robots and Systems*, pp. 3207–3212, Aug. 2005.

[32] C. Ishii, K. Kobayashi, Y. Kamei, and Y. Nishitani, “Robotic forceps manipulator with a novel bending mechanism”, *IEEE/ASME Transactions on Mechatronics*, Vol. 15, No. 5, pp. 671–684, Oct. 2010.

[33] J. Arata, T. Saito, and H. Fujimoto, “Outer shell type 2 dof bending manipulator using spring-link mechanism for medical applications”, In *Proceedings of 2010 IEEE International Conference on Robotics and Automation*, pp. 1041–1046, May 2010.

[34] S. McKinley, A. Garg, S. Sen, R. Kapadia, A. Murali, K. Nichols, S. Lim, S. Patil, P. Abbeel, A. M. Okamura, and K. Goldberg, “A single-use haptic palpation probe for locating subcutaneous blood vessels in robot-assisted minimally invasive surgery”, In *Proceedings of 2015 IEEE International Conference on Automation Science and Engineering*, pp. 1151–1158, Aug. 2015.

[35] C. H. King, M. O. Culjat, M. L. Franco, C. E. Lewis, E. P. Dutson, W. S. Grundfest, and J. W. Bisley, “Tactile feedback induces reduced grasping force in robot-assisted surgery”, *IEEE Transactions on Haptics*, Vol. 2, No. 2, pp. 103–110, Apr.–Jun. 2009.

[36] U. Kim, D. H. Lee, W. J. Yoon, B. Hannaford, and H. R. Choi, “Force sensor integrated surgical forceps for minimally invasive robotic surgery”, *IEEE Transactions on Robotics*, Vol. 31, No. 5, pp. 1214–1224, Oct. 2015.

[37] H. Tanaka, K. Ohnishi, H. Nishi, T. Kawai, T. Morikawa, S. Ozawa, and T. Furukawa, “Implementation of bilateral control system based on acceleration control using fpga for multi-dof haptic endoscopic surgery robot”, *IEEE Transactions on Industrial Electronics*, Vol. 56, No. 3, pp. 618–627, Mar. 2009.

[38] E. Ishii, S. Katsura, H. Nishi, and K. Ohnishi, “Development of multi degrees-of-freedom bilateral forceps robot system using fpga”, *IEEJ Transactions on Industry Applications*, Vol. 127, No. 5, pp. 508–517, 2007.

[39] J. Oguma, S. Ozawa, Y. Morikawa, T. Furukawa, Y. Kitagawa, M. Ueda, and M. Kitajima, “Knot-tying force during suturing and wound healing in the gastrointestinal tract”, *Journal of Surgical Research*, Vol. 140, No. 1, pp. 129–134, Apr. 2007.

[40] W. Motooka, T. Nozaki, T. Mizoguchi, K. Sugawara, F. Mitome, K. Okuda, M. Miyagaki, D. Yashiro, T. Yakoh, K. Ohnishi, Y. Morikawa, and N. Shimojima, “Development of 16-dof telesurgical forceps master/slave robot with haptics”, In *Proceedings of 36th Annual Conference of the IEEE Industrial Electronics Society*, pp. 2081–2086, Nov. 2010.

[41] K. Ohnishi, M. Shibata, and T. Murakami, “Motion control for advanced mechatronics”, *IEEE/ASME Transactions on Mechatronics*, Vol. 1, No. 1, pp. 56–67, Mar. 1996.

[42] T. Murakami, F. Yu, and K. Ohnishi, "Torque sensorless control in multidegree-of-freedom manipulator", *IEEE Transactions on Industrial Electronics*, Vol. 40, No. 2, pp. 259–265, Apr. 1993.

[43] S. Sakaino, T. Sato, and K. Ohnishi, "Multi-dof micro-macro bilateral controller using oblique coordinate control", *IEEE Transactions on Industrial Informatics*, Vol. 7, No. 3, pp. 446–454, Aug. 2011.

[44] T. Nozaki, S. Shimizu, T. Mizoguchi, and K. Ohnishi, "Interpretation of acceleration-based bilateral control standing of impedance control and its application to reduction of haptic data", In *Proceedings of the IEEJ Technical Meeting on Industrial Instrumentation and Control*, pp. 69–74, Mar. 2014.

[45] T. Matsunaga, K. Yu, and K. Ohnishi, "Time scaling changed by force information for high speed reproduced motion of two dof haptic robot", In *Proceedings of the IEEJ International Workshop on Sensing, Actuation, Motion Control, and Optimization*, pp. 1–6, Mar. 2017.

[46] T. Matsunaga, D. Tomizuka, T. Nozaki, S. Yuki, K. Ogawa, K. Ohnishi, N. Wada, and Y. Kitagawa, "Development of miniature haptic forceps for flexible endoscope", *Journal of Japan Society of Computer Aided Surgery*, Vol. 19, No. 3, Jul. 2017.

[47] T. Matsunaga, G. Fau, R. Kozuki, and K. Ohnishi, "Motion control of five degrees of freedom surgical robot to transmit force", In *Proceedings of the IEE Japan Technical Meeting on Industrial Instrumentation and Control*, Mar. 2014.

[48] T. Matsunaga, K. Yu, and K. Ohnishi, "Development of five dof hem^2 using parallel link mechanism", *Journal of the Japan Society for Precision Engineering*, Vol. 85, No. 8, Aug. 2017.

[49] S. Hyodo, Y. Soeda, and K. Ohnishi, "Verification of flexible actuator from position and force transfer characteristic and its application to bilateral teleoperation system", *IEEE Transactions on Industrial Electronics*, Vol. 56, No. 1, pp. 36–42, Jan. 2009.

[50] T. Matsunaga and K. Ohnishi, "Exact kinematics for pitch motion and yaw motion of five degrees of freedom surgical robot", In *Proceedings of 14th IEEE International Workshop on Advanced Motion Control*, pp. 467–472, Apr. 2016.

[51] J. Burgner, D. C. Rucker, H. B. Gilbert, P. J. Swaney, P. T. Russell III, K. D. Weaver, and R. J. Webster III, "A telerobotic system for transnasal surgery", *IEEE Transactions on Mechatronics*, Vol. 19, No. 3, pp. 996–1006, Jun. 2014.

[52] T. Yoshikawa, "Measure of manipulatability for robot manipulators", *Journal of the Robotics Society of Japan*, Vol. 2, No. 1, pp. 63–67, Feb. 1984.

[53] T. Matsunaga, G. Fau, S. Shimizu, K.Tanida, T. Mizoguchi, and K. Ohnishi, "Double hands manipulation with force sensation realized by multi dof forceps robots", In *Proceedings of 41st Annual Conference of the IEEE Industrial Electronics Society*, pp. 002840–002845, Nov. 2015.

[54] T. Matsunaga, D. Tomizuka, K. Yu, T. Mizoguchi, and K. Ohnishi, "Construction of motion reproduction system using haptic forceps robots for needle insertion", In *Proceedings of 42nd Annual Conference of the IEEE Industrial Electronics Society*, pp. 722–727, Oct. 2016.

List of Achievements

Journals (As a first author)

[1] Takuya Matsunaga, Daisuke Tomizuka, Takahiro Nozaki, Saito Yuki, Kenji Ogawa, Kouhei Ohnishi, Norihito Wada, and Yuko Kitagawa, "Development of Miniature Haptic Forceps for Flexible Endoscope," *Journal of Japan Society of Computer Aided Surgery*, Vol. 19, No. 3, (accepted for publication).

[2] Takuya Matsunaga, Koyo Yu, and Kouhei Ohnishi, "Development of Five DoF HEM^2 Using Parallel Link Mechanism," *Journal of the Japan Society for Precision Engineering*, (accepted for publication).

Journals (As a co-author)

[1] Koyo Yu, Takuya Matsunaga, Hiromasa Kawana, Shin Usuda, and Kouhei Ohnishi, "Frequency-Based Analysis of the Relationship between Cutting Force and CT Number for an Implant-Surgery-Teaching Robot," *IEEJ Journal of Industry Applications*, Vol. 6, No. 1, pp. 66–72, Jan. 2017.

[2] Kouhei Ohnishi, Yuki Saito, Satoshi Fukushima, Takuya Matsunaga, Kouhei Ohnishi, and Takahiro Nozaki, "Future Society Opened by Real Haptics," *Journal of the Japan Society of Applied Electromagnetics and Mechanics*, Vol. 25, No. 1, pp. 9–16, Mar. 2017. (in Japanese)

International Conference (As a first author)

[1] Takuya Matsunaga, Guillaume Fau, Ryohei Kozuki, Kazuki Tanida, and Kouhei Ohnishi, "Gripper's Rotation of Five DoF Surgical Robot by Using Coordinate Transformation," In *Proceedings of IEEE International Conference on Mechatronics*, Nagoya, Japan, Mar. 6th–8th, 2015.

[2] Takuya Matsunaga, Guillaume Fau, Shuhei Shimizu, Kazuki Tanida, Takahiro Mizoguchi, and Kouhei Ohnishi, "Double Hands Manipulation with Force Sensation Realized by Multi DoF For-

ceps Robots," In *Proceedings of the 41st Annual Conference of the IEEE Industrial Electronics Society*, Yokohama, Japan, Nov. 9th–12th, 2015.

[3] Takuya Matsunaga and Kouhei Ohnishi, "Exact Kinematics for Pitch Motion and Yaw Motion of Five Degrees of Freedom Surgical Robot," In *Proceedings of the 14th IEEE International Workshop on Advanced Motion Control*, Auckland, New Zealand, Apr. 22nd–24th, 2016.

[4] Takuya Matsunaga, Daisuke Tomizuka, Koyo Yu, Takahiro Mizoguchi, and Kouhei Ohnishi, "Construction of Motion Reproduction System Using Haptic Forceps Robots for Needle Insertion," In *Proceedings of the 42nd Annual Conference of the IEEE Industrial Electronics Society*, Firenze, Italy, Oct. 24th–27th, 2016.

[5] Takuya Matsunaga, Koyo Yu, and Kouhei Ohnishi, "Time Scaling Changed by Force Information for High Speed Reproduced Motion of Two DoF Haptic Robot," In *Proceedings of the IEEJ International Workshop on Sensing, Actuation, Motion Control, and Optimization*, Nagaoka, Japan, Mar. 6th–8th, 2017.

International Conference (As a co-author)

[1] Guillaume Fau, Takuya Matsunaga, and Kouhei Ohnishi, "Development of a Five Degrees of Freedom Master/Slave Robot for Tele-operated Laparoscopic Surgical Operations," In *Proceedings of the 7th IEEE International Conference on Human System Interaction*, Lisbon, Portugal, Jun. 16th–18th, 2014.

[2] Seiji Uozumi, Shuhei Shimizu, Takuya Matsunaga, Tomohiro Nakano, and Kouhei Ohnishi, "Verification of Twist Drive System and Its Application to Haptic Robot Hand," In *Proceedings of 2015 IEEE International Conference on Industrial Technology*, Seville, Spain, Mar. 17th–19th, 2015.

[3] Shuhei Shimizu, Takuya Matsunaga, and Kouhei Ohnishi, "Method of Position Error Compensation in Consideration of Symmetric Structure for Bilateral Control System under Time Delay," In *Proceedings of the 41st Annual Conference of the IEEE Industrial Electronics Society*, Yokohama, Japan, Nov. 9th–12th, 2015.

[4] Daisuke Tomizuka, Takuya Matsunaga, Koyo Yu, and Kouhei Ohnishi, "Decoupling Control Using Gain Scaling Based on Scaling Bilateral Control with Different Inertia," In *Proceedings of the IEEJ International Workshop on Sensing, Actuation, Motion Control, and Optimization*, Nagaoka, Japan, Mar. 6th–8th, 2017.

[5] Tomoyuki Shimono, Hiroshi Asai, Takahiro Fujimoto, Takahiro Mizoguchi, Takuya Matsunaga, Kouhei Ohnishi, "Large Circular Linear Motor for Lower Limb Rehabilitation Robot," In *Proceedings of the IEEJ International Workshop on Sensing, Actuation, Motion Control, and Optimization*, Nagaoka, Japan, Mar. 6th–8th, 2017.

Domestic Conference (As a first author)

[1] Takuya Matsunaga, Guillaume Fau, Ryohei Kozuki, and Kouhei Ohnishi, "Motion Control of Five Degrees of Freedom Surgical Robot to Transmit Force," In *Papers of the IEE Japan Technical Meeting on Industrial Instrumentation and Control,*, Mar. 10th–11th, 2014. (in Japanese)